Université de Liège - Faculté des Sciences Appliquées

Punching shear of deep pile caps

Travail de fin d'études réalisé en vue de l'obtention du grade de Master Ingénieur Civil des Constructions par Jeunehomme Denis

Année académique 2014-1015

Composition du jury :

MIHAYLOV Boyan
FRANSSEN Jean-Marc
COLLIN Frédéric
CERFONTAINE Frédéric

Lundi 1er juin 2015

First of all, I would like to thank Mr. Boyan Mihaylov, the promoter of this thesis, for the continuous help he brought to both the development of the model and the writing of my thesis. His advice were always useful and I have tried to follow them as much as I could. Then, I would to thank the other members of my jury for the interest they brought to my work and for the comments they formulated which were really helpful. I also would like to express my gratitude to my two office coworkers, namely Mrs. Jian Liu and Mr. Nikola Tatar for their patience and their permanent good mood which brought motivation when I had none and to my parents without whom no word of this thesis would have been written. I will finish the acknowledgment by thanking Mrs. Anaïs De Cuyper for kicking my ass when I needed it to work efficiently and for her unconditional support.

Thesis statement

Reinforced concrete pile caps belong to the family of deep elements which work predominantly in shear. As such, they are characterized by complex deformation patterns and cannot be modeled based on the classical assumption that plane sections remain plane. In this context, it is necessary to develop a new approach which captures better their ultimate shear behavior.

This thesis consists of the development and the analysis of a model for the shear strength of caps joining four piles. To do so, it is planned to use the two-parameters kinematic theory (2PKT) previously developed for deep beams by *Mihaylov et al. (2013)*, and extend it to pile caps. The basic idea is to evolve this 2D model into a 3D one. Thus, the same basic phenomena explaining the behavior of deep beams should be taken into account, but the different terms which compose the 2PKT approach have to be adapted in order to capture the specifics of pile caps.

The first step consists of finding in the literature tests performed on four-pile caps and build a database with the properties of each test specimen. The interest is double: on the one hand, it will allow to observe the behavior of as many specimens as possible to identify the common failure modes and more specifically to try to find a reoccurring crack pattern. On the other hand, these tests will serve to evaluate the accuracy of the model.

The final goal of this thesis is to determine the reliability of this model and more precisely to study its behavior in its field of use. So, it will be necessary to vary some key parameters of pile caps and study the results produced by the model. Using the database, it will be possible to determine how accurate the model is in capturing the effect of different experimental variables.

In parallel, a strut-and-tie model will be used to illustrate one way the pile caps are dimensioned nowadays. In that way, comparisons between this approach, the test specimens, and the 2PKT model could be provided.

Signature of the members of the Jury:

MIHAYLOV Boyan (promoter): FRANSSEN Jean-Marc:

COLLIN Frédéric: CERFONTAINE Frédéric:

Abstract

Punching shear of deep pile caps
Jeunehomme Denis
Second year of the Master's degree in Civil Engineering
Academic year 2014-2015

The purpose of this Master's thesis is to develop a model predicting the shear strength of deep pile caps and especially in the case of four-piles specimens. The considered approach consisted of starting from the 2PKT model realized by *B. Mihaylov et al. in 2013 [1]*, which is initially used to predict the shear strength of deep beams, and extending it for deep pile caps. To do so, the different components of the model had to be adapted accordingly to this new configuration. Then, to evaluate both the efficiency and the utility of this model, two verifications were performed. The first one is based one the series of tests realized on such elements in order to experimentally determine their ultimate strength. Thereby, using all data collected during these tests, the model was able to predict the theoretical strength of the different considered elements. As such, these values were then compared to the experimental strengths in order to determine the accuracy it could reach. Besides, the results were hopeful considering the model offers the possibility to approach reality in a safe way while keeping a good efficiency. Then, the utility of the model was evaluated depending on the improvements it can bring compared to the classical design methods. In particular, the pile caps are generally designed using some strut-and-tie models. at this occasion, the realized model should keep it simple and follow reasonable assumptions in order to correspond as well as possible with what is done in practice. Unfortunately, the results of the comparison between the strut-and-tie model and the 2PKT model extended for pile caps showed some mitigated improvements of the predicted values which thus seems to question the use of this model.

Résumé

Résistance au cisaillement des semelles sur pieux
JEUNEHOMME Denis
Deuxième année du grade de master en ingénieur civil des constructions (finalité approfondie)
Année académique 2014-2015

Le but de ce travail de fin d'étude était de développer un modèle permettant d'évaluer la résistance au cisaillement des semelles sur pieux et en particulier dans le cas d'éléments à quatre pieux. L'approche considérée a consisté à partir du modèle 2PKT réalisé par *B. Mihaylov et al. en 2013 [1]*, permettant initialement de prédire la résistance au cisaillement des poutres hautes, et de l'étendre aux éléments de types semelles sur pieux. Pour ce faire, les différents éléments composant ce modèle ont dû être adapté de manière à correspondre à leur nouvelle configuration. De manière à évaluer tant l'efficacité que l'utilité de ce modèle, deux vérifications ont été envisagées. La première se base sur les séries de tests réalisés sur ce type d'éléments pour déterminer expérimentalement leur résistance ultime. Ainsi, en utilisant l'ensemble des données récoltées lors de ces tests, le modèle a pu prédire la résistance théorique des différents éléments considérés. A ce titre, ces valeurs ont ensuite été comparées aux résistances expérimentales de manière à déterminer la précision qu'il pouvait atteindre. Les résultats sont d'ailleurs encourageant dans le sens où le modèle permet d'approcher la réalité de manière sécuritaire tout conservant une bonne efficacité. L'utilité du modèle a ensuite été évaluée en fonction des améliorations qu'il apporte vis-à-vis des méthodes de dimensionnement classique. En l'occurrence, les semelles sur pieux sont généralement dimensionnées à l'aide de modèles bielle-tirant. Le modèle réalisé à cette occasion devait rester simple et suivre des hypothèses raisonnable de manière à correspondre au mieux à ce qui est fait en pratique en bureau d'études. Malheureusement, les résultats de la comparaison entre le modèle bielle-tirant et le modèle 2PKT étendu aux semelles sur pieux n'a permis que d'illustrer une amélioration mittigées des prédictions, ce qui semble rendre discutable l'utilisation de ce modèle.

Contents

1 Introduction

Pile caps are commonly used for supporting heavily loaded columns in order to transfer the loads to the soil through the piles. Such elements generally have a lower span-to-depth ratio and mainly work in shear. Moreover, classical flexural methods cannot be used considering they are characterized by complex deformation patterns. Compared to other reinforced concrete elements, they are generally only reinforced in the bottom and are characterized by a low reinforcement ratio. In that case, the Figure 1 illustrates the three different bar arrangements commonly used :

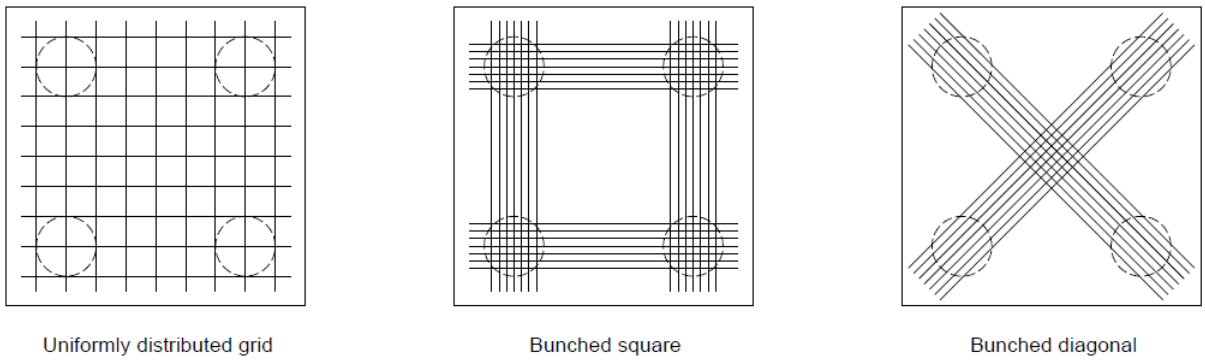

Figure 1: Illustration of the 3 different bar arrangements

In that context, the purpose of this Master's thesis is to proposed a new model which will offer the possibility to evaluate accurately the strength of this kind of elements and propose some improvements compared to the current design methods. In particular, pile caps are generally designed by using some strut-and-tie model and thus, the one used or developed in this thesis to compare the two models has to keep it simple and follow reasonable assumptions in order to correspond to a practical approach.

Concerning the model itself, it will be based on the 2PKT model developed by *B. Mihaylov et al. in 2013 [1]* in order to respond to the same problematics which existed for deep beams. Thereby, regarding the efficiency of this model, it seemed logical to lead a similar approach for pile caps and determine if it brings such encouraging results. To adapt the model to this new configuration, it it will be first necessary to analyze the initial model and then determine how this change impacts each component of the model.

As such, it has to be ensured that the modifications undertaken correspond well with reality. To do so, some series of tests performed on pile caps has to researched in the existing literature. In that way, their results could be gathered in order to understand the behavior of such elements, especially at failure. Moreover, these tests will also contribute to realize database in which the model could find the characteristics it needs to deduce the predicted strength of all the specimens. Finally, the experimental tests will serve to determine the accuracy of the model by comparing the values it furnished to the ultimate load observed experimentally.

2 Literature review

As it was already mentioned, several sources from the literature will be used all along this thesis. All of them have different purpose but they can be synthesized into four different categories:

– Experimental studies of pile caps

This category try to centralize as much as possible tests which were made on pile caps and especially on four-pile caps. By investigating the way the specimens failed, it will be possible to try to draw some reoccurring failure modes and their corresponding crack patterns. Considering the fact that these observations are really useful to understand properly the involved phenomena when the failure occurs.

Moreover, it will permit to gather the different characteristic parameters of the tested specimens. Therefore, they will form a database which could be used to put to test the new model. Indeed, the results it will produce can be compared to the corresponding experimental values which will give information on its accuracy.

– Strut-and-tie model for pile caps

Before developing a new model, it is important to know exactly where the state of the art has reached. To do so, it is necessary to evaluate the strength and more importantly the weaknesses of the current methods in order to identify the fields where some improvements can be made. In the case of deep pile caps, Eurocode 2 remains quite vague regarding these elements. In fact, there is no specific calculation for them and only some recommendations are indicated such as :

Reinforcement in a pile cap should be calculated either by using strut-and-tie or flexural methods as appropriate, Eurocode 2

Knowing that, it will be useful to develop at least one method in order to compare it to the experimental results. In particular, the strut-and-tie model appears to be the best alternative to test the way pile caps are designed nowadays. Indeed, it permits to describe how the forces are flowing through the element fitting better with the phenomena the dimensioning is supposed to describe. Moreover, the flexural method is clearly not the best way to get into the problem while one of the main hypothesis on which this method is based on, namely that "plane sections remain plane" cannot be applied to deep elements, to which most pile caps belong.

The idea was initially to use a strut-and-tie model based on an existing one. However, it appeared that the information given were not sufficient to understand the assumptions used and the geometry considered for the nodes. As such, it was decided to develop a new model which will be developped later in this work.

– 2PKT for deep beams

This is the model which will be extended from 2 dimensions into 3D. As such, it is important to evaluate the quality of the initial model and the accuracy of its results. Indeed, it is useless to try to base this work on a model if this one did not lead to any interesting result.

Then, it is a necessity to understand precisely the phenomena involved in the beam failure and handle them well enough to start the development of the new model. This requires to be able to identify the differences and the similarities between pile caps and beams, but more important, to understand how these changes impact the model and their consequences on the different parameters of the model.

- Upper-bound plasticity models

In the same idea of the 2PKT, a model was developed in the university of Southern, Denmark, to describe the collapse mechanism of pile caps in order to predict their strength. To do so, they identified and parametrized one failure mode in particular. Then, they were able to deduce the values of the different components of the strength based on this particular mode.

Because this thesis tries to solve the same problem than their, it can be interesting to investigate the reasons why they have chosen this particular pattern and not another one in order to try to find new explanations of what happens at failure and also inspire of their pictures to develop some simplified models which could be used through this thesis.

2.1 Experimental studies of pile caps

Six different series of tests were found. They are extending over a period of time from 1967 to 2001. They come from 3 different countries:

- France
- United Kingdom
- Japan

The purpose of this section is to describe each of them in order to draw a fast picture of their content and understand how they will be useful to the development of the new model. Indeed, more than bringing some new data to this study, the observations and the developments performed in parallel can give some precious informations, helping the understanding of the physical phenomena or giving interesting results of pile caps behavior.

Moreover, it is necessary to describe the tests procedures. In that way, it is possible to analyze and interpret the results obtained both concerning the observed values and the conclusions they could draw from them. Thus, the following criteria have to be detailed:

- Description of the specimens
- Test setup
- Main experimental observations

2.1.1 French tests

These are the oldest series of tests found in the literature. They were reported in a paper published by *J. Blévot and R. Frémy in 1967 [2].* This article is organized around two distinct topics. The first one concerns a proposed simplified method for the dimensioning of pile caps based on the "Struts method", while the second part simply gives a report of the tests made on scaled or full size pile caps. The tests were realized to compare different reinforcing bar arrangements in order to evaluate their respective efficiency.

Two series of tests were performed : The first one, realized between 1955 and 1958, used mainly 1/2 - 1/3 scale specimens with different numbers of piles from 2 to 4. The second one was performed right after, using specimens with also composed from 2 to 4 piles but this time designed at full scale. Moreover, most of the four-pile caps were realized with taper whose dimensions varied from specimen to another. Thus, through their tests, Blévot and Frémy showed that grid arrangement of reinforcements is around 20% less effective than bunched square one. They also have reported the crack pattern on some of their tests as shown in Figure 2.

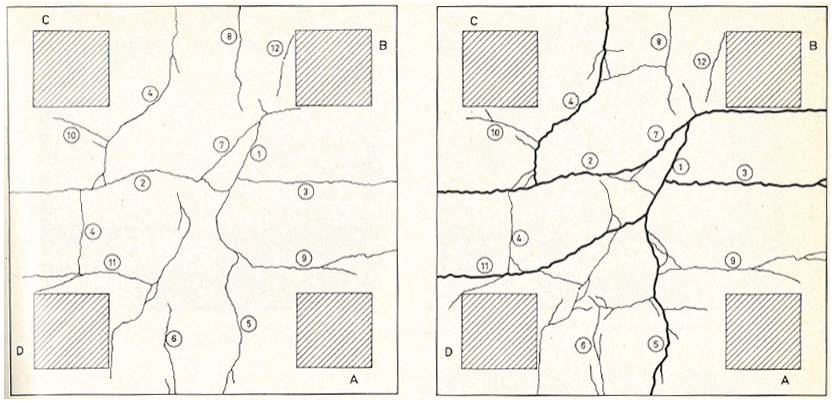

Figure 2: Example of crack pattern at 500t (left) at failure (right) [2]

All the specimens were tested by increasing the load on the column until reaching the failure. However, to make sure that their tests could be correctly analyzed, they have imposed several characteristics to them:

- Center the force applied on the column as much as possible
- Free the rotation of the lower sections of the piles
- Free the horizontal translation of the lower sections of the piles

These measures were taken in order to ensure that the piles and the column did not behave like fixed support and develop frictional effects. Indeed, these would have created some unwanted phenomena and would have noised the final results. To do so, they placed one ball under each pile and above the column to allow the rotation. After some unsuccessful tests, they have finally added smaller balls under the piles to free their horizontal translation. Thus, the final test statement is illustrated in Figure 3.

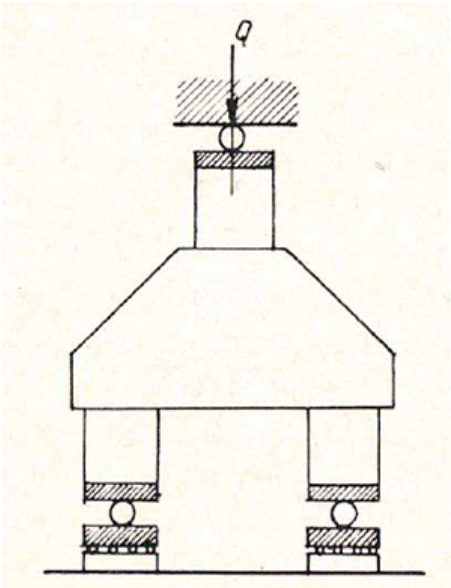

Figure 3: Test arrangement chosen by *J. Blévot and R. Frémy [2]*

2.1.2 English tests

This series of tests was realized by *J. L. Clarke et al. in 1973 [3].* They were aimed at increasing the number of experimental results in order to evaluate the different ways to design pile caps. They also have taken the opportunity to compare common bar arrangements and the efficiency of different bar anchorage. During this study, they tested fifteen four-pile caps and based on the observation they made, they tried to describe the characteristic shape of the failure surface, see Figure 4.

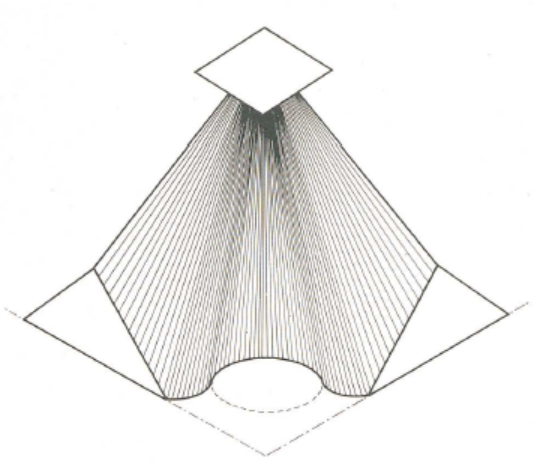

Figure 4: Suggested shape of failure surface by *Clarke et al. [3]*

This shape is obviously too complex to be exploited as such, but the informations it gives can be useful to understand how the force flows in the cap and how the specimens fail. Moreover,

it can be adapted and simplified for the development of kinematic model.

Unlike the previous tests, these were made by loading the piles and not the column. Moreover, the hydraulic jack loading each pile rested on several rollers to free the horizontal displacement. However, it seems that no measure was taken to allow the rotation of the piles. The picture in Figure 5 illustrates the final design of the test setup used:

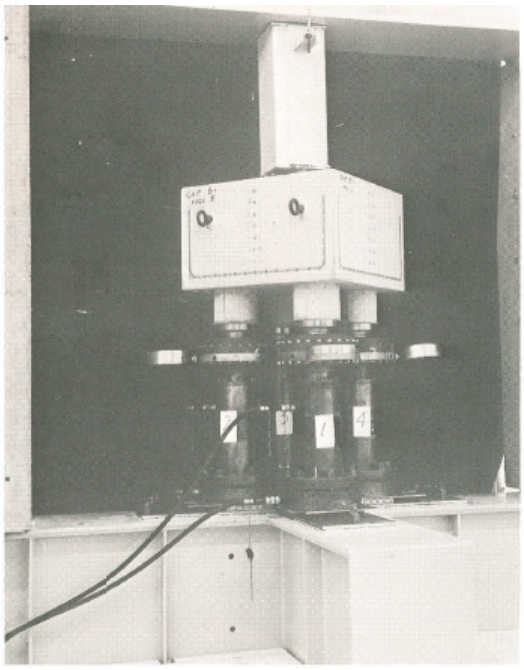

Figure 5: Final test arrangement used by *Clarke et al. [3]*

2.1.3 Japanese tests

More recently, several tests were performed in Japan to improve the knowledge on pile caps. Apparently performed by the same group of research, they tried to study the influence of some specific characteristics of pile caps.

In particular, the same test setup was used all along these series of tests. In this case, a Amsler machine was used. This kind of testing machines consist on loading the piles of the element through two hydraulic jacks supporting two loading beams. Thus, the reactions of the piles have to be equal each others in respect of the static equilibrium of each beam. An illustration of this material is given in Fig.6.

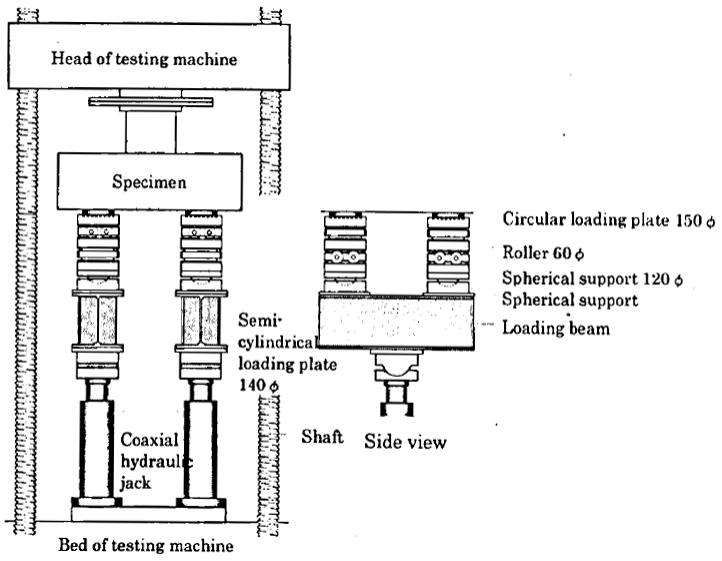

Figure 6: Test arrangement used in each Japanese series

Moreover, the rotation and the horizontal translation of the piles were set free respectively by a spherical support and two-stage rollers positioned under each piles. In that way, they ensured that the results would not be noised by some unwanted resistance.

The first test performed was written in *1998 by K. Suzuki, K. Otsuki and T. Tsubata [4]* tries to answer to two problematics. First, they undertook to study the impact of the bar arrangement on the strength of pile caps. By varying the bottom reinforcement layout, they tried to clarify their respective efficiency. Then, they performed a comparative study to evaluate the impact of the distance from the center of the pile and the edge of the cap. In that way, they were able to show that bunched square bar offers higher strength than uniform square grid as it was illustrated by the previous authors. Moreover, it appears that the edge distance has a beneficial effect on the pile cap strength as it is represented on the graph in Figure 7.

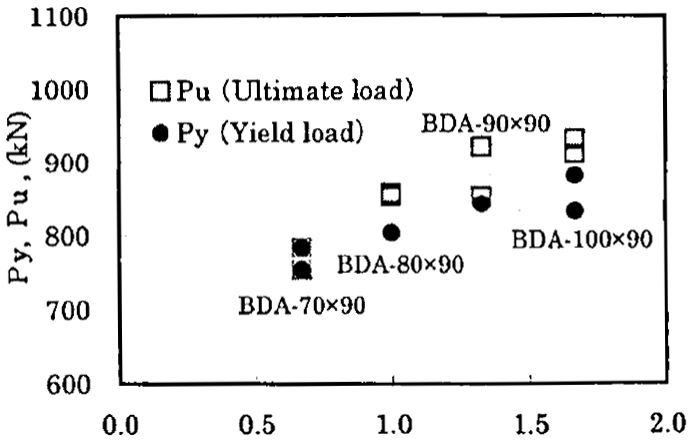

Figure 7: Impact of edge distance on yield and ultimate load by *Suzuki et al. [4]*

They also used their tests to gather the observed crack pattern and analyze them in order to represent the characteristic crack distribution on each type of specimens.

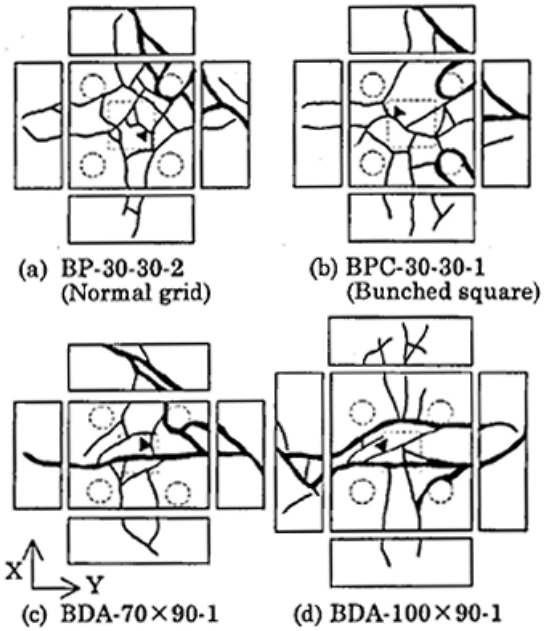

Figure 8: Crack pattern on several specimens tested by *Suzuki et al. [4]*

Where it appears that the common failure mode occurred either by corner shear failure or by flexural failure. However, they also have noticed two others failure modes which happened less frequently, namely the punching shear and one way shear failure.

The tests performed in *1999* by the same scientists [5] used some four-pile caps with tapper. They have decided to study these particular elements because, even if some previous studies seemed to show that there is no difference between tapered and non tapered footings, some

properties had to be clarified as the failure behavior of such elements. In parallel, they tried to measure the influence of the amount of reinforcement on the load when the first cracks appear and compared the experimental values to the classical design methods.

All the specimens were reinforced with a uniformly distributed grid whose mesh dimensions changed in order to vary the reinforcement ratio. Thus, they arrived to the conclusion that the more the reinforcement, the lower the cracking load, as it seems to be depicted on their results.

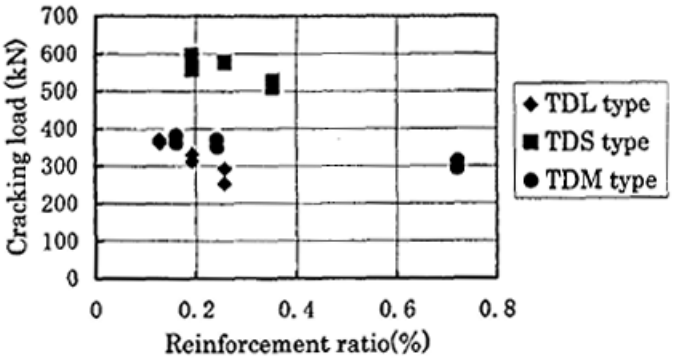

Figure 9: Relationship between cracking load and reinforcement ratio by *Suzuki et al. [5]*

Concerning the failure mode of the tapered pile caps, the authors reported once again the crack pattern at failure which allowed them to determine the reoccurring ones.

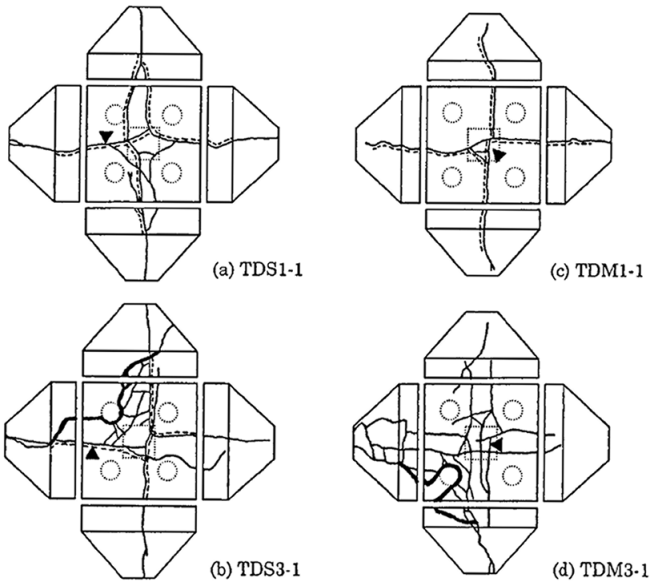

Figure 10: Characteristic crack patterns on several tested specimens by *Suzuki et al. [5]*

Two different modes were observed : Flexural failure, see top two diagrams in Figure 10, and

corner shear failure, see bottom diagrams in Figure 10. However, regarding their detailed results, it appears that most of the specimens failed by flexure instead of shear.

The year after, they published a new paper whose authors are *K. Suzuki, K. Otsuki and T. Tsuchiya [6]* in order to describe the tests they performed to identify once again the influence of the edge distance. To do so, they used three different parameters: the pile cap depth, the column width and the edge distance. Then, they varied the third one in three different configurations in order to show how the flexural strength and the ultimate load are affected. In addition and in the same way they did during their previous studies, they reported the failure modes of each specimen and some characteristic crack patterns they were able to observe after the failure.

This time they used classical pile caps whose reinforcement was composed of a uniformly distributed grid. Thereby, they arrived to the conclusion that a shortening of the edge distance leads to decrease both the yield and the maximal load as it is shown in Figure 11.

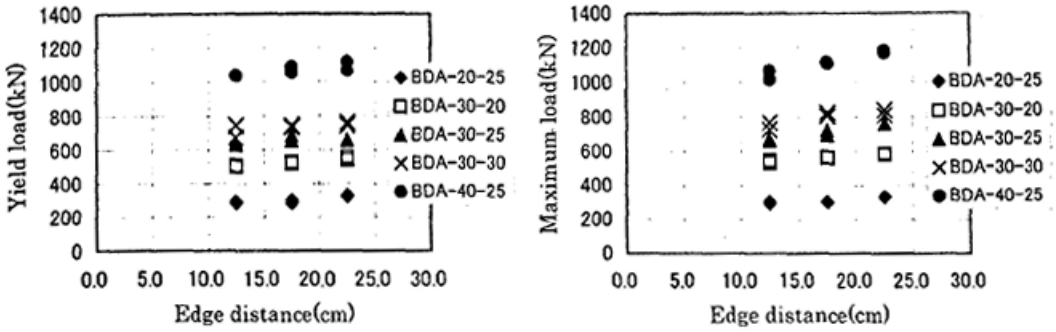

Figure 11: Relationship between yield/maximum load and edge distance by *Suzuki et al. [6]*

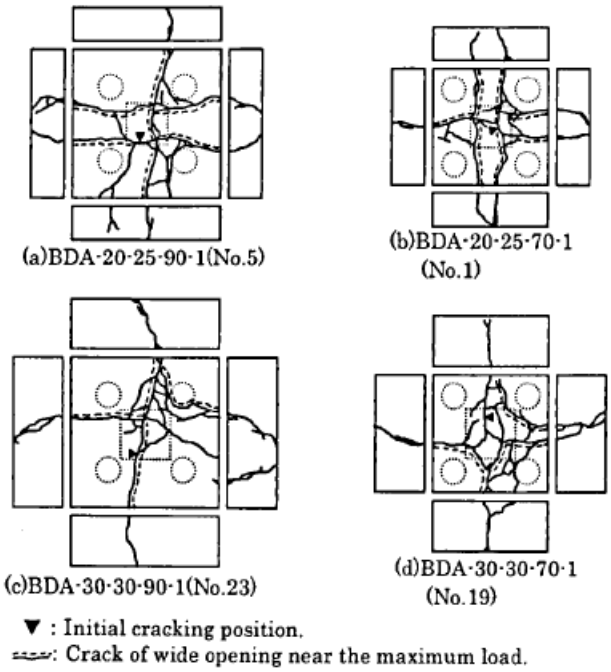

Figure 12: Crack patterns recovered by *Suzuki et al. [6]*

Figure 12 shows the different interesting crack patterns they observed at failure. Here, it is more difficult to clearly distinguish the failure modes of the specimens. Indeed, it seems that both flexure and corner shear failure occurred in the same time as shown by the combination of vertical lines on the faces of the caps and inclined lines surrounding one pile. These observations are confirmed by the failure modes observed experimentally during the tests when apparently an important number of specimens failed by flexural shear failure. However, flexural failure was still the most observed.

The last paper, written in *2001 by K. Suzuki and K. Otsuki [7]* is based on the tests they previously made. However, they tried to go a bit further and used this series to depict the influence of the concrete strength and the type of anchorage of reinforcing bars on the strength of four-pile caps. Then, they have contributed to enlarge the observations made during the previous tests by reporting once again the failure modes and trying to describe the characteristic crack pattern.

In this context, the tests clearly showed that concrete strength only have a small impact. They also illustrated that most specimens failed in corner shear before flexural failure. The strain measurement along the different bars of the reinforcement grid also allowed to show that each bar has different effectiveness, depending of its position in the cap, see Figure 13. It clearly appears that the reinforcement becomes less and less effective when it is far way from the pile.

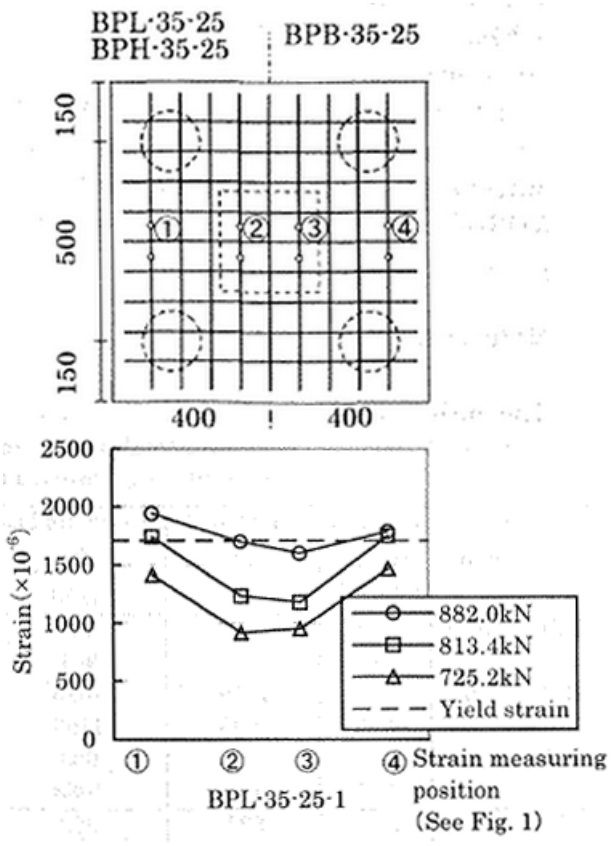

Figure 13: Strain distribution of reinforcing bars by *Suzuki et al. [7]*

All of these tests combined represent a total number of tests equal to 179, which is, compared to the number of tests which can be found for beams, relatively few.

2.1.4 Database description

The database has the function to summarize the relevant parameters describing the specimens tested. In that way, they could easily be passed through the model and help it improve until it reaches the level wanted for this thesis. Moreover, the corresponding results could be exploited to analyze the accuracy and the characteristics of the model.

First, it is necessary to sort all the tests to determine which one are useful and which one are not. Indeed, some series contain specimens whose particularities can have some unexpected impacts on the final strength. However it is first necessary to focus on the basic phenomena which are governing the failure of pile caps to ensure that the approach of the problem capture them well. At this stage, try to take into account more complex and developed components so early in the process could skew the results and bring false conclusions.

That is the case for some specimens from *Clarke's tests [3]* where the anchorage of the bottom reinforcement was sometimes extended to form half a loop as it is shown in Figure 14. In this particular case, the strength of the specimens is improved but the way such an-

chorage contributes to the strength remains unclear and difficult to evaluate. Moreover, this detail in pile caps design is uncommon which motivates the choice to neglect the specimens containing it.

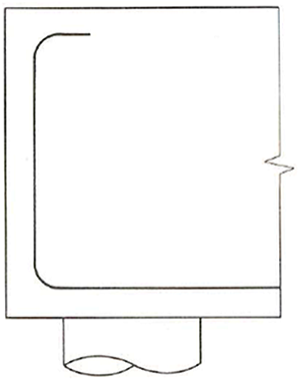

Figure 14: Half loop anchorage sometimes used in Clarke's specimens [3]

Another example concerns the symmetry of the pile caps. Indeed, symmetrical elements offer the possibility to simplify the phenomena or at least to reduce the complexity of the model by assuming identical behavior in both directions. Thus, it is not necessary to distinguish them and we can assume that the different associated values are equal. That is why only symmetrical specimens should be considered in order to respect this hypothesis. It appears that most of the tests were designed in this way. However *Suzuki, Otsuki and Tsubata [4]* realized some special specimens whose dimensions and reinforcement differed in the two directions. Once again, these were neglected in the context of this work.

Even if they are not used in this thesis, it's important to note that they can be used in future work. Indeed, further improvement of the model would look at make it more developed in order to catch better the complex phenomena such as those previously described.

Concerning the different parameters which are gathered in the database, they can be classified into 3 different categories:

Dimensions of the pile caps

These values described the geometrical properties of the pile caps whose notations are represented in Figure 15.

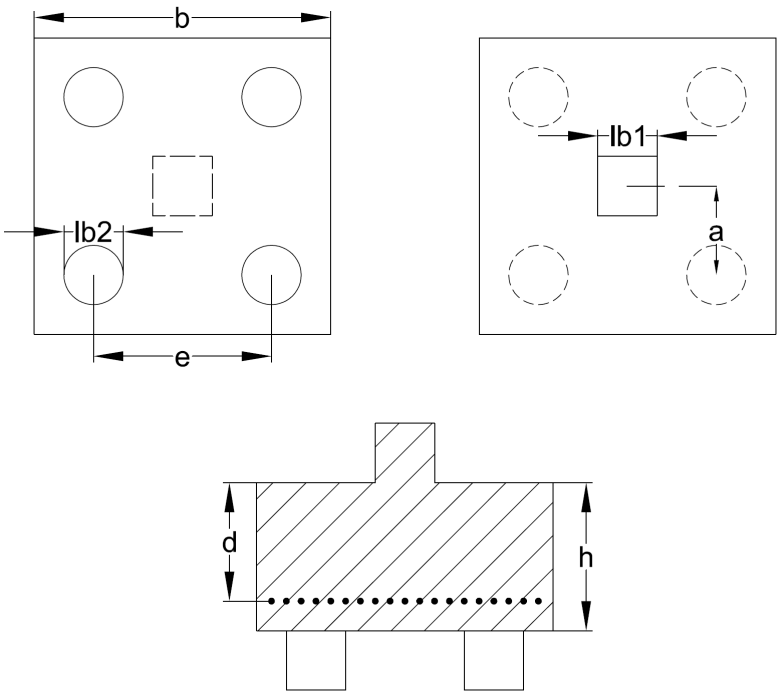

Figure 15: Representation of the notations used to describe pile cap geometry

As such, they are representing respectively:

- b: The length of the cap
- h: The total depth of the cap
- d: The effective depth of the cap
- e: The axial distance between two piles
- a: The shear span
- lb_1: The size of the top column
- lb_2: The size of the pile

Reinforcement

This part principally contains the parameters of the pile cap relative to its strength and also covers the characteristics of the reinforcement and the concrete. Thus, are represented there:

- d_g,A_g,n_g: The diameter, the area and the number of bars disposed in grid in one direction
- d_{bsq},A_{bsq},n_{bsq}: The diameter, the area and the number of bunched square bars in one direction
- d_{bd},A_{bd},n_{bd}: The diameter, the area and the number of bunched diagonal bars along one diagonal

Material properties

- a_g: The size of the coarse aggregates
- f_c: The compressive strength of the concrete
- $f_{y,g}$,$f_{y,bsq}$,$f_{y,bd}$: The yielding strength of the bottom reinforcement. Respectively in grid, bunched square and bunched diagonal
- $f_{u,g}$,$f_{u,bsq}$,$f_{u,bd}$: The ultimate strength of the bottom reinforcement. Respectively in grid, bunched square and bunched diagonal
- $\varepsilon_{u,g}$,$\varepsilon_{u,bsq}$,$\varepsilon_{u,bd}$: The ultimate strain of the bottom reinforcement. Respectively in grid, bunched square and bunched diagonal

Test results

- *Name*: Permits to identify the origin of the current specimen and to distinguish the tests made during the same series.
- *Series N°*: It is a pointer I used to separate the different series each other to make easier the graph drawings.
  - 1 = *J. Clarke [3]*
  - 2 = *J. Blévot and R. Frémy [2]*
  - 3 = *K. Suzuki, K. Otsuki (2001) [7]*
  - 4 = *K. Suzuki, K. Otsuki, T. Tsubata (1999) [5]*
  - 5 = *K. Suzuki, K.Otsuki, T. Tsubata (1998) [4]*
  - 6 = *K. Suzuki, K. Otsuki, T. Tsuchiya(2000) [6]*
- $N_{u,e}$: The ultimate load observed at failure during the test.
- *EFL*: Describe the failure mode of the specimen.
  - "c" = Corner shear failure
  - "f" = Flexural failure
  - "p" = Punching shear failure
  - "f+c" = Combination of flexural and corner shear failure
  - "f+p" = Combination of flexural and punching shear failure

Most of these parameters were given for the different tests. If they were not, it was necessary to make a reasonable assumption. In particular, this was the case for the a_g and ε_u values for which only the Japanese authors indicated both while [3] reported only the size of the coarse aggregates. For the missing ones, the following values were used:

- $a_g = 9.5mm$
- $\varepsilon_u = 10\%$

Finally, from the 174 initial specimens,145 remain. Unfortunately, most of the specimen were small ($d \leq 400mm$) which generally decreases the reliability of the test results. The smaller the element, the greater the impact of imperfections. Thus, we can fear some noisy results for the smallest values of d and an increase of accuracy for higher ones.

N°	b, m	h, m	d, m	e, m	a,m	lb1, m	lb2, m	ag	dg	Ag	ng	dbsq	Absq	nbsq	dbd	Abd	nbd	eu	fc, MPa	fyg, MPa	fug, Mpa	fybsq, MPa	fubsq, Mpa	fybd, MPa	fubd, Mpa	|Nf,e|, kN	EFL	Name	Serie N°
1	0.95	0.45	0.4	0.6	0.3	0.2	0.2	9.5	10	785.398163	10	10	0	0	10	0	0	0	26.6	410	590	410	590	410	590	1110	c	Clarke - A1	1
2	0.95	0.45	0.4	0.6	0.3	0.2	0.2	9.5	10	0	0	10	785.398163	10	10	0	0	0	34	410	590	410	590	410	590	1420	c	Clarke - A2	1
3	0.95	0.45	0.4	0.6	0.3	0.2	0.2	9.5	10	0	0	10	0	0	10	549.778714	7	0	38	410	590	410	590	410	590	1340	c	Clarke - A3	1
4	0.95	0.45	0.4	0.6	0.3	0.2	0.2	9.5	10	785.398163	10	10	0	0	10	0	0	0	26.7	410	590	410	590	410	590	1230	c	Clarke - A4	1
5	0.95	0.45	0.4	0.6	0.3	0.2	0.2	9.5	10	0	0	10	785.398163	10	10	0	0	0	33.2	410	590	410	590	410	590	1400	c	Clarke - A5	1
6	0.95	0.45	0.4	0.6	0.3	0.2	0.2	9.5	10	0	0	10	0	0	10	549.778714	7	0	32.3	410	590	410	590	410	590	1230	c	Clarke - A6	1
7	0.95	0.45	0.4	0.6	0.3	0.2	0.2	9.5	10	0	0	10	785.398163	10	10	0	0	0	34	410	590	410	590	410	590	1510	c	Clarke - A8	1
8	0.95	0.45	0.4	0.6	0.3	0.2	0.2	9.5	10	785.398163	10	10	0	0	10	0	0	0	33.2	410	590	410	590	410	590	1450	c	Clarke - A9	1
9	0.6	0.3	0.25	0.42	0.21	0.15	0.14	9.5	0	0	0	8	402.12386	8	0	0	0	0	29.1	439.7	613.3	439.7	613.3	439.7	613.3	850	c	Blevot - 1,1	2
10	0.6	0.3	0.268	0.42	0.21	0.15	0.14	9.5	0	0	0	0	0	0	10	314.159265	4	0	27.85	451.7	591.3	451.7	591.3	451.7	591.3	880.4	c	Blevot - 1,2	2
11	0.6	0.3	0.262	0.42	0.21	0.15	0.14	9.5	0	0	0	8	201.06193	4	10	157.079633	2	0	31.3	444.963158	613.3	439.7	613.3	451.7	591.3	871	c	Blevot - 1,3	2
12	0.6	0.3	0.2781	0.42	0.21	0.15	0.14	9.5	0	0	0	10	628.318531	8	0	0	0	0	32.6	283.5	409.5	283.5	409.5	283.5	409.5	747.5	c	Blevot - 2,1	2
13	0.6	0.3	0.276	0.42	0.21	0.15	0.14	9.5	0	0	0	0	0	0	12	452.389342	4	0	32.8	355	427.5	355	427.5	355	427.5	810	c	Blevot - 2,2	2
14	0.6	0.3	0.269	0.42	0.21	0.15	0.14	9.5	0	0	0	10	314.159265	4	10	157.079633	2	0	31.6	304.833333	397	290.5	397	333.5	420	740	c	Blevot - 2,3	2
15	0.6	0.2	0.18	0.42	0.21	0.15	0.14	9.5	0	0	0	8	402.12386	8	0	0	0	0	32.1	469	642.7	469	642.7	469	642.7	475	c	Blevot - 3,1	2
16	0.6	0.3	0.177	0.42	0.21	0.15	0.14	9.5	0	0	0	0	0	0	10	314.159265	4	0	37.2	447.3	588.7	447.3	588.7	447.3	588.7	540	c	Blevot - 3,2	2
17	0.6	0.3	0.173	0.42	0.21	0.15	0.14	9.5	0	0	0	8	201.06193	4	10	157.079633	2	0	30.9	440.296491	594.7	431.7	594.7	451.3	585	510	c	Blevot - 3,3	2
18	0.6	0.3	0.27	0.42	0.21	0.15	0.14	9.5	0	0	0	11.045361	766.548607	8	0	0	0	0	26.6	494.5	581.070492	492.6065574	581.0704918	494.5	581.070492	1150	c	Blevot - 1A,1	2
19	0.6	0.3	0.27	0.42	0.21	0.15	0.14	9.5	0	0	0	0	0	0	13.0384048	534.070751	4	0	36.8	503.15	567.468235	503.15	567.4682353	504.809412	567.468235	900	c	Blevot - 1A,2	2
20	0.6	0.3	0.27	0.42	0.21	0.15	0.14	9.5	0	0	0	0	0	0	13.0384048	534.070751	4	0	33.2	503.15	567.468235	503.15	567.4682353	504.809412	567.468235	1177.5	c	Blevot - 1A,2 bis	2
21	0.6	0.3	0.27	0.42	0.21	0.15	0.14	9.5	0	0	0	11.045361	383.274304	4	11.045361	191.637152	2	0	36.6	510.566667	595	523	595	485.7	547.5	1185	c	Blevot - 1A,3	2
22	0.6	0.2	0.17	0.42	0.21	0.15	0.14	9.5	0	0	0	11.045361	766.548607	8	0	0	0	0	29.15	509.35	580.240984	505.6803279	580.2409836	511.35	580.240984	815	c	Blevot - 3A,1	2
23	0.6	0.3	0.17	0.42	0.21	0.15	0.14	9.5	0	0	0	0	0	0	13.0384048	534.070751	4	0	39.2	503.15	580.885882	503.15	580.8858824	505.054118	580.885882	900	c	Blevot - 3A,2	2
24	0.6	0.2	0.172	0.42	0.21	0.15	0.14	9.5	0	0	0	11.045361	383.274304	4	11.045361	191.637152	2	0	32	500.433333	582.7	508	582.7	485.3	556.6	665	c	Blevot - 3A,3	2
25	0.6	0.3	0.172	0.42	0.21	0.15	0.14	9.5	0	0	0	11.045361	383.274304	4	11.045361	191.637152	2	0	46.1	500.433333	582.7	508	582.7	485.3	556.6	842.5	c	Blevot - 3A,3 bis	2
26	0.6	0.2	0.17	0.42	0.21	0.15	0.14	9.5	8	402.12386	8	0	0	0	0	0	0	0	33.9	459.5	607.8	459.5	607.8	459.5	607.8	408	c	Blevot - Q,1	2
27	0.6	0.3	0.27	0.42	0.21	0.15	0.14	9.5	10	628.318531	8	0	0	0	0	0	0	0	30.75	342.3	442	342.3	442	342.3	442	650	c	Blevot - Q,2	2
28	0.6	0.3	0.27	0.42	0.21	0.15	0.14	9.5	8	402.12386	8	0	0	0	0	0	0	0	21	325.3	464	325.3	464	325.3	464	510	c	Blevot - Q,2 bis	2
29	0.6	0.14	0.11	0.42	0.21	0.15	0.14	9.5	0	0	0	10	628.318531	8	0	0	0	0	13.15	498	592	498	592	498	592	250	c	Blevot - 6,1	2
30	0.6	0.14	0.11	0.42	0.21	0.15	0.14	9.5	0	0	0	14	1231.50432	8	0	0	0	0	13.15	461	534.5	461	534.5	461	534.5	290	c	Blevot - 6,2	2
31	0.6	0.2	0.18	0.42	0.21	0.15	0.14	9.5	0	0	0	10	628.318531	8	0	0	0	0	22.05	512	593	512	593	512	593	650	c	Blevot - 6,3	2
32	0.6	0.2	0.17	0.42	0.21	0.15	0.14	9.5	0	0	0	14	1231.50432	8	0	0	0	0	30.6	476	558	476	558	476	558	850	c	Blevot - 6,4	2
33	0.6	0.3	0.26	0.42	0.21	0.15	0.14	9.5	0	0	0	12	904.778684	8	0	0	0	0	18.4	517.5	617.5	517.5	617.5	517.5	617.5	842.5	c	Blevot - 6,5	2
34	0.6	0.3	0.28	0.42	0.21	0.15	0.14	9.5	0	0	0	16	1608.49544	8	0	0	0	0	18.4	468	555	468	555	468	555	810	c	Blevot - 6,6	2
35	0.6	0.5	0.47	0.42	0.21	0.15	0.14	9.5	0	0	0	12	904.778684	8	0	0	0	0	27.27	459	635	459	635	459	635	1200	c	Blevot - 9,A1	2
36	0.6	0.5	0.47	0.42	0.21	0.15	0.14	9.5	0	0	0	16	1608.49544	8	0	0	0	0	40.81	467	595	467	595	467	595	1900	c	Blevot - 9,A2	2
37	0.6	0.5	0.47	0.42	0.21	0.15	0.14	9.5	12	904.778684	8	12	904.778684	8	0	0	0	0	34.4	435.2	587.2	465.3	644.2	450.25	644.2	1700	c	Blevot - 9,A3	2
38	0.6	0.25	0.23	0.42	0.21	0.15	0.14	9.5	0	0	0	12	904.778684	8	0	0	0	0	34.6	446	605	446	605	446	605	850	c	Blevot - 10,1a	2
39	0.6	0.25	0.2211	0.42	0.21	0.15	0.14	9.5	0	0	0	12	452.389342	4	14	307.87608	2	0	43.11	456	616	456	616	480	568.2	800	c	Blevot - 10,1b	2
40	0.6	0.25	0.22	0.42	0.21	0.15	0.14	9.5	0	0	0	12	904.778684	8	0	0	0	0	33.93	453.3	615.3	453.3	615.3	453.3	615.3	750	c	Blevot - 10,2a	2
41	0.6	0.25	0.2202	0.42	0.21	0.15	0.14	9.5	0	0	0	12	452.389342	4	14	307.87608	2	0	31.43	462	615.3	462	615.3	480	562.2	800	c	Blevot - 10,2b	2
42	0.6	0.25	0.2231	0.42	0.21	0.15	0.14	9.5	0	0	0	12	904.778684	8	0	0	0	0	28.38	462	630	462	630	462	630	760	c	Blevot - 10,3a	2
43	0.6	0.25	0.2154	0.42	0.21	0.15	0.14	9.5	0	0	0	12	452.389342	4	14	307.87608	2	0	33.38	463.5	631.5	463.5	631.5	480	568.2	740	c	Blevot - 10,3b	2
44	0.6	0.3	0.27	0.42	0.21	0.15	0.14	9.5	0	0	0	12	904.778684	8	0	0	0	0	26.88	311	431	311	431	311	431	562.5	c	Blevot - 11,1a	2
45	0.6	0.3	0.27	0.42	0.21	0.15	0.14	9.5	0	0	0	12	904.778684	8	0	0	0	0	19.48	311	431	311	431	311	431	492.5	c	Blevot - 11,1b	2
46	0.6	0.3	0.29	0.42	0.21	0.15	0.14	9.5	0	0	0	10	628.318531	8	0	0	0	0	30.86	444.7	545.3	444.7	545.3	444.7	545.3	557.5	c	Blevot - 11,2a	2
47	0.6	0.3	0.27	0.42	0.21	0.15	0.14	9.5	0	0	0	10	628.318531	8	0	0	0	0	30	440.7	546	440.7	546	440.7	546	585	c	Blevot - 11,2b	2
48	0.6	0.2	0.17	0.42	0.21	0.15	0.14	9.5	0	0	0	12	904.778684	8	0	0	0	0	20.78	318.7	436	318.7	436	318.7	436	840	c	Blevot - 12,1a	2
49	0.6	0.2	0.17	0.42	0.21	0.15	0.14	9.5	0	0	0	12	904.778684	8	0	0	0	0	21.88	318.7	436	318.7	436	318.7	436	692.5	c	Blevot - 12,1b	2
50	0.6	0.2	0.17	0.42	0.21	0.15	0.14	9.5	0	0	0	10	628.318531	8	0	0	0	0	32.43	435.7	540.6	435.7	540.6	435.7	540.6	750	c	Blevot - 12,2a	2
51	0.6	0.2	0.17	0.42	0.21	0.15	0.14	9.5	0	0	0	10	628.318531	8	0	0	0	0	26.1	431.7	542.6	431.7	542.6	431.7	542.6	640	c	Blevot - 12,2b	2
52	1.85	0.75	0.67461538	1.2	0.6	0.5	0.35	9.5	16	1407.43351	7	32	6433.98175	8	0	0	0	0	37.25	279.3	401	276.2	401.5	277.75	401.5	7000	c	Blevot - 4N1	2
53	1.85	0.75	0.68164447	1.2	0.6	0.5	0.35	9.5	12	791.681349	7	25	3926.99082	8	0	0	0	0	40.8	516.7	822.7	443	764	479.55	764	6700	c	Blevot - 4N1 bis	2
54	1.85	0.75	0.66409301	1.2	0.6	0.5	0.35	9.5	0	0	0	32	4825.48632	6	25	1963.49541	4	0	37.1	278.5	407.5	278.5	407.5	300.3	431.7	6580	c	Blevot - 4N2	2
55	1.85	0.75	0.67303738	1.2	0.6	0.5	0.35	9.5	0	0	0	25	2945.24311	6	20	1256.63706	4	0	34.15	498	819	498	819	474.5	776.5	7390	c	Blevot - 4N2 bis	2
56	1.85	1	0.92	1.2	0.6	0.5	0.35	9.5	12	904.778684	8	28.714108	5180.48629	8	0	0	0	0	34.15	293.1	397.4	262.1979381	382.6810188	274.96	382.681019	6500	c	Blevot - 4N3	2
57	1.85	1	0.92	1.2	0.6	0.5	0.35	9.5	10	628.318531	8	22.6384628	3220.13247	8	0	0	0	0	49.3	429.5	683.5	469.4756098	805.0853659	453.33	805.085366	9000	c	Blevot - 4N3 bis	2
58	1.85	1	0.915	1.2	0.6	0.5	0.35	9.5	0	0	0	25	3926.99082	8	25	1963.49541	4	0	35.35	291.4	412.9	291.4	412.9	291.4	412.9	7530	c	Blevot - 4N4	2
59	1.85	1	0.9225	1.2	0.6	0.5	0.35	9.5	0	0	0	20	2513.27412	8	20	1256.63706	4	0	42.3	486.4	811.3	486.4	811.3	486.4	811.3	8750	c	Blevot - 4N4 bis	2
60	0.8	0.35	0.29	0.5	0.25	0.3	0.15	25	10	641.7	9	0	0	0	0	0	0	0.285	24.1	353	505	353	505	353	505	960	c	Suzuki - BPL 35/30 1	3
61	0.8	0.35	0.29	0.5	0.25	0.3	0.15	25	10	641.7	9	0	0	0	0	0	0	0.285	25.6	353	505	353	505	353	505	941	c	Suzuki - BPL 35/30 2	3
62	0.8	0.35	0.29	0.5	0.25	0.3	0.15	25	10	641.7	9	0	0	0	0	0	0	0.285	23.7	353	505	353	505	353	505	1029	f+c	Suzuki - BPB 35/30 1	3
63	0.8	0.35	0.29	0.5	0.25	0.3	0.15	25	10	641.7	9	0	0	0	0	0	0	0.285	23.5	353	505	353	505	353	505	1103	f+c	Suzuki - BPB 35/30 2	3
64	0.8	0.35	0.29	0.5	0.25	0.3	0.15	25	10	641.7	9	0	0	0	0	0	0	0.285	31.5	353	505	353	505	353	505	980	c	Suzuki - BPH 35/30 1	3
65	0.8	0.35	0.29	0.5	0.25	0.3	0.15	25	10	641.7	9	0	0	0	0	0	0	0.285	32.7	353	505	353	505	353	505	1088	f+c	Suzuki - BPH 35/30 2	3
66	0.8	0.35	0.29	0.5	0.25	0.25	0.15	25	10	641.7	9	0	0	0	0	0	0	0.285	27.1	353	505	353	505	353	505	902	f+c	Suzuki - BPL 35/25 1	3
67	0.8	0.35	0.29	0.5	0.25	0.25	0.15	25	10	641.7	9	0	0	0	0	0	0	0.285	25.6	353	505	353	505	353	505	872	c	Suzuki - BPL 35/25 2	3
68	0.8	0.35	0.29	0.5	0.25	0.25	0.15	25	10	641.7	9	0	0	0	0	0	0	0.285	23.2	353	505	353	505	353	505	911	f+c	Suzuki - BPB 35/25 1	3
69	0.8	0.35	0.29	0.5	0.25	0.25	0.15	25	10	641.7	9	0	0	0	0	0	0	0.285	23.7	353	505	353	505	353	505	921	f+c	Suzuki - BPB 35/25 2	3
70	0.8	0.35	0.29	0.5	0.25	0.25	0.15	25	10	641.7	9	0	0	0	0	0	0	0.285	36.6	353	505	353	505	353	505	882	c	Suzuki - BPH 35/25 1	3
71	0.8	0.35	0.29	0.5	0.25	0.25	0.15	25	10	641.7	9	0	0	0	0	0	0	0.285	37.9	353	505	353	505	353	505	951	c	Suzuki - BPH 35/25 2	3
72	0.8	0.35	0.29	0.5	0.25	0.2	0.15	25	10	641.7	9	0	0	0	0	0	0	0.285	22.5	353	505	353	505	353	505	755	c	Suzuki - BPL 35/20 1	3
73	0.8	0.35	0.29	0.5	0.25	0.2	0.15	25	10	641.7	9	0	0	0	0	0	0	0.285	21.5	353	505	353	505	353	505	735	c	Suzuki - BPL 35/20 2	3
74	0.8	0.35	0.29	0.5	0.25	0.2	0.15	25	10	641.7	9	0	0	0	0	0	0	0.285	20.4	353	505	353	505	353	505	755	f+p	Suzuki - BPB 35/20 1	3
75	0.8	0.35	0.29	0.5	0.25	0.2	0.15	25	10	641.7	9	0	0	0	0	0	0	0.285	20.2	353	505	353	505	353	505	804	f+c	Suzuki - BPB 35/20 2	3
76	0.8	0.35	0.29	0.5	0.25	0.2	0.15	25	10	641.7	9	0	0	0	0	0	0	0.285	31.4	353	505	353	505	353	505	813	c	Suzuki - BPH 35/20 1	3
77	0.8	0.35	0.29	0.5	0.25	0.2	0.15	25	10	641.7	9	0	0	0	0	0	0	0.285	30.8	353	505	353	505	353	505	794	c	Suzuki - BPH 35/20 2	3
78	0.9	0.35	0.3	0.6	0.3	0.25	0.15	25	10	285.2	4	0	0	0	0	0	0	0.284	30.9	356	501	356	501	356	501	392	f	Suzuki - TDL1 1	4
79	0.9	0.35	0.3	0.6	0.3	0.25	0.15	25	10	285.2	4	0	0	0	0	0	0	0.284	28.2	356	501	356	501	356	501	392	f	Suzuki - TDL1 2	4
80	0.9	0.35	0.3	0.6	0.3	0.25	0.15	25	10	427.8	6	0	0	0	0	0	0	0.284	28.6	356	501	356	501	356	501	519	f	Suzuki - TDL2 1	4
81	0.9	0.35	0.3	0.6	0.3	0.25	0.15	25	10	427.8	6	0	0	0	0	0	0	0.284	28.8	356	501	356	501	356	501	472	f	Suzuki - TDL2 2	4
82	0.9	0.35	0.3	0.6	0.3	0.25	0.15	25	10	570.4	8	0	0	0	0	0	0	0.284	29.6	356	501	356	501	356	501	608	f	Suzuki - TDL3 1	4
83	0.9	0.35	0.3	0.6	0.3	0.25	0.15	25	10	570.4	8	0	0	0	0	0	0	0.284	29.3	356	501	356	501	356	501	627	f	Suzuki - TDL3 2	4
84	0.9	0.35	0.3	0.45	0.225	0.25	0.15	25	10	427.8	6	0	0	0	0	0	0	0.284	25.6	356	501	356	501	356	501	921	f	Suzuki - TDS1 1	4
85	0.9	0.35	0.3	0.45	0.225	0.25	0.15	25	10	427.8	6	0	0	0	0	0	0	0.284	27	356	501	356	501	356	501	833	f	Suzuki - TDS1 2	4
86	0.9	0.35	0.3	0.45	0.225	0.25	0.15	25	10	570.4	8	0	0	0	0	0	0	0.284	27.2	356	501	356	501	356	501	1005	f	Suzuki - TDS2 1	4
87	0.9	0.35	0.3	0.45	0.225	0.25	0.15	25	10	570.4	8	0	0	0	0	0	0	0.284	27.3	356	501	356	501	356	501	1054	f	Suzuki - TDS2 2	4
88	0.9	0.35	0.3	0.45	0.225	0.25	0.15	25	10	784.3	11	0	0	0	0	0	0	0.284	28	356	501	356	501	356	501	1299	f+c	Suzuki - TDS3 1	4
89	0.9	0.35	0.3	0.45	0.225	0.25	0.15	25	10	784.3	11	0	0	0	0	0	0	0.284	28.1	356	501	356	501	356	501	1303	f+c	Suzuki - TDS3 2	4
90	0.9	0.3	0.25	0.5	0.25	0.25	0.15	25	10	285.2	4	0	0	0	0	0	0	0.267	27.5	383	522	383	522	383	522	490	f	Suzuki - TDM1 1	4
91	0.9	0.3	0.25	0.5	0.25	0.25	0.15	25	10	285.2	4	0	0	0	0	0	0	0.267	26.3	383	522	383	522	383	522	461	f	Suzuki - TDM1 2	4
92	0.9	0.3	0.25	0.5	0.25	0.25	0.15	25	10	427.8	6	0	0	0	0	0	0	0.267	29.6	383	522	383	522	383	522	657	f	Suzuki - TDM2 1	4
93	0.9	0.3	0.25	0.5	0.25	0.25	0.15	25	10	427.8	6	0	0	0	0	0	0	0.267	27.6	383	522	383	522	383	522	657	f	Suzuki - TDM2 2	4

94	0.9	0.3	0.25	0.5	0.25	0.25	0.15	25	13	1270	10	0	0	0	0	0	0	0.288	27	370	528	370	528	370	528	1245	c	Suzuki - TDM3 1	4
95	0.9	0.3	0.25	0.5	0.25	0.25	0.15	25	13	1270	10	0	0	0	0	0	0	0.288	28	370	528	370	528	370	528	1210	c	Suzuki - TDM3 2	4
96	0.9	0.2	0.15	0.54	0.27	0.3	0.15	25	10	570.4	8	0	0	0	0	0	0	0.256	21.3	413	606	413	606	413	606	519	f+c	Suzuki - BP 20 1	5
97	0.9	0.2	0.15	0.54	0.27	0.3	0.15	25	10	570.4	8	0	0	0	0	0	0	0.256	20.4	413	606	413	606	413	606	480	f+c	Suzuki - BP 20 2	5
98	0.9	0.2	0.15	0.54	0.27	0.3	0.15	25	0	0	0	10	570.4	8	0	0	0	0.256	21.9	413	606	413	606	413	606	519	f+p	Suzuki - BPC 20 1	5
99	0.9	0.2	0.15	0.54	0.27	0.3	0.15	25	0	0	0	10	570.4	8	0	0	0	0.256	19.9	413	606	413	606	413	606	529	f+p	Suzuki - BPC 20 2	5
100	0.9	0.25	0.2	0.54	0.27	0.3	0.15	25	10	713	10	0	0	0	0	0	0	0.256	22.6	413	606	413	606	413	606	735	c	Suzuki - BP 25 1	5
101	0.9	0.25	0.2	0.54	0.27	0.3	0.15	25	10	713	10	0	0	0	0	0	0	0.256	21.5	413	606	413	606	413	606	755	c	Suzuki - BP 25 2	5
102	0.9	0.25	0.2	0.54	0.27	0.3	0.15	25	0	0	0	10	713	10	0	0	0	0.256	18.9	413	606	413	606	413	606	818	f+c	Suzuki - BPC 25 1	5
103	0.9	0.25	0.2	0.54	0.27	0.3	0.15	25	0	0	0	10	713	10	0	0	0	0.256	22	413	606	413	606	413	606	813	f+p	Suzuki - BPC 25 2	5
104	0.8	0.2	0.15	0.5	0.25	0.3	0.15	25	10	427.8	6	0	0	0	0	0	0	0.272	29.1	405	592	405	592	405	592	485	f+c	Suzuki - BP 20/30 1	5
105	0.8	0.2	0.15	0.5	0.25	0.3	0.15	25	10	427.8	6	0	0	0	0	0	0	0.272	29.8	405	592	405	592	405	592	480	f+c	Suzuki - BP 20/30 2	5
106	0.8	0.2	0.15	0.5	0.25	0.3	0.15	25	0	0	0	10	427.8	6	0	0	0	0.272	29.8	405	592	405	592	405	592	500	f	Suzuki - BPC 20/30 1	5
107	0.8	0.2	0.15	0.5	0.25	0.3	0.15	25	0	0	0	10	427.8	6	0	0	0	0.272	29.8	405	592	405	592	405	592	495	f	Suzuki - BPC 20/30 2	5
108	0.8	0.3	0.25	0.5	0.25	0.3	0.15	25	10	570.4	8	0	0	0	0	0	0	0.272	27.3	405	592	405	592	405	592	916	c	Suzuki - BP 30/30 1	5
109	0.8	0.3	0.25	0.5	0.25	0.3	0.15	25	10	570.4	8	0	0	0	0	0	0	0.272	28.5	405	592	405	592	405	592	907	f+c	Suzuki - BP 30/30 2	5
110	0.8	0.3	0.25	0.5	0.25	0.3	0.15	25	0	0	0	10	570.4	8	0	0	0	0.272	28.9	405	592	405	592	405	592	1039	f+c	Suzuki - BPC 30/30 1	5
111	0.8	0.3	0.25	0.5	0.25	0.3	0.15	25	0	0	0	10	570.4	8	0	0	0	0.272	30.9	405	592	405	592	405	592	1029	f+c	Suzuki - BPC 30/30 2	5
112	0.8	0.3	0.25	0.5	0.25	0.25	0.15	25	10	570.4	8	0	0	0	0	0	0	0.272	30.9	405	592	405	592	405	592	794	f+c	Suzuki - BP 30/25 1	5
113	0.8	0.3	0.25	0.5	0.25	0.25	0.15	25	10	570.4	8	0	0	0	0	0	0	0.272	26.3	405	592	405	592	405	592	725	c	Suzuki - BP 30/25 2	5
114	0.8	0.3	0.25	0.5	0.25	0.25	0.15	25	0	0	0	10	570.4	8	0	0	0	0.272	29.1	405	592	405	592	405	592	853	f+c	Suzuki - BPC 30/25 1	5
115	0.8	0.3	0.25	0.5	0.25	0.25	0.15	25	0	0	0	10	570.4	8	0	0	0	0.272	29.2	405	592	405	592	405	592	872	f+c	Suzuki - BPC 30/25 2	5
116	0.7	0.2	0.15	0.45	0.225	0.25	0.15	25	10	285.2	4	0	0	0	0	0	0	0.3	26.1	358	496	358	496	358	496	294	f	Suzuki - BDA 20/25/70 1	6
117	0.7	0.2	0.15	0.45	0.225	0.25	0.15	25	10	285.2	4	0	0	0	0	0	0	0.3	26.1	358	496	358	496	358	496	304	f	Suzuki - BDA 20/25/70 2	6
118	0.8	0.2	0.15	0.45	0.225	0.25	0.15	25	10	285.2	4	0	0	0	0	0	0	0.3	25.4	358	496	358	496	358	496	304	f	Suzuki - BDA 20/25/80 1	6
119	0.8	0.2	0.15	0.45	0.225	0.25	0.15	25	10	285.2	4	0	0	0	0	0	0	0.3	25.4	358	496	358	496	358	496	304	f	Suzuki - BDA 20/25/80 2	6
120	0.9	0.2	0.15	0.45	0.225	0.25	0.15	25	10	285.2	4	0	0	0	0	0	0	0.3	25.8	358	496	358	496	358	496	333	f	Suzuki - BDA 20/25/90 1	6
121	0.9	0.2	0.15	0.45	0.225	0.25	0.15	25	10	285.2	4	0	0	0	0	0	0	0.3	25.8	358	496	358	496	358	496	333	f	Suzuki - BDA 20/25/90 2	6
122	0.7	0.3	0.25	0.45	0.225	0.2	0.15	25	10	427.8	6	0	0	0	0	0	0	0.3	25.2	358	496	358	496	358	496	534	f	Suzuki - BDA 30/20/70 1	6
123	0.7	0.3	0.25	0.45	0.225	0.2	0.15	25	10	427.8	6	0	0	0	0	0	0	0.3	24.6	358	496	358	496	358	496	549	f+c	Suzuki - BDA 30/20/70 2	6
124	0.8	0.3	0.25	0.45	0.225	0.2	0.15	25	10	427.8	6	0	0	0	0	0	0	0.3	25.2	358	496	358	496	358	496	568	f	Suzuki - BDA 30/20/80 1	6
125	0.8	0.3	0.25	0.45	0.225	0.2	0.15	25	10	427.8	6	0	0	0	0	0	0	0.3	26.6	358	496	358	496	358	496	564	f	Suzuki - BDA 30/20/80 2	6
126	0.9	0.3	0.25	0.45	0.225	0.2	0.15	25	10	427.8	6	0	0	0	0	0	0	0.3	26	358	496	358	496	358	496	583	f	Suzuki - BDA 30/20/90 1	6
127	0.9	0.3	0.25	0.45	0.225	0.2	0.15	25	10	427.8	6	0	0	0	0	0	0	0.3	26.1	358	496	358	496	358	496	588	f	Suzuki - BDA 30/20/90 2	6
128	0.7	0.3	0.25	0.45	0.225	0.25	0.15	25	10	427.8	6	0	0	0	0	0	0	0.267	28.8	383	522	383	522	383	522	662	f+c	Suzuki - BDA 30/25/70 1	6
129	0.7	0.3	0.25	0.45	0.225	0.25	0.15	25	10	427.8	6	0	0	0	0	0	0	0.267	26.5	383	522	383	522	383	522	676	f+c	Suzuki - BDA 30/25/70 2	6
130	0.8	0.3	0.25	0.45	0.225	0.25	0.15	25	10	427.8	6	0	0	0	0	0	0	0.267	29.4	383	522	383	522	383	522	696	f+c	Suzuki - BDA 30/25/80 1	6
131	0.8	0.3	0.25	0.45	0.225	0.25	0.15	25	10	427.8	6	0	0	0	0	0	0	0.267	27.8	383	522	383	522	383	522	725	f+c	Suzuki - BDA 30/25/80 2	6
132	0.9	0.3	0.25	0.45	0.225	0.25	0.15	25	10	427.8	6	0	0	0	0	0	0	0.267	29	383	522	383	522	383	522	764	f+c	Suzuki - BDA 30/25/90 1	6
133	0.9	0.3	0.25	0.45	0.225	0.25	0.15	25	10	427.8	6	0	0	0	0	0	0	0.267	26.8	383	522	383	522	383	522	764	f	Suzuki - BDA 30/25/90 2	6
134	0.7	0.3	0.25	0.45	0.225	0.3	0.15	25	10	427.8	6	0	0	0	0	0	0	0.3	26.8	358	496	358	496	358	496	769	f+c	Suzuki - BDA 30/30/70 1	6
135	0.7	0.3	0.25	0.45	0.225	0.3	0.15	25	10	427.8	6	0	0	0	0	0	0	0.3	25.9	358	496	358	496	358	496	730	f+c	Suzuki - BDA 30/30/70 2	6
136	0.8	0.3	0.25	0.45	0.225	0.3	0.15	25	10	427.8	6	0	0	0	0	0	0	0.3	27.4	358	496	358	496	358	496	828	f+c	Suzuki - BDA 30/30/80 1	6
137	0.8	0.3	0.25	0.45	0.225	0.3	0.15	25	10	427.8	6	0	0	0	0	0	0	0.3	27.4	358	496	358	496	358	496	809	f+c	Suzuki - BDA 30/30/80 2	6
138	0.9	0.3	0.25	0.45	0.225	0.3	0.15	25	10	427.8	6	0	0	0	0	0	0	0.3	27.2	358	496	358	496	358	496	843	f+c	Suzuki - BDA 30/30/90 1	6
139	0.9	0.3	0.25	0.45	0.225	0.3	0.15	25	10	427.8	6	0	0	0	0	0	0	0.3	24.5	358	496	358	496	358	496	813	f+c	Suzuki - BDA 30/30/90 2	6
140	0.7	0.4	0.35	0.45	0.225	0.25	0.15	25	10	570.4	8	0	0	0	0	0	0	0.3	25.9	358	496	358	496	358	496	1019	c	Suzuki - BDA 40/25/70 1	6
141	0.7	0.4	0.35	0.45	0.225	0.25	0.15	25	10	570.4	8	0	0	0	0	0	0	0.3	24.8	358	496	358	496	358	496	1068	f+c	Suzuki - BDA 40/25/70 2	6
142	0.8	0.4	0.35	0.45	0.225	0.25	0.15	25	10	570.4	8	0	0	0	0	0	0	0.3	26.5	358	496	358	496	358	496	1117	f	Suzuki - BDA 40/25/80 1	6
143	0.8	0.4	0.35	0.45	0.225	0.25	0.15	25	10	570.4	8	0	0	0	0	0	0	0.3	25.5	358	496	358	496	358	496	1117	f+c	Suzuki - BDA 40/25/80 2	6
144	0.9	0.4	0.35	0.45	0.225	0.25	0.15	25	10	570.4	8	0	0	0	0	0	0	0.3	25.7	358	496	358	496	358	496	1176	f	Suzuki - BDA 40/25/90 1	6
145	0.9	0.4	0.35	0.45	0.225	0.25	0.15	25	10	570.4	8	0	0	0	0	0	0	0.3	26	358	496	358	496	358	496	1181	f	Suzuki - BDA 40/25/90 2	6

2.2 Upper-bound plasticity models

I mainly used the following paper to help my understanding of the four-pile caps failure. Both to try to find a recurring crack pattern and to figure out the mechanisms involved.

This paper was realized by *U.G Jensen and L.C Hoang in 2012 [8]* and consists on the development of an upper bound plasticity approach to predict the strength of reinforced pile caps. The research started with the determination and the parametrization of the collapse mechanism of four-pile caps. The objective was to develop several ones and then compare their predicted failure load, the lowest one corresponding to the answer. To determine the strength of each case, the virtual displacement theorem was used. It consists to express that the internal work is equal to the external work.

$$W_I = W_E \tag{1}$$

During the process, they to compared the strength predicted by the model to the results given by previous tests performed on four-pile caps to have an idea of the accuracy of their approach. Thus, this paper offers the opportunity to get some detailed pictures on the failure shape which makes an easier understanding of the phenomena and can gives some leads on how to develop the current model. For example, here is one of the considered mechanism

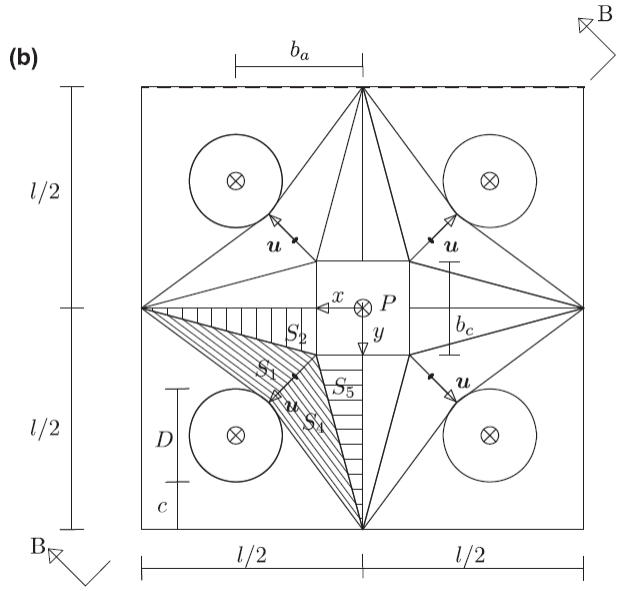

Figure 16: Illustration of the collapse mechanism developed by [8]

It's important to notice that this failure mode is similar to this detailed by *Clarke et al.* in their suggestions and represented in the Figure 4 of this work. Indeed, they also inspired from the observations made by previous researchers. In that context, they started from something existing and tried to extend it into something more successful.

In fact, the phenomena they assumed to be involved in the failure of pile caps are similar to those described in the 2PKT model. Indeed, while the 2PKT model considered that failure occurs with a combination of a vertical displacement with the rotation of the rigid block, this paper combined instead a vertical displacement with an horizontal one as it is depicted on the following picture:

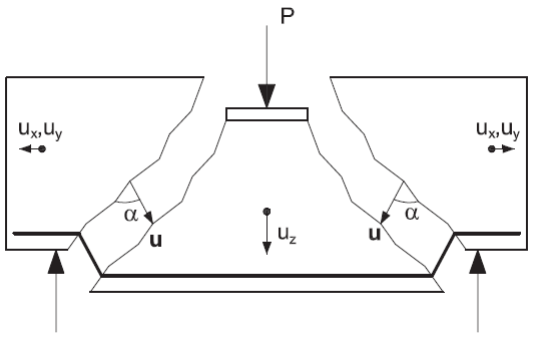

Figure 17: Combination of vertical and horizontal displacement at failure by [8]

By comparing the strength predicted by the model and the experimental values, they were able to draw the following graph:

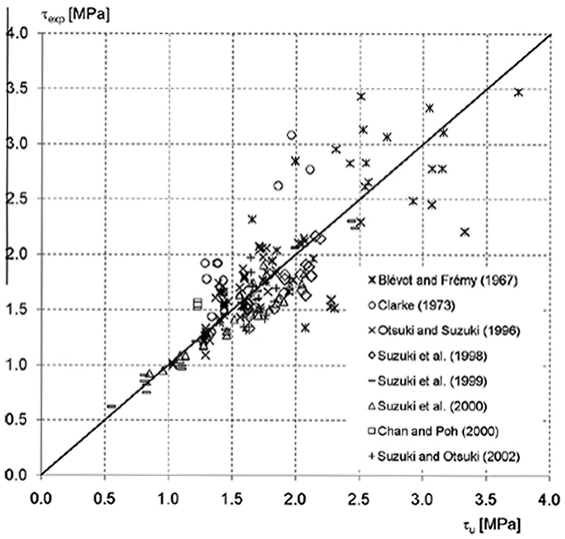

Figure 18: Results of the model developed by [8]

Where the results seem to fit pretty well with reality. Given the similarities between this model and the 2PKT one on which is based this thesis, it comforts the legitimacy of this attempt. Moreover, it can be seen that most of the tests used during their work will be also used here. Thus, the fact that these tests were already employed for previous works gives them some credibility on their results.

3 Validation of strut-and-tie model

The purpose of this section is to develop a simple strut-and-tie model based on the design rules of the Eurocode 2. The idea is to follow the same kind of design process than the one commonly used for determine the strength of the pile caps and to compare this method to the experimental results furnished by the different series of tests. In that way, it will be possible to evaluate the efficiency of this method to capture well the physics of the phenomena and its ability to determine accurately the strength of such an element.

3.1 Presentation of the strut-and-tie model

Basically, a strut-and-tie model describes an idealization of the stresses flowing into the specimen. As such, the Figure 19 represents a simple way to model the force paths in the case of pile caps.

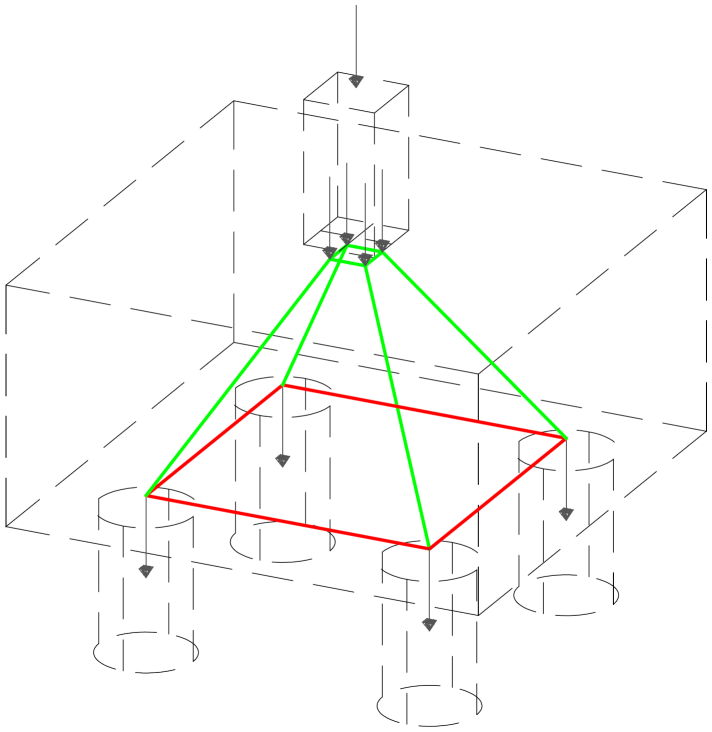

Figure 19: Illustration of a simple strut-and-tie model for four-pile caps

Thereby, pushing on the column leads to generate compression on the top of the cap which is then spread between the different pile caps through four different inclined struts which transfer vertical load the piles. Moreover, these phenomena are still governed by the equilibrium equations. Therefore, the struts have to be horizontally equilibrated at the piles by some ties, dealing with the tension generated by the tilts of the struts. Similarly, four horizontal struts equilibrate the horizontal forces on the top of the cap.

From this diagram, the strength of the pile cap can be determined by evaluating the strength of each the components which compose it. In this case, three different types can be distinguished

- The struts representing the concrete working in compression.
- The ties corresponding to the bottom reinforcement working in tension.
- The nodes which characterize the links between several elements.

Each of them are governed by their own equations which depend on the materials considered and the disposition of the considered element. In full generality all of these have to be calculated and transformed into the corresponding applied load. Thus, the lowest one indicates to the final strength of the pile cap. However, the simplicity of the phenomena involved in this case reduces this number to three. Indeed, it is reasonable to assume that the pile caps do not fail in flexure by excess of compression in the concrete which means that the horizontal struts are not critical. Moreover, the struts themselves are stronger than the connected nodes which means that their strength is not relevant.

Thereby, the remaining possible failure modes can correspond to:

- Crushing of the inclined struts at the nodes
- Excess of tension in the bottom reinforcement

Physically, the first mode corresponds to a shear failure while the second one describes a flexural failure. According to the strut-and-tie model represented by the Figure 19, shear failure can occurs both on the top and the bottom nodes while flexural one can only happens on the bottom ties. Moreover, taking into account the symmetry of the pile cap, it is possible to reduce this study to one quarter of the entire specimen and only focus on the two corresponding nodes which are represented in the Figure 20

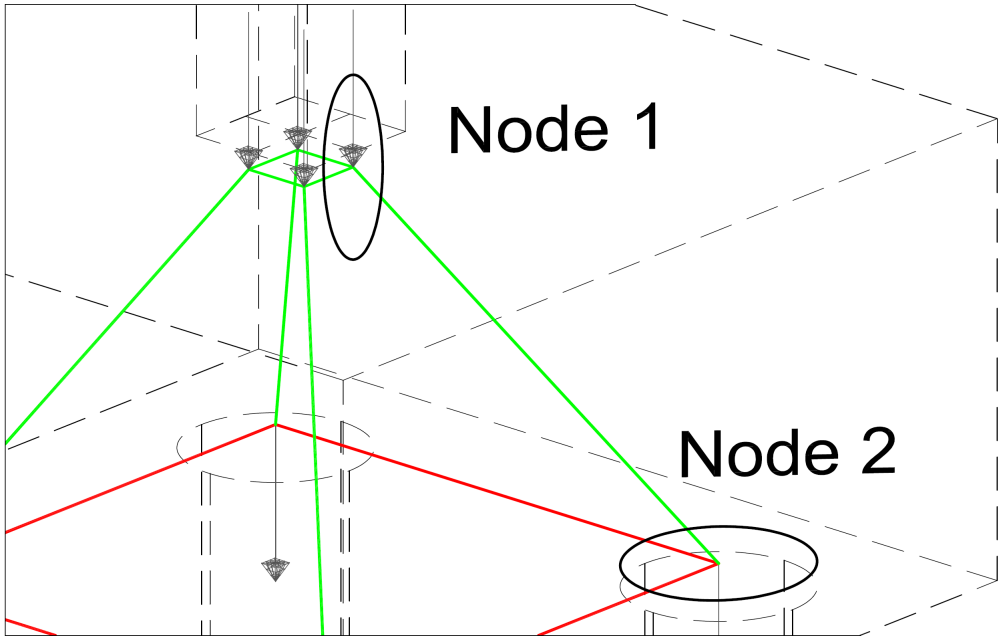

Figure 20: Identification of the nodes to verify

3.2 Evaluation of the $\sigma_{R,max}$

Before expressing the equations of each components, it is necessary to remember that this study it is not a matter of designing conservatively these element but rather to evaluate its accuracy against reality. As such, the different terms will correspond to the basic properties they described without taking into account the safety factors usually considered. The consequences of this concern especially the calculation strength of the materials which will now correspond to

$$f_{c,k} = f_{c,d} \tag{2}$$
$$f_{y,k} = f_{y,d} \tag{3}$$

That being said, each configuration has to be detailed in order to identify the corresponding expression of the maximum stress. Thereby, the node 1 located on the top of the pile cap is only submitted to compression. In such a case, the stress can reach the following value:

$$\sigma_{nt,max} = 0.85\nu' f_{c,d} \tag{4}$$
$$\nu' = 1 - \frac{f_{c,k}}{250} \tag{5}$$

In the bottom node, two verifications have to be led. The first one aims to determine the strength on the inclined strut and the second one concerns the strength of the horizontal ties.

Concerning the node itself, it is submitted to both compression and traction. Moreover, two different ties meet there. For these reasons, the maximum compression stress cannot exceed the following expression:

$$\sigma_{nb,max} = 0.75\nu' f_{c,d} \tag{6}$$

However, the expression corresponding to the strength of the tie is easier to determine considering it simply expresses that failure occurs if the bottom reinforcement reaches its yielding strength. Thereby,

$$\sigma_{t,max} = f_y \tag{7}$$

3.2.1 Confinement of the top node

It has to be mentioned that these stresses and more precisely the maximum stress on the top node $\sigma_{nt,max}$ will give really conservative results. Indeed, considering the top node is submitted to compression in all direction knowing that the external load acts vertically and the horizontal struts bring compression in the horizontal plan. As such, this triaxial confinement tends to increase the maximum stress reachable in the node. In particular, Eurocode 2 specifies that triaxially compressed nodes may be checked according:

$$\begin{array}{ll} \sigma_{n,max} = f_{c,k}(1 + 5\sigma_2/f_{c,k}) & \text{for } \sigma_2 \leq 0.05 f_{c,k} \\ \sigma_{n,max} = f_{c,k}(1.125 + 2.5\sigma_2/f_{c,k}) & \text{for } \sigma_2 > 0.05 f_{c,k} \end{array} \tag{8}$$

Where σ_2 represents the lowest main stress in the plan perpendicular to the strut. Moreover, Eurocode 2 imposes a maximal value by limiting the maximum stress to

$$\sigma_{n,max} \leq 3\nu' f_{c,d} \tag{9}$$

In particular, that means that it would be necessary to use the Mohr circle of this plan to express the two corresponding main stresses and choose the lowest one. However, it seems unrealistic to consider such an approach in a classic design. Therefore, some assumptions can be expressed to evaluate the impact of the confinement.

First of all, it is commonly recognized that the biaxial confinement can reach at maximum the value of $1.25 f_{c,d}$. Extending this concept to the current case, it seems realistic to consider that reaching this value for a triaxial confinement constitute a conservative approach. Then, by coupling this assumption to the maximum value recommended by Eurocode 2, it appears that the confinement is contained between two bounds:

$$\sigma_{c,min} = 1.25\nu' f_{c,d} \tag{10}$$

$$\sigma_{c,max} = 3\nu' f_{c,d} \tag{11}$$

In particular, these two expressions will serve to depict the extreme results of the strut-and-tie model

3.3 Maximum force in each component

Now when the stresses are determined, the associated area permit to evaluate the corresponding forces passing through each component. Once again, the tie is the easiest element to measure. Indeed, it corresponds to the total steel area A_s reaching one pile in one direction. Thereby, the resulting force can be directly obtained by:

$$F_{tie} = A_s.f_y \tag{12}$$

The evaluation of the surface of the strut at each node requires a little more developments. By definition, it corresponds to the surface perpendicular to the strut whose dimensions are delimited by the shape of the node. This shape represents here the tricky part of this kind of dimensioning. Indeed, in the case of pile caps, the corresponding strut-and-tie model has to be developed in 3D regarding the physics of such elements. By definition, each node represents a location where several non-coplanar ties or struts meets. As such, the resulting geometry of the node is composed by the intersections of different plans which finally leads to delimit the researched node. As an example, the Figure 21 describes the bottom node resulting of the intersection of the two perpendicular bottom ties and the inclined strut:

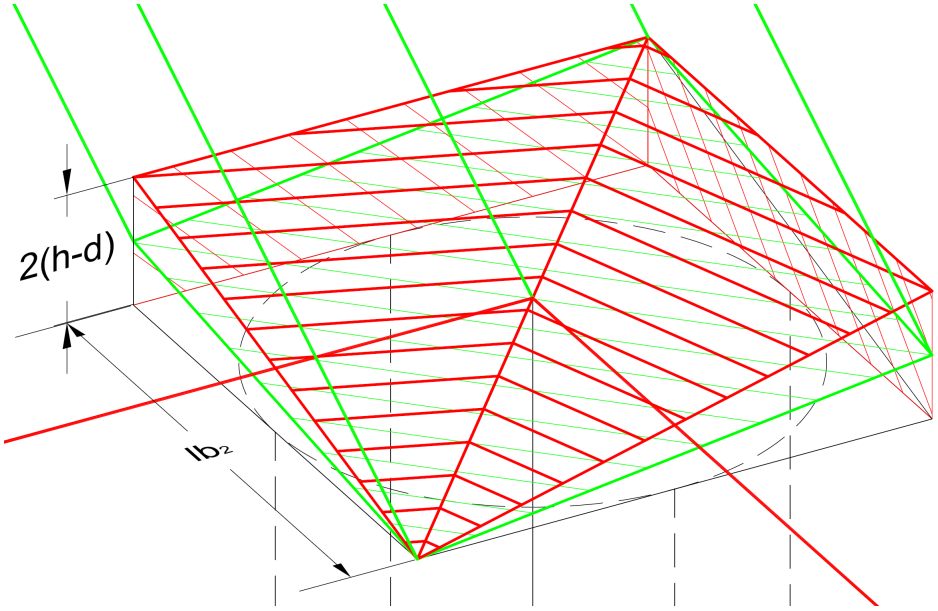

Figure 21: Geometry of the bottom node

In particular, the dimensions of the node can be determined by the classical simplified approach used in strut-and-tie models. First, it is the place where the vertical loading is transmitted to the pile which means that the length of the node is limited by the size of the pile lb_2. Moreover, the height of the effect zone of a tie is commonly supposed equal to twice the distance between the reinforcement and the bottom face of the element. Knowing that the distance between the top of the cap and the bottom reinforcement correspond to the effective depth d, the researched height correspond well to the notation used, namely:

$$h_{tie} = 2(h - d) \tag{13}$$
$$= h_{\text{bot node}} \tag{14}$$

Thus, the node corresponds to the combination of the two pyramid characterizing the two ties (in red in the Figure 21). Then, it is necessary to project the two red surfaces onto the green one. Therefore, the resulting rhombus is still inscribed in the node and its center of gravity corresponds to the center of gravity of the strut. As such, it represents the plane section of the strut projected on the node. Moreover, the formula of the rhombus surface can be calculated with its two diagonals which can be determined directly from the size of the node given previously. Thus,

$$d_b = \sqrt{2} l b_2 \tag{15}$$
$$D_b = \sqrt{d_b^2 + (2(h - d))^2} \tag{16}$$
$$A_b = \frac{d_b + D_b}{2} \tag{17}$$

On the top node, the same reasoning can be executed to determine the corresponding area. However, the dimensions of the node have to be adapted to take into account the geometry of the horizontal struts. In that case, the length of the node correspond to half of the column size $lb_1/2$ considering that the total load is spread into four identical parts. Then, it is necessary to evaluate the height of the compression zone. This value can be approximated the same way it is done by the simplified method to determine the flexural strength of beams. in particular, this method assumes that the lever arm between the tension in the bottom reinforcement and the compression in the concrete is equal to $h = 0.9d$. Under this condition, the height of the compression zone can be expressed by:

$$h_{strut} = 2(0.1d) \tag{18}$$
$$= h_{\text{top node}} \tag{19}$$

Now the dimensions of the top node are known, the same developments can be followed to evaluate the area of the new rhombus. Thereby,

$$d_t = \frac{\sqrt{2} l b_1}{2} \tag{20}$$
$$D_t = \sqrt{d_t^2 + (0.2d)^2} \tag{21}$$
$$A_t = \frac{d_t + D_t}{2} \tag{22}$$

At this point, the surfaces calculated correspond to projection of the strut on each node. However, to determine the maximum forces reachable in the strut at the nodes, it is necessary

to know the section of the strut which represents the surface perpendicular to its direction. Therefore, the angles between the researched sections and the actual rhombuses have to be evaluated. To do so, the geometrical properties of the pile cap can be used once again. Following that idea, the Figure 22 illustrates a cut performed at 45° and thus passes all along the considered strut.

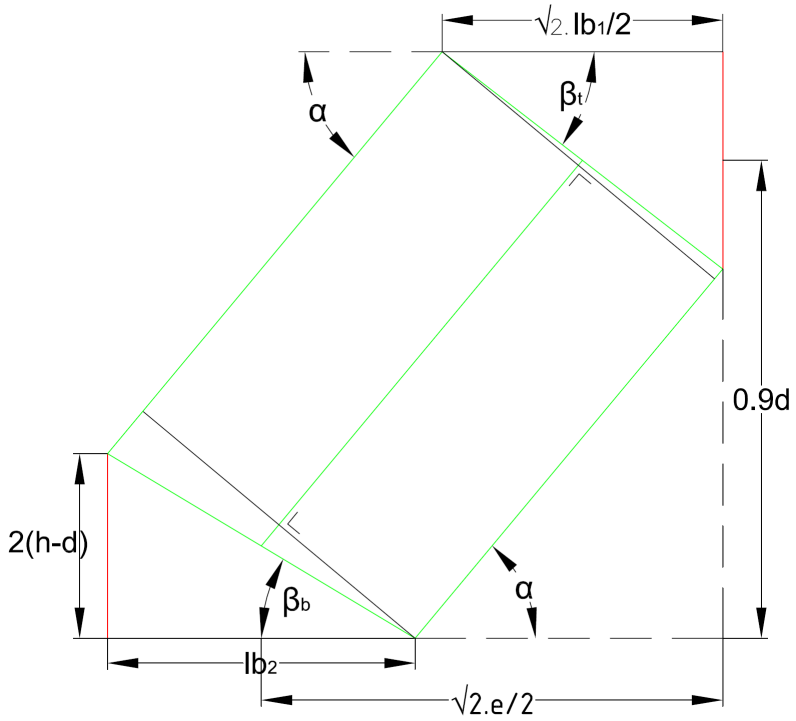

Figure 22: Vertical cut on nodes

Where the tilts of the bottom and top rhombuses correspond respectively to β_b and β_t and the slope of the tie is given by the value of α. In particular, these values are given by the following expressions:

$$\beta_b = atan(\frac{2(h-d)}{\sqrt{2}lb_2}) \tag{23}$$

$$\beta_t = atan(\frac{0.2d}{\sqrt{2}lb_1/2}) \tag{24}$$

$$\alpha = atan(\frac{0.9d}{\sqrt{2}e/2 - \sqrt{2}lb_1/4}) \tag{25}$$

Then, the angles between the rhombuses and the perpendicular sections are directly deduced from these values. Indeed,

$$\gamma_b = 90 - \alpha - \beta_b \tag{26}$$

$$\gamma_t = 90 - \alpha - \beta_t \tag{27}$$

In that way, the sections of the strut can be obtained by projecting the surface of the rhombuses according to these angles. Finally, the expressions of the different forces reachable in the top and bottom node as well as in the bottom tie can be respectively expressed by:

$$F_{strut,b} = \cos\gamma_b A_b.\sigma_{nb,max} \tag{28}$$
$$F_{strut,t} = \cos\gamma_t A_t.\sigma_{nt,max} \tag{29}$$
$$F_{tie} = A_s.f_y \tag{30}$$

3.4 Determination of the ultimate load

At this point, the maximum forces passing through each component are know. It is now possible to deduce the load which generates them. To do so, it is simply necessary to use the geometry of the pile caps and to express the equilibrium equations. Thereby, the loads corresponding to the force in the nodes are directly obtained by projecting them vertically according to the slope of the strut they characterized. Thus, reusing the value of α from the Equation 25,

$$V_{strut,b} = F_{strut,b}\sin(\alpha) \tag{31}$$
$$V_{strut,t} = F_{strut,t}\sin(\alpha) \tag{32}$$

To determine the corresponding value for the tie, it is necessary to use the moment equilibrium expressed parallel to the bottom tie, in the top node. Thereby, the Figure 23 illustrates the configuration of this equilibrium:

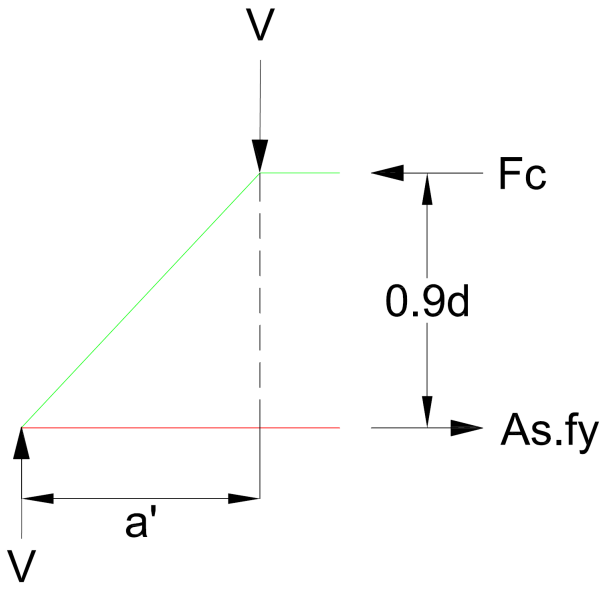

Figure 23: Static diagram of a quarter of the strut-and-tie model

Where a' represents the projection of the horizontal distance between the bottom and the top node. In particular, this distance was already represented in the Figure 22 where it corresponded to $\sqrt{2}e/2 - \sqrt{2}lb_1/4$. Thereby, a' can be expressed as follows:

$$a' = \cos 45(\sqrt{2}e/2 - \sqrt{2}lb_1/4) \tag{33}$$

Therefore, the corresponding moment equilibrium express that:

$$V_{tie}a' = F_{tie}0.9d \Rightarrow V_{tie} = \frac{F_{tie}0.9d}{a'} \tag{34}$$

Which express that the vertical reaction under the pile multiplied by its lever arm has to be compensated by the moment generated by the force in the bottom tie.

Now when the different maximal load are known, the strut-and-tie model simply considers that the failure mode is due to the minimum value of these three and thus that

$$V_{R,d} = min(V_{ties}, V_{strut,b}, V_{strut,t}) \tag{35}$$

3.5 Results

By performing this method for all the specimens of the database, it will be possible to compare for each of them the ratio

$$R = \frac{V_{exp}}{V_{\text{pred}}} \tag{36}$$

Which gives an information of the accuracy of the model while the closer to one, the better. As such, the following data gives the results for both bounds of the confinement. As such, their efficiency will be illustrated and some characteristic statistic values will complete them by giving some more informations to refine the observations. However, the results will not be discussed in the section but will be further in this thesis. Thereby, they are just shown to give a quick idea on the what the strut-and-tie model can predict.

Moreover, the detailed results calculated by the strut-and-tie model are joined in the Appendix in the end of this work.

3.5.1 Lower bound of the confinement

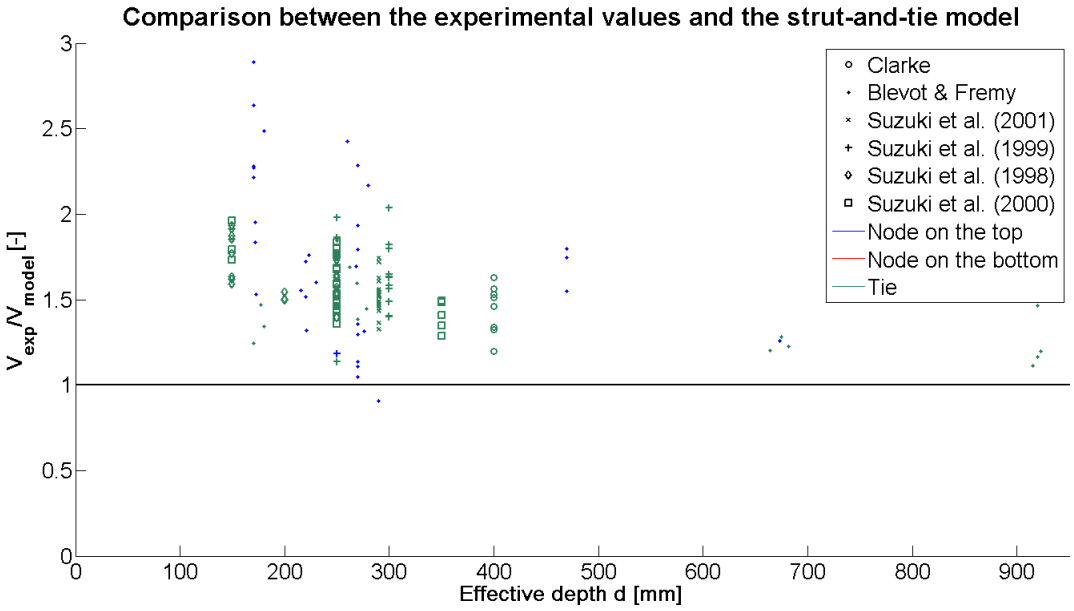

Figure 24: Results of the strut-and-tie model with the minimum confinement

R_{min}	R_{max}	$\bar{R}$	$\sigma/\bar{R}[\%]$
0.908	3.87	1.655	25.8%

Table 1: Characteristic numbers of the strut-and-tie model with the minimum confinement

3.5.2 Upper bound of the confinement

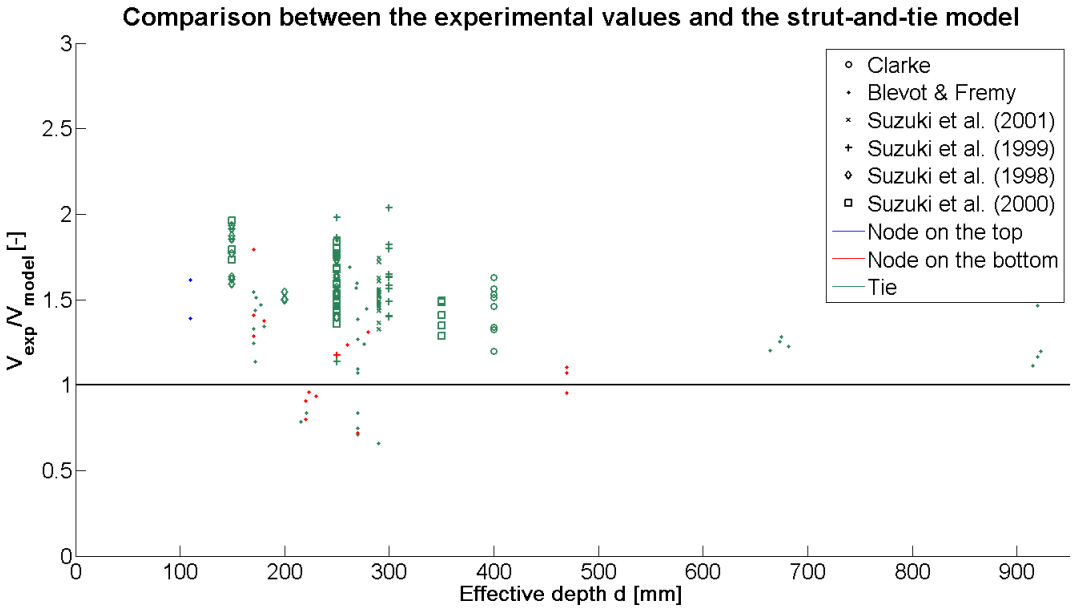

Figure 25: Results of the strut-and-tie model with the maximum confinement

R_{min}	R_{max}	$\bar{R}$	$\sigma/\bar{R}$
0.659	2.03	1.461	19.7%

Table 2: Characteristic numbers of the strut-and-tie model with the maximum confinement

4 2PKT for deep beams

The purpose of this thesis is to extend the two-parameter kinematic theory (2PKT) for deep beams proposed by *Mihaylov et al. [1]* to the four-pile caps. Therefore, most of the following developments will be based on the phenomena which compose the initial model. This section only aims to summarize the 2PKT and introduce the principal results.

First, the 2PKT approach describes more accurately the failure mode of deep beams and thus obtain better results than classic design models. In particular, it is based on a kinematic approach which is able to determine the strain distribution across the beam. Secondly, a comparative study was undertook in order to evaluate the efficiency of the different models commonly used and the 2PKT. Besides, these results were extended in order to show the field of use of each model.

4.1 Description of the model

The 2PKT approach assumes that shear failure occurs along a diagonal crack which extends from the inner edge of the support to the plate where the force is applied. Then it assumes that the crack opening is govern by two separate phenomena : In one hand, the concrete block above the critical crack rotates and in another hand, the concrete below vertically translates.

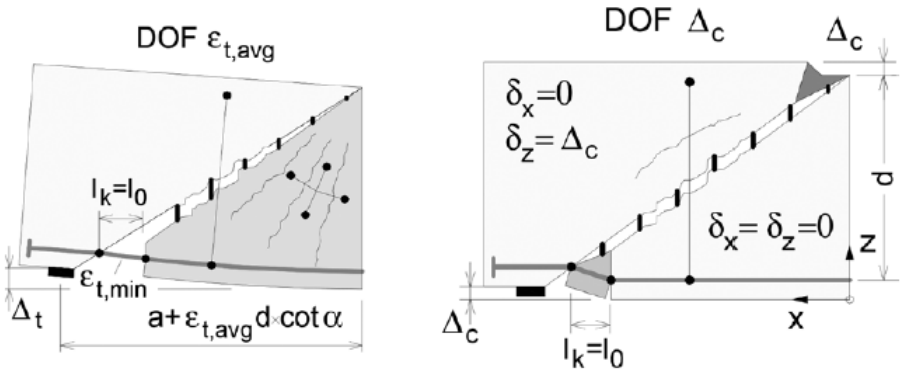

Figure 26: Illustration of the two degrees of freedom [1]

The first displacement can be correlated to the strain in the bottom reinforcement ε_t and the second one is generated by the crushing of the concrete zone right under the loading plate. This zone, called Critical Loading Zone (or CLZ), is responsible of the vertical translation Δ_c.

These two both have a direct impact on the critical crack behavior. Indeed, while the vertical displacement Δ_c in the critical loading zone generates widening and slip of the crack, the elongation of the bars ε_t causes only widening. Thereby, the crack width can be expressed

by:

$$w = \Delta_c \cos\alpha_1 + \frac{\varepsilon_t l_k}{2\sin\alpha_1} \tag{37}$$

Where α_1 corresponds to the angle of the critical crack and l_k represents the length of the bottom reinforcement which contributes to width the crack, see Figure 26.

Extending this concept, it was shown by *Mihaylov et al. [1]* that the vertical reaction applied on the support at failure is a sum of four different components:

- The strength of the CLZ, V_{CLZ}
- The interlocking of the two lips of the critical crack, V_{ci}
- The dowel effect generated by the bottom reinforcement, V_d
- The stress in the stirrups crossing the critical diagonal crack, V_s

In other words, this reaction can be expressed as:

$$V = V_{CLZ} + V_{ci} + V_s + V_d \tag{38}$$

4.2 Critical Loading Zone

The critical loading zone includes the area right under the loading plate which is subjected to high stresses. At failure, the compression reaches the concrete strength and this zone start to crush. Moreover, the strains start to reach higher values and the corresponding deformation becomes important. Thus, a vertical displacement Δ_c can be observed between the two edges as suggested in Figure 27.

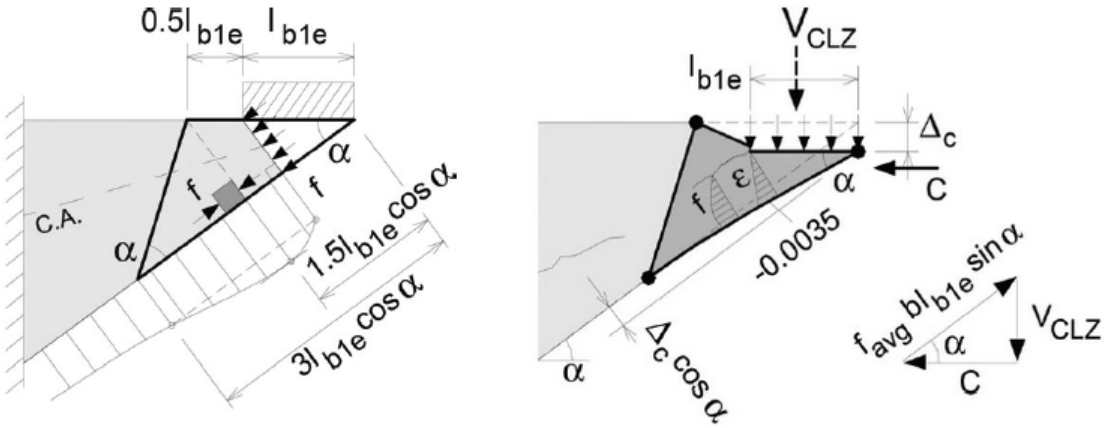

Figure 27: Description of the Critical Loading Zone by [1]

To evaluate the strength of this zone, it can be modeled as a variable-depth cantilever. Thus, the different developments of the 2PKT model and the assumption made permitted to express the shear strength of the critical loading zone as:

$$V_{CLZ} = k1.43 f_c^{0.8} b l_{b1e} \sin^2 \alpha \tag{39}$$

Where k represents the crack shape and l_{b1e} the length of the critical loading zone.

The force in the CLZ is parallel to the diagonal crack, and V_{CLZ} is the vertical of this zone.

Moreover, the value of Δ_c is only governed by the crushing of the critical loading zone. Thereby, it can simply be expressed as the deflection of a cantilever on which is applied a uniformly distributed force at its edge

$$\Delta_c = 0.0105 l_{b1e} \cot \alpha \tag{40}$$

Where l_{b1e} corresponds to the effective width of the loading plate parallel to the longitudinal dimension of the beam. In particular, this value depends on the position of the loading plate. For example, when it lays in the middle of the member, the force is equally redistributed between the two supports and then:

$$l_{b1e} = 0.5 l_{b1} \tag{41}$$

where l_{b1} is the width of the loading plate.

4.3 Interlock strength

The interlock strength takes into account the friction between the two sides of the crack and especially between the aggregates of each side and can be expressed by the following equation:

$$V_{ci} = \frac{0.18\sqrt{f_c}}{0.31 + \frac{24w}{a_{ge}+16}} bd \tag{42}$$

Here, w represents the crack width and illustrates that the wider the crack, the less the sides of the crack are able to develop friction. It is the opposite for the aggregates size which has a positive effect on the interlock strength because biggest aggregates offer a higher resistance to the translation.

Concerning the surface concerned, the friction develops from the top to the bottom reinforcement all along the width of the section b. However, it is once again the vertical component which is interesting to determine the vertical reaction and in this particular case, the projected length of the crack is equal to the effective height d.

4.4 Dowel action

When the failure occurs and the critical crack appears, the beam is separated onto two parts. However, they are still connected by the critical loading zone, the stirrups and the bottom reinforcement. As such, the vertical translation of the concrete under the crack subjects this reinforcement to a double curvature as it is represented on the second picture of Figure 26. Thus the bars will start to resist to this deformation in the same way the dowels resist to the shear in composite floors.

Thereby, the expression of the dowel action developed in that way is given by the following equation:

$$V_d = n_b f_{ye} \frac{d_b^3}{3l_k} \tag{43}$$

Of course, the total strength is a function of the characteristics of the bars knowing that the more they are, the higher the strength as it is depicted by the number of bars n_b, the stress in the bars f_{ye} and the bars diameter d_b. It is also necessary to take into account l_k which also represents the length of the reinforcement between the two kinks formed by the dowel action. Thus, the larger it is, the lower the stiffness of the portion of the bars involved in the dowel effect. Consequently, the corresponding strength will be diminished.

It is also important to note that the stress in the bars does not represent the yielding strength of the bars. Indeed, it is described by the following expression:

$$f_{ye} = f_y \left[1 - \left(\frac{T_{min}}{f_y A_s} \right)^2 \right] \leq 500MPa \tag{44}$$

$$\geq 0 \tag{45}$$

This equation describes the fact that the total stress in the bars cannot exceed the yield strength of the steel. Thereby, the remaining strain available to develop the dowel effect depends on the difference between the yield strength and the tension in the bars. When These two becomes equal, the reinforcement starts yielding and it is not any more able to resist the vertical displacement. In this case, the strength of the dowel effect falls to 0 and of course cannot reach negative values.

4.5 Stirrups

The critical crack develops through the stirrups which resists to its widening. The strength of each stirrups is known by definition but it remains to determine the number of concerned stirrups. Thus, the maximum strength supported by the stirrups can be expressed as follows:

$$V_s = \rho_v b(d \cot \alpha 1 - l_0 - 1.5 l_{b1e}) f_v \geq 0 \tag{46}$$

Where $(d \cot \alpha 1 - l_0 - 1.5 l_{b1e})$ represents the horizontal projection of the crack which is multiplied by the width of the beam b in order to determine the horizontal surface to consider. Then, the stirrups ratio ρ_v allows to convert this concrete area into a steel one which can be directly used to calculate V_s.

4.6 Model implementation

As it was shown in the previous development, the values of the shear components depend especially on the two degrees of freedom Δ_c and ε_t. However they are not themselves sufficient to determine the maximum strength of the pile cap. Indeed, this equation only describes the evolution of the strength of the specimen without any consideration of the state of stresses generated by the external forces. To do so, it is necessary to add the equilibrium equation in order to determine the way the load equilibrated:

$$V_{CLZ} + V_{ci} + V_s + V_d = \frac{\varepsilon_t E_s A_s (0.9d)}{a} \tag{47}$$

In that way, the model enters into an iterative process in which the value of the strain ε_t is varied until the two sides of this equation reach the same value. At that particular point, the external forces reach the shear strength of the specimen and failure occurs.

4.7 Model results

Some tests on realistic deep beams were performed in parallel of the development of the model. In that way, the results produced by the model have been compared to the experimental values. Figure 28 illustrates one of these comparisons.

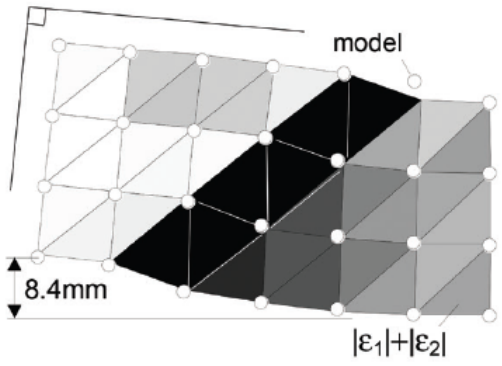

Figure 28: Comparison experimental (mesh)/predicted (circles) displacement [1]

It can be seen that the predicted displacements fit pretty well with the observed one. In fact, only one point is misplaced. Indeed, its position regarding the critical crack was miscalculated. In particular, it was supposed to be above the crack, in the rigid block while it normally stands right under the crack where the deformations are way higher.

Moreover, it is also necessary to evaluate the efficiency of the 2PKT model through the accuracy of its strength prediction. To do so, the ratio between the experimental ultimate load V_{exp} and the strength predicted by the model V_{model} is define.

$$r = \frac{V_{exp}}{V_{model}} \tag{48}$$

And is expressed according to the effective depth d or the span-to-depth ratio a/d.

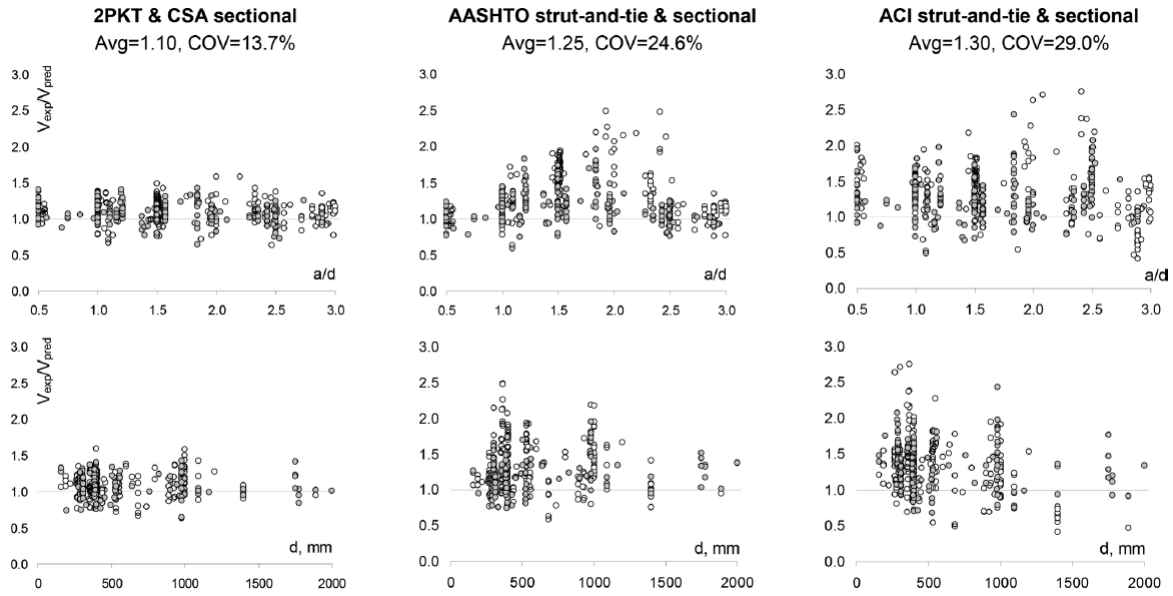

Figure 29: Comparative study of 2PKT/current models [1]

Once again, the results given by the 2PKT model reach really accurate values. Moreover, when they are compared to the other models, they seem to be more stable which strengthen the idea that the phenomena involved during the failure of deep beams are represented better than before.

5 Crack patterns in pile caps

Now when the basics of the 2PKT model are presented, the adaptation of the model can start. It is first necessary to choose the crack pattern on which it will be based. To do so, the different papers and especially the series of tests will be analyzed in order to determine the failure modes which were observed recurrently during the tests.

The different proposed model will be presented depending on their complexity. The first one will be the simplest and the degree of complexity will grow progressively.

5.1 One way shear

In that particular case, the failure mode is similar to those for the deep beams. Indeed, the crack develops continuously throughout the cap and separate the element into two parts, see Fig.30.

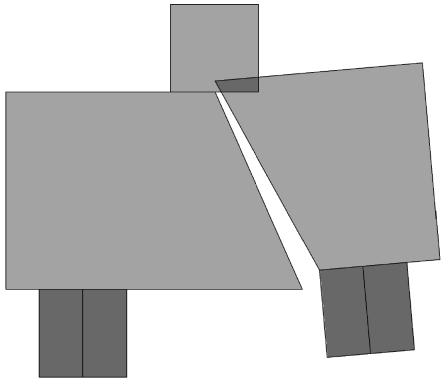

Figure 30: One way shear failure pattern

This is one of the failures observed during the *Japanese [4–7]* tests. However, this information has to be considered carefully. Indeed, the authors forced the reactions under the piles to be equal by joining the piles in pairs with a repartition beam. Thereby, once the first pile reached its strength, the simulation was not able to increase the loading because of the equality of support reactions of the beam. On the contrary, real specimens can continue to increase the load by redistributing the forces on the three remaining piles. Consequently, the crack pattern cannot develops entirely and it is possible that the failure mode observed could be incomplete compared to the real one.

That is why the failures occurred only involving one or two corners at a same time and instead of the whole cap which can explain why the Japanese tests were the only ones to report this kind of failure. Thus, even if this simple approach offers the possibility to bring a first approach on the pile caps behavior, it seems that this failure mode is too uncommon to represent accurately the phenomena the extended 2PKT model is supposed to capture. For that reason, the one way shear will be used in a first approach to test roughly the ability of

such a model. Then, the failure mode will be improved in order to fit better with the purpose of this thesis.

5.2 Punching shear

The second proposed failure mode was developed based on experimental observations reported by both the *French [2]* and *English [3]* tests. It consists on the formation of a pyramid extending from the column to the piles.

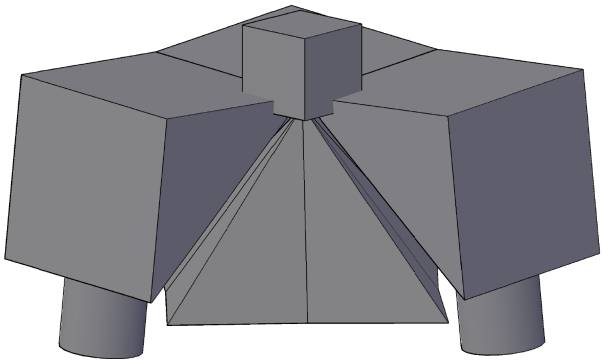

Figure 31: Punching shear failure pattern

Here, the base of the pyramid is a square which joins the center of each side of the cap and is tangent to the piles. The global shape of this model is similar to what can be observed at the failure of the reinforced flat slabs. In that case, a cone develops above the supporting column and extends in a circle to the top of the slab. Indeed, because of the uniformly distributed reinforcement used in such elements, the load has no preferential flow path which allow the formation of a circular base instead of an angular one. Of course, this is not the case for pile caps where the struts are concentrated in the paths joining the column to the piles which justify the square shape of the pyramid.

Once again, this failure mode is far from perfect. Regarding the different crack patterns reported by the series of tests, even if the global result seems to be messy, some reoccurring cracks can be noticed. For example, by looking at Figure 54, it appears that the four specimens have several cracks in common. One of them develops on the side of the cap, from the inner edge of the pile to the middle of the column. However, this is not represented by the current model where the main crack on each side is vertical and is located in the middle of the face. From this point of view, the previous mode was better than this one.

Moreover, the orientation of the pyramid does not fit with the observations made during previous studies concerning the failure modes in pile caps. Indeed, Figure 4 made by *Clarke et al. [3]* shows that the corners of the base are directed towards the piles instead of the sides of the cap.

In conclusion, this model offers the opportunity to describe another failure mode currently observed during the tests. However the crack pattern corresponding to this failure mode is completely different from the previous one while the physical phenomena leading to failure are exactly the same. In particular, experimentations showed that the crack pattern develops in the same way for each different type of failure mode. The only difference comes from the way how this crack pattern reaches failure. In other word, based a model on some crack patterns which do not correspond to the observations made during the tests is inconsistent with physics. Thereby, even if can represent another failure mode, this model has to be improved to correspond better to reality. For that reason, it will be used in a first approach but will not be used further.

5.3 Corner shear

From the previous analysis, it was shown that the crack pattern related to the one way shear fitted relatively well with reality but some improvement was necessary to describe properly the failure mode. The drawing in Fig.32 was realized to reach that purpose.

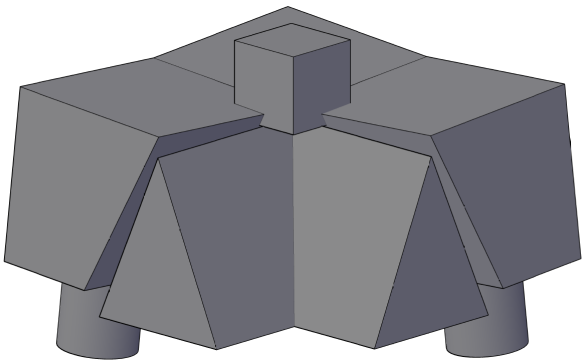

Figure 32: Corner shear failure pattern

It consists of a combination of several one way shear cracks which allow to isolate the four corners of the cap: Once the strength of the element is reached, inclined critical cracks will develop on each side of the element, from the inner edge of the pile to the top middle of the side. Thus, the pile cap will be separated into five pieces: one at each corner which will start to rotate and the last one which will be formed by the remaining element and will undergo the vertical translation.

This model offers the possibility to use use a crack pattern similar to what was described during the experimentations and in the same time to develop a failure mode which corresponds better to reality. Moreover, the global shape of this model remains simple which will permit to keep an easier formulation of the model.

5.4 Improved punching shear

A similar approach can be led in order to develop a new punching shear failure. Indeed, if several one way shear cracks are once again combined but this time not to isolate the corner but to cut the cap through its whole length, the resulting failure mode includes a pyramid forms at failure, see Figure 33. Its base still corresponds to a square whose orientation is now correctly represented. Thereby, this failure mode permits to conciliate both a reasonable crack pattern and a punching shear model which fit better with experimental observations.

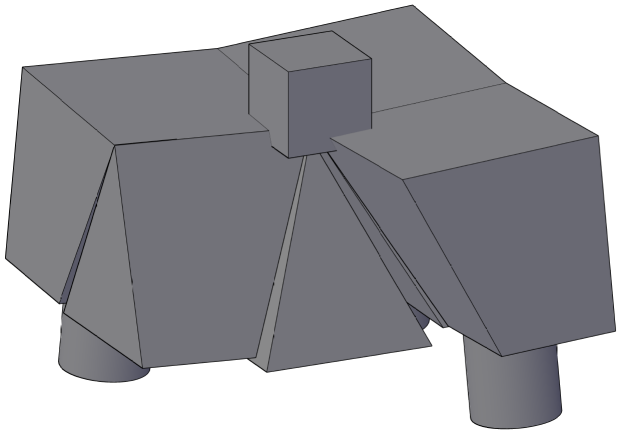

Figure 33: Punching failure pattern with a combination of one way shear

Concerning the behavior of this model, it can be seen that the shape of the corners are conserved: Inclined cracks still develop in the same way as previously mentioned which isolates the four corners from the rest of the pile cap. The main difference comes from the central part of the cap: While it remained in only one block in the corner shear model, it is now cut into five different pieces where the pyramid represents the central element. In that configuration, most of the elements rotate and only the pyramid moves downward.

5.5 Final model

The advantage of the two models presented in 5.3 and 5.4 is that they are based on the same scheme. Thereby it is possible to combine them in order to obtain a new one which is able to represent the two expected failure modes into only one model.

This model reuses the previous model considering the fact the central part is cut in several elements. However, the pyramid does not undergo any more the vertical displacement alone. Indeed, the total displacement Δ_c is now divided equally between the pyramid and the four lateral elements. Moreover, the corners become again the only parts to rotate as it was the case for the corner shear model. Thus, following this model, the failure of the pile cap can be shown in Fig.34.

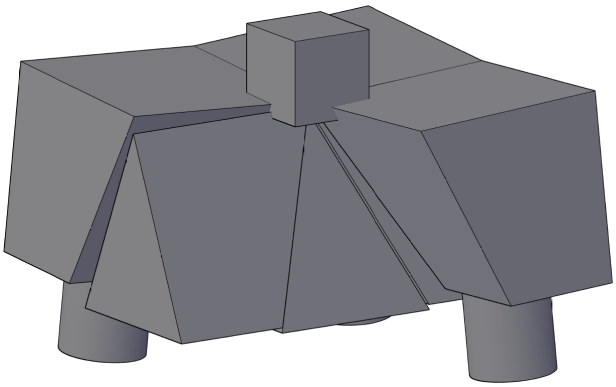

Figure 34: Final model combining punching and corner shear

This model describes the interactions which exist between these two failure modes and the fact that the two are the result of the same phenomena which develop differently. Thereby, the model evaluates the corner shear failure by considering displacement $\frac{\Delta_c}{2}$ between the corners and the lateral elements. Similarly, the punching shear failure occurs with the displacement $\frac{\Delta_c}{2}$ between the lateral elements and the central pyramid.

Obviously, the model remains very simple in comparison with the real failures and especially when the two crack patterns are compared. However, it is not the purpose of this thesis which rather tries to develop a new approach to evaluate the strength of pile caps by staying simple enough in order to describe distinctly the phenomena it attempts to represent.

In this particular context, it responds well to the current problematic considering what was previously discussed. Indeed, the 2PKT model and especially the components involved in the strength of the pile cap can easily be applied to this model. Moreover, its simple shape contributes to ease the writing of the equations describing the different phenomena and thus simplifies the calculation process. At last but surely most importantly, the failures it describes corresponds to the observations reported during the series of tests, both regarding the crack pattern and the failure mode. For that reasons, this model will be the final one used in this thesis.

6 2D kinematic approach

All the tools required to build the 2PKT model for pile caps are now presented. It is now possible to start from the failure modes previously described and adapt the equations of the 2PKT for deep beams in a way they describe the chosen mode. Thereby, this section will consist of establishing and describing the model based on the one way shear failure.

To do so, the kinematics of the model will be presented in more details than what was done in the previous section. In that way, each component involved in the strength of the pile cap will be clearly identified in order to associate them with the right term.

Then, each term will be developed in order to detail how the initial expressions of the 2PKT for deep beams have to be adapted to correspond to this new configuration.This includes the description of the evolution of the equation characterizing these different terms but it will be also necessary to detail how each parameter which composes them is impacted by this change. Moreover, a variability study for the parameter ε_t will be performed for each of them in order to predict their evolution during the iterative process and more important do understand their behavior when the applied force increases.

Finally, all this information will be regrouped and assembled to form the complete model. In parallel, some explanation will be given concerning some specificities of the computer code used for the calculations, especially concerning the iterative process and the choice whether to consider or not the yielding of the flexural reinforcement.

6.1 Kinematics

When the applied force increases, the concrete zone right under the column plate becomes more and more loaded and the compression flowing to the supports increases. At failure, a crack develop from the column plate to the piles where the slip is avoid by the interlock of the two faces of the crack and by the dowel effect brought by the bottom reinforcement. Moreover, the critical loading zone starts crushing and creates a vertical displacement between the parts on either side of the crack.

Figure 35 shows another picture of the current failure mode which is now represented in 3D in order to illustrate better how the different parts move with respect to each other:

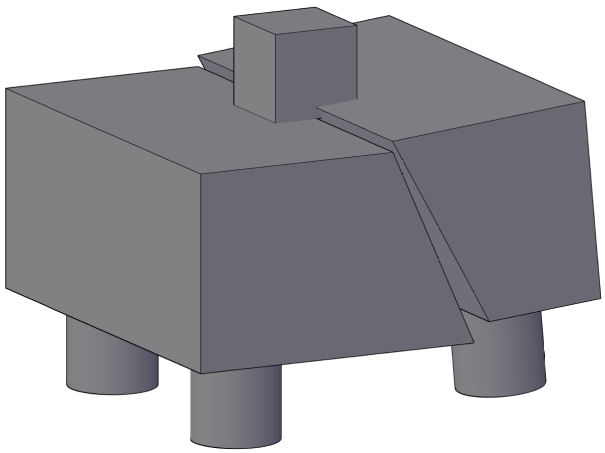

Figure 35: Description of the one way shear failure

Under this configuration, the failure mode is similar to which observed for deep beams and the components contributing to the strength of the element are almost the same. The first difference comes from the absence of stirrups. Indeed, pile caps are typically designed without any stirrup which means that the shear component V_s is 0. Moreover, it appears that the critical loading zone is concentrated under the column and does not extend trough the entire width of the pile cap as it was the case for deep beams.

Concerning the aggregate interlock area, it can at maximum develop all along the failure crack which corresponds to the whole length and the whole height of the cap. Finally, the dowel action which represent the last component involved in the strength of pile caps remains unchanged compared to what is done for deep beams. Of course, the ratio of reinforcement, its location and its arrangement have an impact on the final value but the basic principles remain the same.

All the different parts are now identified and it is now possible to analyze them separately in order to adapt their expression to the current configuration.

6.2 $V - \varepsilon_{t,avg}$ relationship based on moment equilibrium

As it was previously mentioned, the strength of the pile caps will be calculated by determining the value of the strain on the bottom reinforcement ε_t under which the shear force transfered through the critical crack

$$V = V_{CLZ} + V_{ci} + V_s + V_d \tag{49}$$

is in equilibrium with the shear force derived from moment equilibrium

$$V = \frac{\sigma_t A_s (0.9d)}{a} \tag{50}$$

Where A_s corresponds to the bottom reinforcement crossing the critical crack. As such, it can be composed by the three different type of bar arrangements commonly used in pile caps.

These two equations are exactly the same that those used for deep beams because this failure mode assumes that the pile cap works the same way than beams. Thereby, it is normal to observe that they are governed by the same equations. Moreover, the expression of the shear span a remains unchanged and can be written as

$$a = \frac{e}{2} \tag{51}$$

In this particular context, it is important to focus first on equation (50) and more specifically on the relationship between the applied force F and the strain in the bottom reinforcement ε_t.

The previous equations are both related to the pile reaction V under the block above the critical crack while the experimental data available correspond to the total applied force F. However, these two are directly connected by the geometry of the pile cap. Indeed, because of the symmetry of the elements, their 2D static scheme can be represented as shown in Figure **??**.

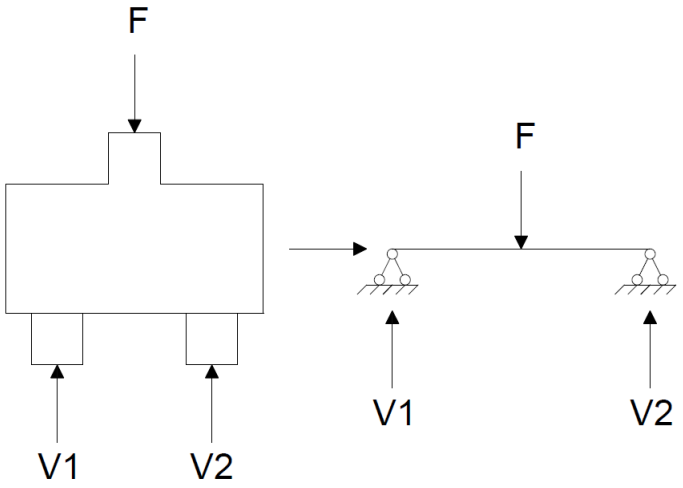

Figure 36: 2D static scheme of the considered pile caps

Under this configuration,

$$V_1 = 0.5F \tag{52}$$
$$= V_2 \tag{53}$$

6.2.1 Steel constitutive law

During this work, two different approaches were considered for the modeling of the steel reinforcement:

– Infinitely elastic

It is assumed that the steel keeps a linear elastic behavior until failure. In this way, it will not be necessary to distinguish the elastic and plastic domain in the model which simplifies the model. Thus, the governing equation will correspond to Hook's law:

$$\sigma = E\varepsilon \tag{54}$$

– Elastic-plastic with strain hardening

Conversely to the previous one, this approach is more accurate. However, this assumption could seam unusual in comparison with those commonly used for the classic design of steel reinforcement. Indeed, the yielding plateau is generally preferred for its safety and its better representation of the behavior of the steel right after reaching the yield strain where the strain suddenly increases without significant increment of the stress, see Figure 37. This leads to complicate the expression of the stress in the reinforcement:

$$\begin{cases} \sigma = E\varepsilon & \text{If } E\varepsilon \leq f_y \\ \sigma = f_y + \frac{f_u - f_y}{\varepsilon_u - \frac{f_y}{E}}(\varepsilon - \frac{f_y}{E}) & \text{Otherwise} \end{cases} \tag{55}$$

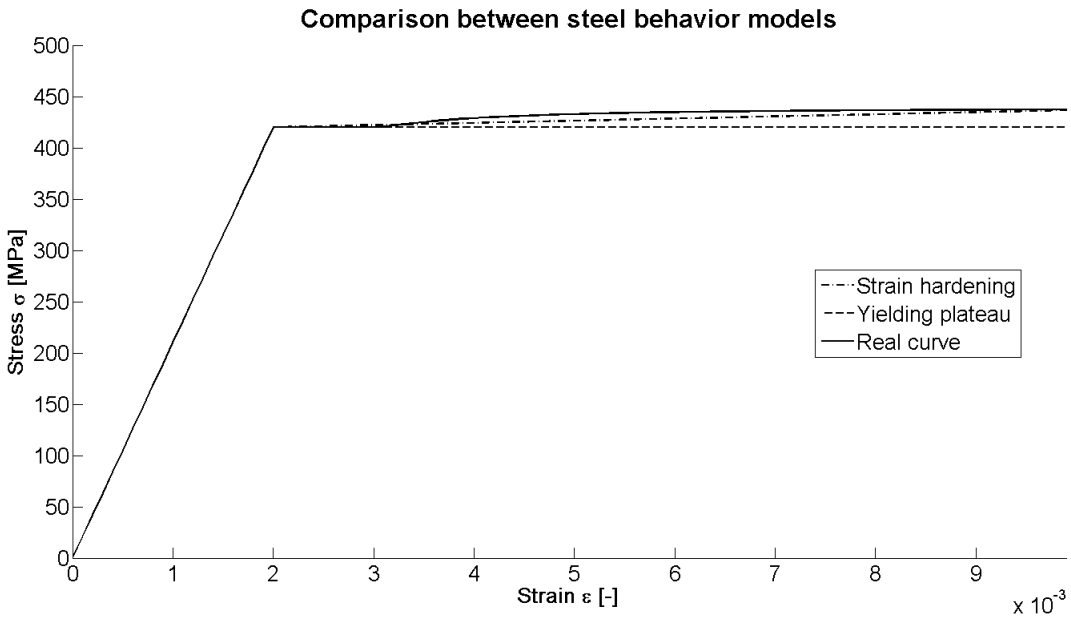

Figure 37: Representation of the different approach of the steel behavior

Thereby, when the reaction under the pile V is evaluated following the equilibrium Eq.50, these two approaches gives the following results:

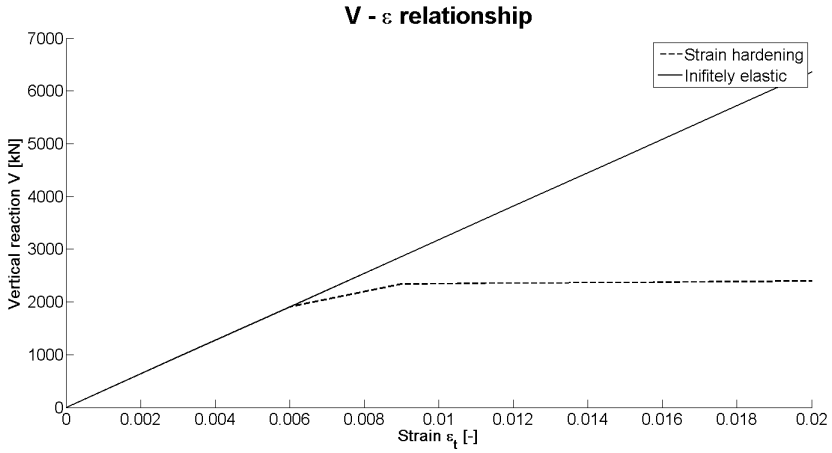

Figure 38: Relationship between the vertical reaction and the strain on the steel

Where the change of slope of the strain hardening curve corresponds to the strain ε_t for which the bottom reinforcement reach its plastic range. Moreover, because the specimens combine different bar arrangements with different yield strength f_y, several changes of slope are captured.

As expected, the two curves are identical until the strain reaches the yielding point $\frac{f_y}{E}$. At this point, the infinitely elastic law continues to follow the same slope while the plastic softening sees its own drastically falls because of the entry in the plastic range.

This means that these two approaches are equivalent as long as the strain remains low considering the fact that common yielding strains have an order of magnitude of a few per thousand while the ultimate strain of steel can reach the tens of percent. Moreover, considering the gap between those two, it can be deduced that the differences between the two approaches reach quite quickly some high values. Thus, it is important to determine in which field of use they will be used to ensure the accuracy of the answer.

Regarding classical pile caps design, it appears that this type of element is relatively little reinforced which leads to heavily load the reinforcement and to reach higher values of strain. In particular, some tests in Japan reported the strain reached in the reinforcement bars at failure. Thereby, it was observed that a lot of them had reached the yielding point and had entered into the plastic range as it is shown in the report of the tests performed in 1998 [4]. Knowing that, the use of the infinitely approach could bring some unrealistic results in comparison with the values obtained during the experimentations. However, this is only a hypothesis and this point will be discussed later in this thesis.

6.2.2 Bars arrangement

Another important detail to mention concerns the bottom reinforcement itself: Longitudinal reinforcement for deep beams are commonly uniformly distributed on the thickness of the element. Moreover, the impact generated by the modification of the bar arrangement

have almost no impact on the strength of the beam.

However, these remarks are not true any more for pile caps. Indeed, considering the size of such elements and the space available to split the reinforcement, three different arrangements can be used:

- Uniformly distributed grid
- Bunched square
- Bunched diagonal

These arrangements are illustrated in Figure 39.

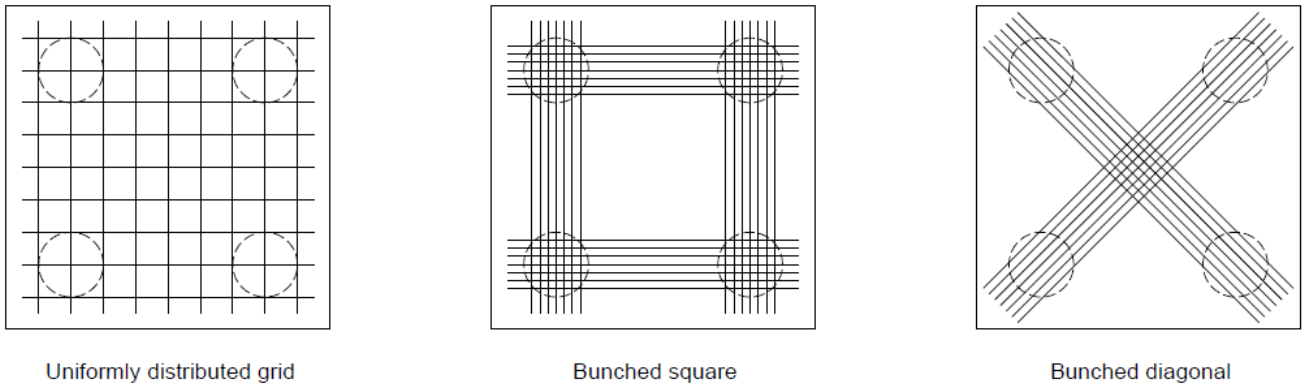

Figure 39: Bar arrangements in pile caps

In addition, they are not equivalent in terms of stiffness and flexural strength. Thus, for the same amount of reinforcement, the distributed grid is less efficient than the two others as observed *J. Blévot and R. Frémy [2]* during their tests. That can be explained by using the same strut-and-tie model used previously. For example, if we consider bunched square reinforcement, the force path is as shown is Fig.40.

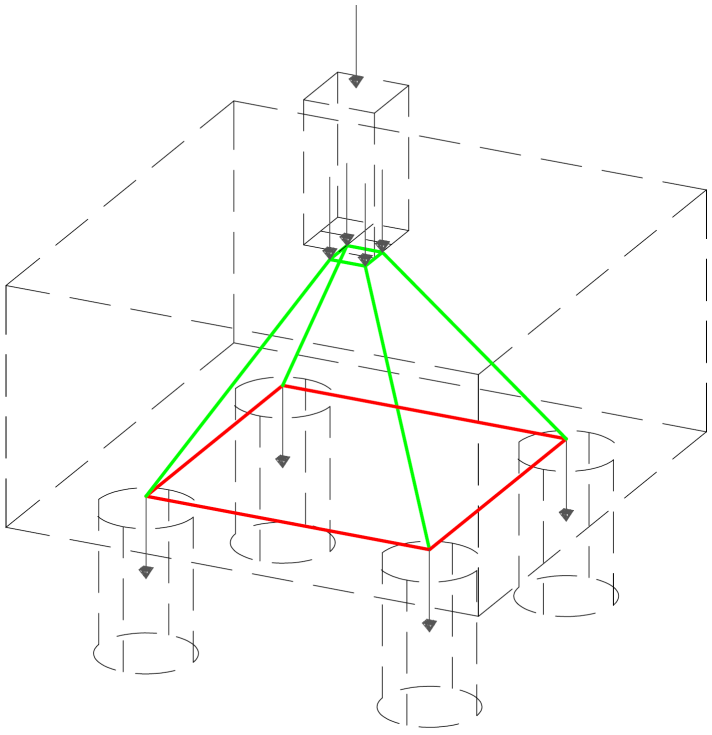

Figure 40: Force transmission in a pile cap with bunched square reinforcement

It can be seen that the tension force in the reinforcement is mainly concentrated on the piles alignment. Thus, the more away the bars, the less effective. That's why an effectiveness coefficient is necessary to express this particular behavior.

In that context, the total width of the reinforcement layer whose stress is not uniformly distributed will be replaced by an effective width where all the bars are identically loaded, neglecting all those outside this area.

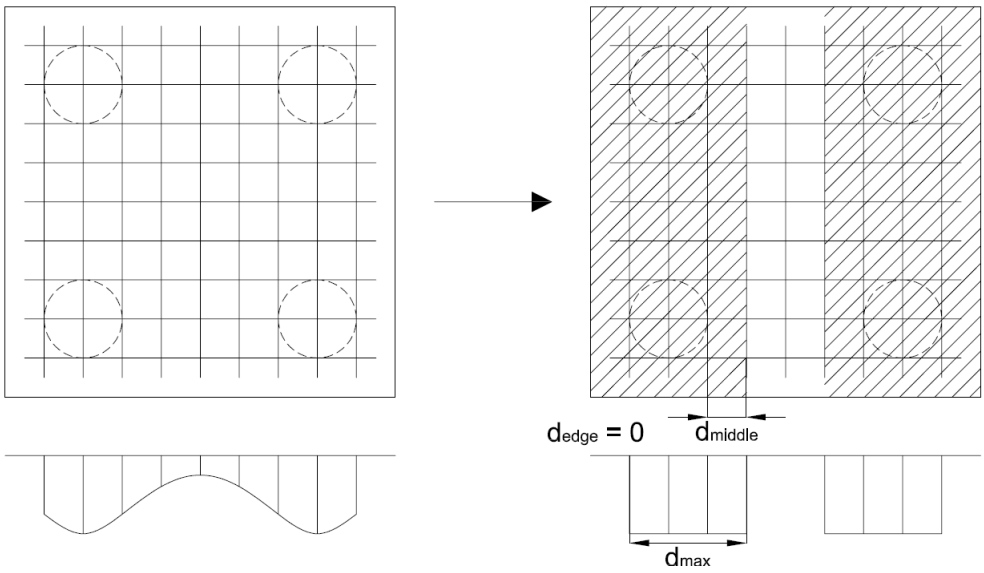

Figure 41: Effective area for an uniformly distributed grid

Now when the principle is explained, it remains to determine the maximum value. For that, it was assumed that the stress can fully develop on a distance until three time the pile width which includes the concerned pile and another time a pile width on either sides. It is however necessary to check if the edge of the cap and its size are large enough to reach it.

Finally, the effectiveness coefficient can be expressed by:

$$eff_{ratio} = \frac{d_{max}}{b/2} \tag{56}$$

$$d_{max} = d_{edge} + lb_2 + d_{middle} \tag{57}$$

$$d_{edge} = min(\frac{b - e - lb_2}{2}, lb_2) \tag{58}$$

$$d_{middle} = min(\frac{e - lb_2}{2}, lb_2) \tag{59}$$

It has to be mentioned that this effective ratio also affects the number of bars considered in the calculations. Indeed, the grid reinforcement which does not lay in the effective width is simply neglected which concerns all the parameters relative to this reinforcement distribution. Thereby,

$$n_{g,eff} = eff_{ratio}.n_g \tag{60}$$

However, this coefficient only affects the grid distribution whereas some differences can still be observed depending on the orientation of the bars (if they are put in diagonal or in square). To determine the conversion coefficient, the stiffness for both of them will be evaluated for a unit elongation, see Fig.42.

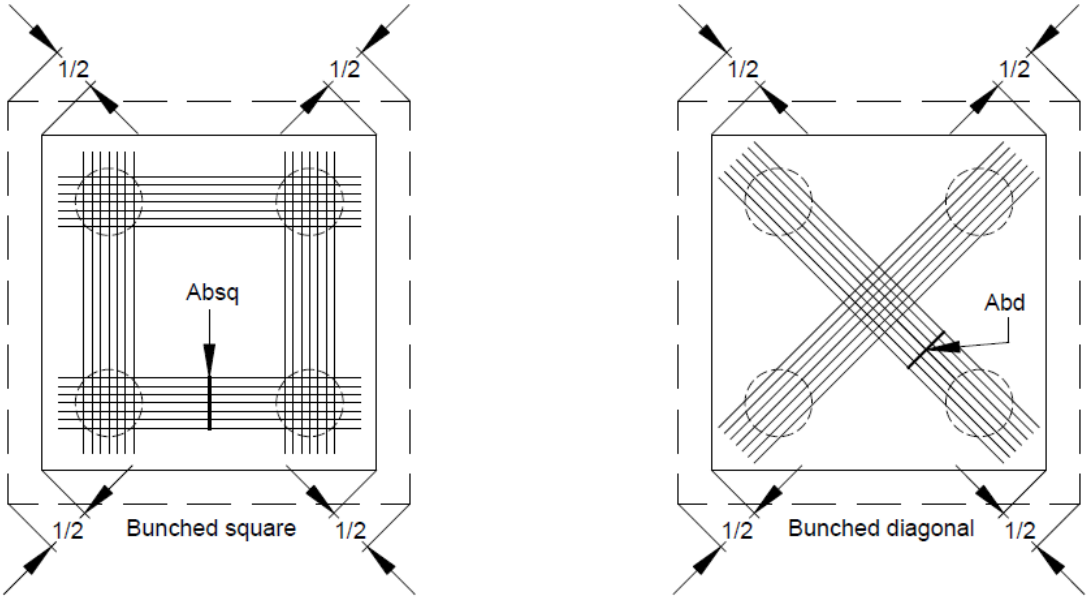

Figure 42: Unit elongation for both arrangements

Bunched square:

The total strain has first to be projected in the bars axis to obtain the following expression:

$$\varepsilon_{bsq} = \frac{1 \cos 45}{l_{bsq}} \tag{61}$$

$$= \frac{\sqrt{2}}{2l_{bsq}} \tag{62}$$

By using the Hook law, one can determine successively the force taken in each direction and the resulting force:

$$F_{bsq,1} = A_{bsq} E \frac{\sqrt{2}}{2l_{bsq}} \tag{63}$$

$$= F_{bsq,2} \tag{64}$$

$$F_{bsq,total} = \sqrt{F_{bsq,1} + F_{bsq,2}} \tag{65}$$

$$= \sqrt{2} \frac{A_{bsq} E \sqrt{2}}{2l_{bsq}} \tag{66}$$

$$= \frac{A_{bsq} E}{l_{bsq}} \tag{67}$$

where $F_{bsq,total}$ is the resulting force along the diagonal of the pile caps.

Bunched diagonal:

In that case, and using the same principle, the following equation is obtained:

$$F_{bd} = \frac{A_{bd}E}{l_{bd}} \tag{68}$$

To determine the conversion coefficient, it remains to express the fact that $F_{bsq,total} = F_{bd}$ in order to determine the area of steel required in each case. Moreover, it is necessary to take into account that the length of the bunched diagonal reinforcement are longer than bunched square one:

$$\sqrt{2}l_{bsq} = l_{bd} \tag{69}$$

Thus,

$$\frac{A_{bsq}E}{l_{bsq}} = \frac{A_{bd}E}{l_{bd}} \tag{70}$$

$$\Rightarrow \sqrt{2}A_{bsq} = A_{bd} \tag{71}$$

Which means that for an equivalent result, it is necessary to place $\sqrt{2}$ time more reinforcement if the bars are positioned in diagonal rather than in square.

However, the reinforcement is generally expressed direction by direction. So, A_{bsq} includes all the bars in one direction instead of considering only one path between two piles (as it was defined in Figure 42).

As such, the previous coefficient has to be adapted to correspond to this convention. Thus,

$$\Rightarrow \frac{\sqrt{2}A_{bsq}}{2} = A_{bd} \tag{72}$$

Which gives the final expression allowing to convert one type of bar arrangement into another. For example, if it is necessary to convert the different reinforcement onto an equivalent bunched square area, each types of bar can be expressed as follows:

$$A_{g\rightarrow bsq} = eff_{ratio}A_g \tag{73}$$

$$A_{bsq\rightarrow bsq} = A_{bsq} \tag{74}$$

$$A_{bd\rightarrow bsq} = \frac{2A_{bd}}{\sqrt{2}} \tag{75}$$

Which finally gives the total amount of steel to consider for the calculation of the bottom reinforcement crossing the critical crack (as required for example in the Equation 50 for the calculation of the moment equilibrium).

$$A_s = A_{g\rightarrow bsq} + A_{bsq\rightarrow bsq} + A_{bd\rightarrow bsq} \tag{76}$$

6.3 Critical loading zone

This part is dedicated to the determination of an expression of the shear V_{CLZ} carried by the CLZ. In that context, the initial equation expressed for deep beams will be adapted to fit with this new configuration but the terms that compose it will also be analyzed to determine how this change affect their value. To do so, the governing equation of the critical loading zone will be decomposed and the transition from the initial model to the pile caps will be explained.

First, to understand properly the particularities of this component of the 2PKT model, Fig.43 a representation of the rigid block above the critical crack on which develops the critical loading zone. Where the critical loading zone is represented by the hatched area right under the column. In there, lb_{1e} represents the width of the critical loading zone and depends on the position of the column on the cap. Following the current geometry, it is positioned in the middle of the crack which means that the applied force is equally distributed between each pile.

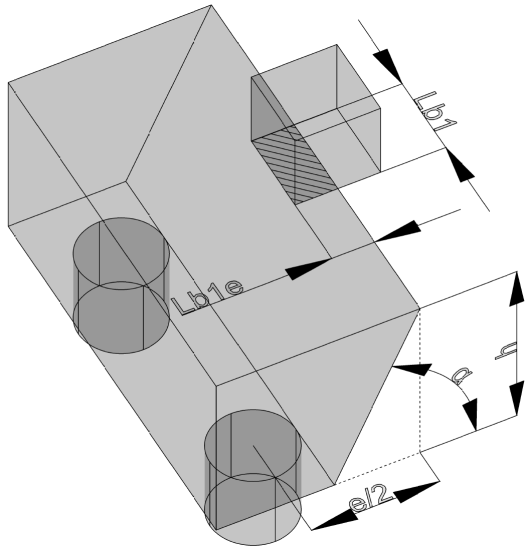

Figure 43: Illustration of the critical loading zone for one way shear failure

Thereby, the critical crack will develop from the inner edge of the piles to the middle of the column which corresponds to :

$$lb_{1e} = 0.5lb_1 \tag{77}$$

Knowing that, the expression of the strength of the critical loading zone becomes:

$$V_{CLZ} = k.f_{avg}.lb_1.lb_{1e}.\sin\alpha^2 \tag{78}$$

Concerning the value of the angle of the crack α, it is still determined by the same equation used for deep beam considering the fact that the one way shear model tends to describe the same failure mode expressed for another type of element. Thereby:

$$\alpha = atan\left(\frac{h}{e/2 - lb_2/2}\right) \tag{79}$$

Finally, by analyzing the expression of the strength of the critical loading zone, it appears it only depends on geometrical components and material characteristics. This means that the result has to be constant, no matter of the value of ε_t is.

6.4 Aggregate interlock

Similarly, the expression of the aggregate interlock for one way shear failure slightly differs from how it is calculated for deep beams. Thereby, the following developments will detail how the differences between those two cases have an impact on the governing equations by explaining the changes affecting the terms which compose them.

Thereby, the contribution of the aggregate interlock is generated by the stress flowing through the specimen. In that particular case, it appears that considering the entire section as fully effective is really unconservative regarding the strut-and-tie model shown in Figure 40 which represents well the flow of forces in the specimen.

In this case, the compression stresses are mainly concentrated in the diagonals linking the column to the pile. Thus, it seems logical to expect that the external zones will not contribute much to the strength granted by the interlock between the two faces of the critical crack. More precisely, the concerned surface will consist of the parallelogram whose bases are composed by the distance between the outer edges of the piles and the size of the column as illustrated in Figure 44:

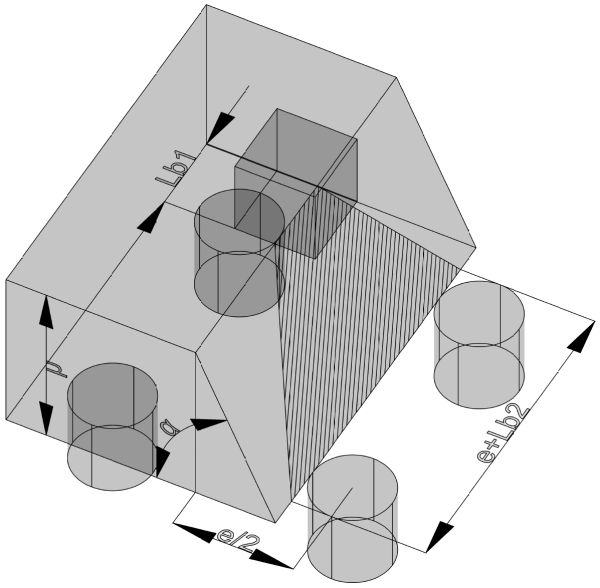

Figure 44: Illustration of the aggregate interlock for one way shear failure

Once again, this means that surface to consider has changed while the physical phenomena remain the same. Thus, the expression of the strength of the aggregate interlock has to be changed accordingly:

$$V_{ci} = \frac{0.18\sqrt{f_c}}{0.31 + \frac{24w}{a_{ge}+16}} \frac{((e + lb_2) + lb_1)\, d}{2} \tag{80}$$

Concerning the terms which compose it, they are similar to those describing this expression for deep beams. Indeed, It was already shown that the angle of the critical crack α was identical. Moreover, the equation of the critical crack width w (Equation 37) and especially those of the vertical displacement Δ_c (Equation 52) remain unchanged. As such, to change the model from deep beam to this one has no other significant impact on the expression of the aggregate interlock.

As it was previously discussed, the strength provided by the friction between the two faces of the crack decreases when the crack width increases because the two interfaces spread and they are less and less able to develop some friction between each other. In particular, Equation 37 expresses that the strain in the bottom reinforcement ε_t contributes to widen the crack. Thereby, more the column will be loaded, more ε_t will increase which will in the same time diminish the efficiency of the aggregate interlock.

6.5 Dowel action

Unlike the two previous components, there is no reason to modify directly the expression of the strength provided by the dowel effect (Equation 43). Indeed, this term is generated by the double curvature to which the bottom reinforcement is subjected. Thus, it only depends

on the characteristic of the bars. For that reason, the transition from a model to another one does not affect the expression of the dowel action and the equation remains:

$$\begin{aligned} V_d &= n_b f_{ye} \frac{d_b^3}{3l_k} \\ f_{ye} &= f_y \left[1 - \left(\frac{T_{min}}{f_y A_s}\right)^2\right] \quad \leq 500MPa \\ &\qquad\qquad\qquad\quad \geq 0 \end{aligned} \tag{81}$$

However, some terms which composed it have to be evaluated carefully. For example, it was mentioned that several bar arrangement exist and these different solutions can potentially be combined in some pile caps. In that context, it is necessary to be consistent when the global reinforcement area is expressed. To do so, it should convert all the different types into the arrangement which is fully effective in the chosen failure mode. For the case of the "one way shear failure", here is how the critical crack is oriented compared to the bottom reinforcement:

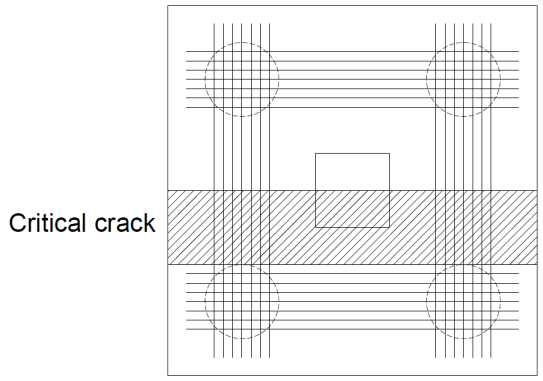

Figure 45: Orientation of the critical cracks of the one way shear model

This means that the total reinforcement have to be expressed following the bunched square arrangement. Thus, following the converting coefficient previously developed and expressed by the Equations 59 and 72, it can be written that:

$$A_{g\to bsq} = eff_{ratio} A_g \tag{82}$$

$$A_{bsq\to bsq} = A_{bsq} \tag{83}$$

$$A_{bd\to bsq} = \frac{2A_{bd}}{\sqrt{2}} \tag{84}$$

$$A_s = A_{g\to bsq} + A_{bsq\to bsq} + A_{bd\to bsq} \tag{85}$$

Not forgetting to also apply this reasoning to the number of bars to consider for the grid arrangement by using the Equation60.

Of course, the interest of these results is not limited to the dowel effect through the values of T_{min} or A_s but will be useful all along the model. Especially, it allows to evaluate the

equilibrium equation and to determine the reinforcement ratio ρ_l used to determine the value of the length of the contributing reinforcement l_k.

$$\rho_l = \frac{A_s}{db} \tag{86}$$

Moreover, each arrangement can have different characteristics, both at the number of bars, their size or even their yielding strength. This means that the yielding is not reached in the same time Consequently, it is not possible to evaluate the strength provided by the dowel effect by simply combining the different terms. In that case, it was decided to keep them split, evaluate the strength of each component separately and recombine them at the end of the process to obtain the final value of the dowel action.

By looking more carefully to the expression of l_k, it appears that it is a function of the bar diameter

$$l_k = min\left(l_0 + d(\cot\alpha - \cot\alpha_1), d\cot\alpha\right) \tag{87}$$

$$l_0 = max(1.5(h-d)\cot\alpha_1, s_{max}) \tag{88}$$

$$s_{max} = \frac{0.28 d_b}{\rho_l}\frac{2.5(h-d)}{d} \tag{89}$$

Here, it would not be practical to evaluate several values for l_k considering it represent a geometrical property of the failure and has to be unique. In that context, the model assumes that l_k is governed by the maximum diameter in order to stay in a conservative approach. Indeed, it maximizes the value of l_k which lead to minimize the value of V_d and in the same time increase the crack width w.

Concerning the evolution of the dowel action, it was already explained that the Equation 81 illustrates the distribution of the total strength of the bottom reinforcement between axial load and dowel effect. Thereby, when the applied load increases, the axial solicitations increase too which decreases the remaining capacity to develop and dowel action. In conclusion, it is expected that the maximum value of V_d is reached when ε_t is equal to zero. Then, this value will progressively decrease while the strain is increased until it fall to zero.

6.6 Solution procedure

The interest of this section is twofold. First, the numerical process will be detailed in order to present how the convergence process is performed and explain how the different key values are calculated. On this occasion, the global evolution of the pile cap strength will be introduced. Moreover, il will be decomposed into all its components in order to compare these results to the comments made for each of them.

Basically, the 2PKT model assumes that at failure, the vertical force V_{equ} which verifies the moment equilibrium reaches the shear strength of the pile cap $V_{strength}$. Moreover, it

was already explained that each of them can be expressed as a function of the strain in the bottom reinforcement ε_t. Thereby, Figure 46 represents their evolution for increasing values of ε_t.

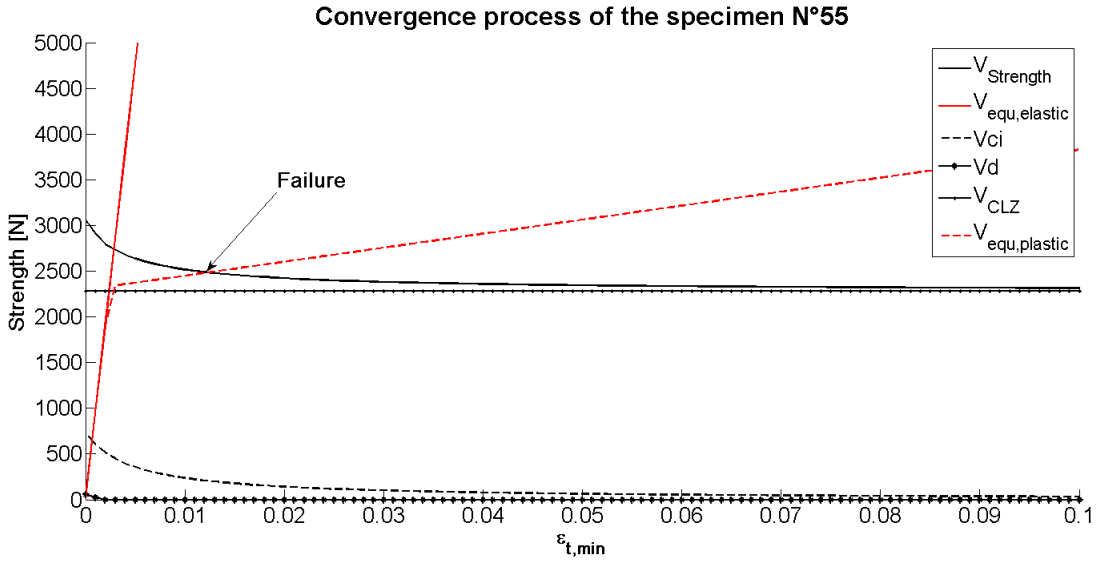

Figure 46: Convergence of the model

Thereby, the failure of the specimen is represented by the intersection between the strength of the pile cap and the strength required by the equilibrium equation. A comparison between the two models for the steel behavior was also added. It appears that the infinitely elastic approach gives a higher strength than the strain hardening. Indeed, as it was presumed, the failure occurred after the reinforcement reached its yielding strain. For that reason, the first model underestimates the strain at failure and thus gives really optimistic results. Conversely, the second one captures better the loss of stiffness and seems to offer more realistic results.

To determine this particular value of ε_t, the model operates by iterating on the value of ε_t, increasing its value until the equilibrium between the pile cap capacity and the equilibrium equation is reached. As such, regarding the value the strain can reach, it is necessary to cover an important domain of values ($\varepsilon_t \in [00.3]$ to entirely describe the whole behavior of some bars used during the tests). Moreover, the value of the increment between two following iterations has to be small enough to provide an accurate answer. For these reasons and to avoid a prohibitive calculation time, it was decided to elaborate a bit more the matlab routine by separating it into two parts.

The first one roughly run through the entire domain in order to identify the iteration during which the strength of the pile caps becomes lower than the strength required by the equilibrium equation. In that way, a shorter domain is defined in which the full accuracy could be used. Then, the routine enter into a new iterative process based on the bi-section

method which diminishes the size of the domain by two until the result has reached the desired accuracy. In that context, the admissible error was fixed to

$$\begin{aligned} e_{adm} &= 100\frac{V_{strength} - V_{equilibrium}}{V_{equilibrium}} \\ &\leq 10^{-4}\% \end{aligned} \tag{90}$$

The model was also supposed to determine if the considered specimen fails by shear or flexural failure. In a first approach, the flexural strength of the element was determined. To do so, the pile cap was idealized as a beam supported at both ends by the piles. Thereby, a classical flexural analysis was led in order to determine the ultimate moment M_u directly linked to the applied force $F_{flexural}$ through the equilibrium equations. Then, this result could be compared to those determined experimentally F_{exp} to be sure of the reliability of the reference values. In that way, if

$$F_{flexural} \geq F_{exp} \tag{91}$$

Then, the specimen fails in shear and otherwise, the failure mode occurs in flexure.

This method is effective when the steel is assumed infinitely elastic because in that case, the reinforcement never reaches the failure and the model is forced to converge. Thus it is necessary to identify which cases correspond to a real equilibrium and which ones were obtained because of the weakness of the current approach. In other words, the flexural method is used as a filter passed trough the model to eliminate the wrong values.

However, when the strain hardening is chosen, the problem does not occur any more. Indeed, the strength of the steel is correctly represented and cannot be exceeded. Consequently, if the specimen has to fail in flexure, it will be correctly represented by the model through the fact that the reinforcement is not any more able to reach the shear strength of the pile cap as it is represented in Figure 47.

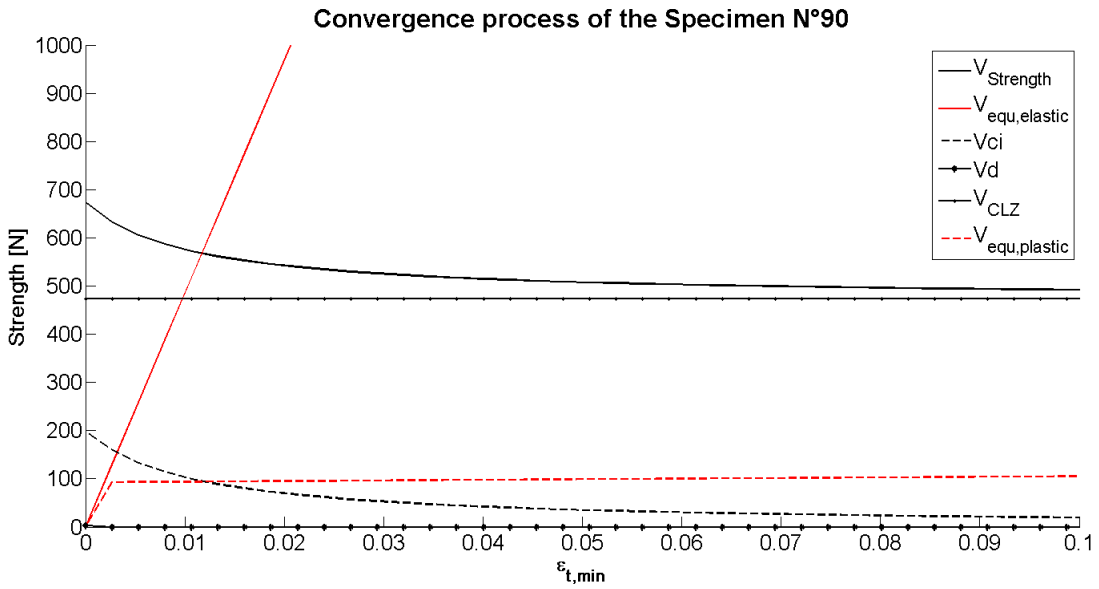

Figure 47: Example of a specimen failing in flexure

It can be seen that the plastic softening model is able to detect when a specimen fails in flexure because the steel is not able to reach the shear strength of the pile cap while the infinitely elastic model cannot.

6.7 Results

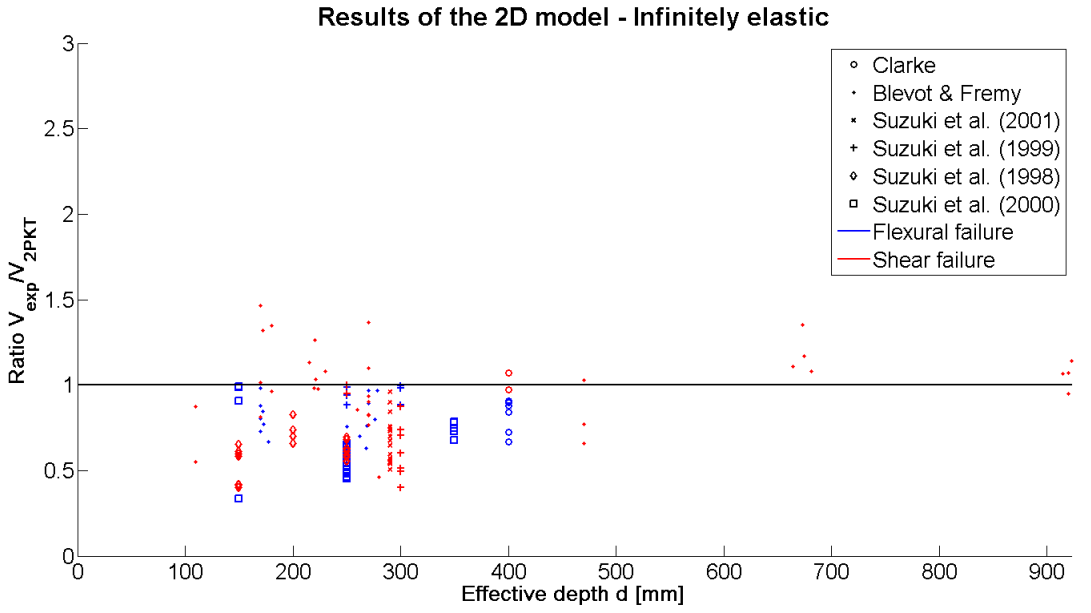

Figure 48: Results furnished by the 2D model with infinitely elastic steel

R_{min}	R_{max}	$\bar{R}$	$\sigma/\bar{R}$
0.335	1.687	0.827	33.2%

Table 3: Characteristic numbers of the 2D model with infinitely elastic steel

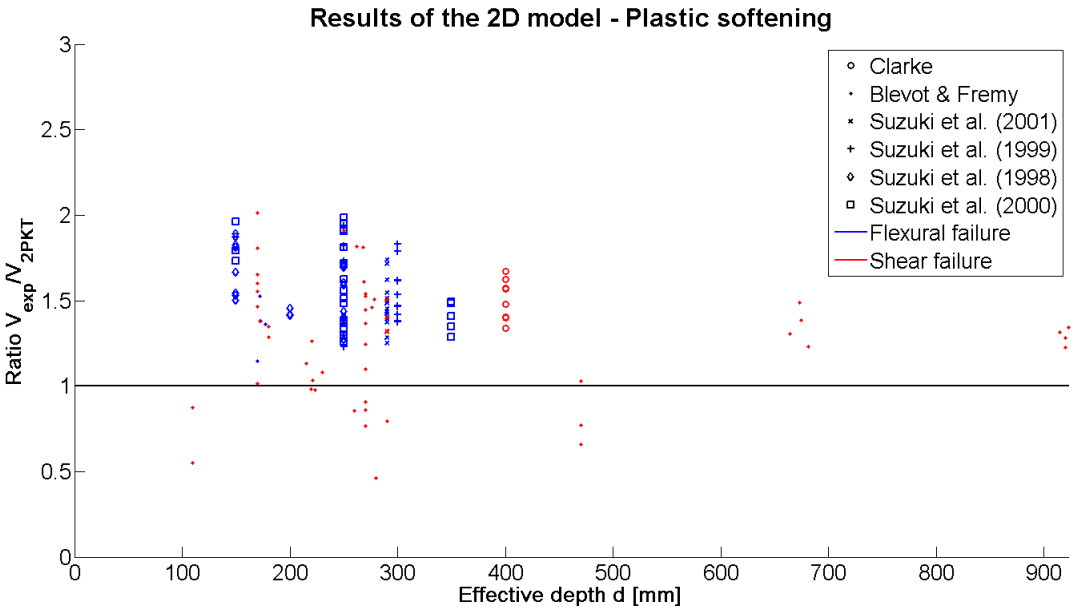

Figure 49: Results furnished by the 2D model with plastic softening steel

R_{min}	R_{max}	$\bar{R}$	$\sigma/\bar{R}$
0.793	2.16	1.495	16.5%

Table 4: Characteristic numbers of the 2D model with plastic softening steel

7 3D kinematic approach

The two simple models are now presented. Through the reasoning detailed in the section related to the crack patterns, they have progressively evolved in order to propose only one single model and to improve the representation of the physical phenomena. Thereby, the final model had to satisfy the following criteria:

- Being able to describe both corner shear and punching shear failure
- Correspond well with the experimental observations
- Furnish results as accurate as possible.

while remaining simple enough to be used with basic computation tools. As such, this section aims to introduce the final model in the same way the simple ones were and illustrate that it fit pretty well with the first prerequisites.

7.1 Kinematics

As it was previously mentioned, this model is a combination between the corner shear and the punching shear failure. Of course, only one mode occurs at failure which means that the crack pattern progressively evolved to either isolate the corner or form the central pyramid, according to the characteristics of the pile cap. However, it is assumed that the vertical displacement Δ_c is equally distributed between the two modes, representing the fact that both of them influence the shear strength of the element.

In that way, when failure occurs, the total vertical displacement is still equal to Δ_c but now two elements are concerned by this translation. First of all, the central element goes down compared to the corner from which it is separated, see Figure 50. This displacement corresponds to the corner failure. In the same time, the pyramid which composes the central element goes down itself and separates from the rest of the central element, Fig.51. In particular, this translation illustrates the punching shear failure.

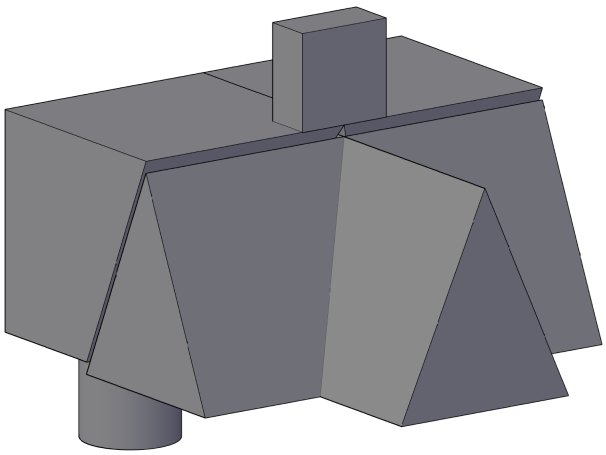

Figure 50: Corner shear displacement

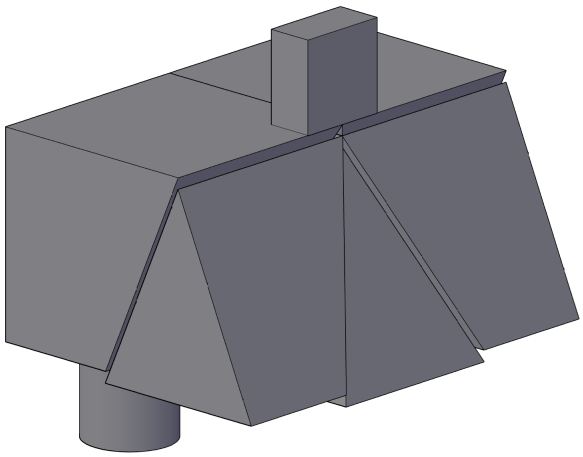

Figure 51: Punching shear displacement

In total, the vertical displacement is equally distributed between these two elements. That means that the vertical gap which develops at failure is the same between the corner and the central element and between the central element and the pyramid. Thereby, each of them is equal two $\frac{\Delta_c}{2}$ as shown in Figure 52.

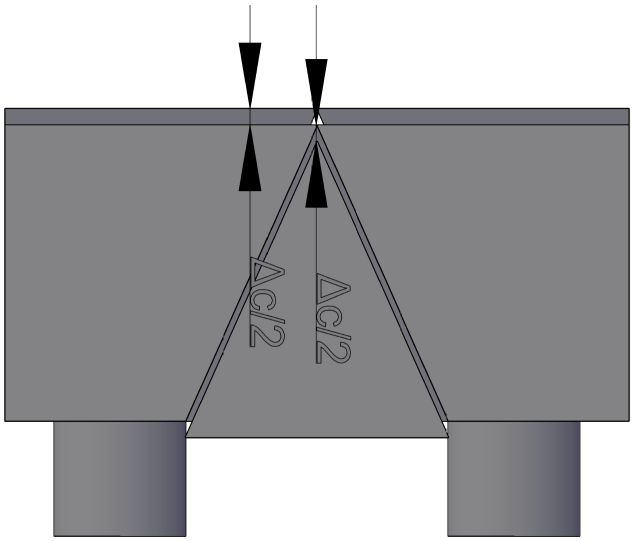

Figure 52: Distribution of the vertical displacement Δ_c

However, even if the two failure modes are represented, only one will induce the failure. In particular, it depends on the strength of each mode. Indeed, it is possible to express for each of them an expression for V_{CLZ}, V_{ci} and V_d. Based on this principle, the weakest failure mode can be theoretically determined which represents the more general way to calculate the final strength of the pile cap.

However, the different series of tests showed that the corner shear failure occurred much more frequently. Moreover, the tests which failed by punching shear failure reached almost the same strength than those which failed by the other mode.

For these reasons, only the first failure mode was considered for the final model. Of course, this leads to a loss of accuracy caused by the exclusion of the punching shear failure. However, the previous explanations showed that the consequences of this will remain low compared to the complexity required to fully implement the model.

Finally, the strength which will be calculated will only concern one corner of the pile cap. Indeed, as it was described, the 3D failure mode is doubly symmetrical: The central piece is identical in each direction and each corner separated from the rest of specimen by the critical cracks is the same than the others. In that way, evaluating the strength of one corner only is equivalent to evaluating a quarter of the total strength.

7.2 $V - \varepsilon_{t,avg}$ relationship based on moment equilibrium

Concerning the equilibrium equation previously used (see Equation 50) to determine the strength of the pile cap at failure, some assumptions were made to simplified its expression. Thereby, the lever arm between the bottom reinforcement reaction and the concrete one z was fixed to $0.9d$. Similarly, the horizontal distance between the support and the concrete reaction was supposed to be equal to the shear span a. This approach brought some inaccuracies in the final result but was consistent with the purpose of the 2D model which was to have an idea of the potential of the 2PKT model for pile caps.

However, which the development of the 3D model, it seems better to improve a little these assumptions in order to increase the accuracy of the model and thus the quality of the results. To to so, it is necessary to return to the basics governing the moment equilibrium. Thereby, the equilibrium of the concrete block above the critical crack can be illustrated by:

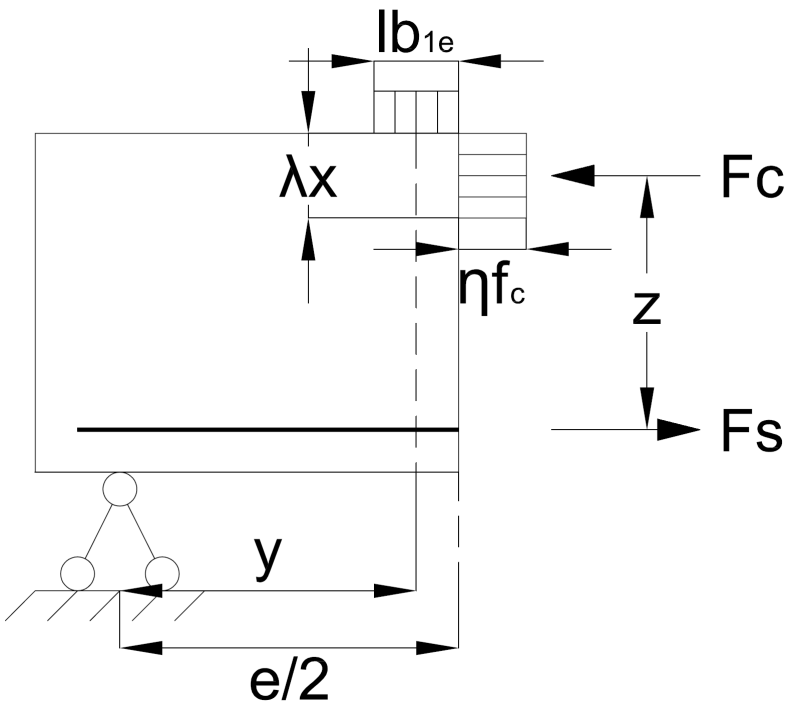

Figure 53: Moment equilibrium

It remains to express analytically the moment equilibrium of this element where the value of V_d can be neglected comparing to the others. By positioning the center of rotation on the concrete reaction, the equilibrium becomes:

$$V.y = F_s.z \tag{92}$$

In particular, the horizontal position of the concrete reaction will be assumed to occur somewhere in the middle of the critical loading zone. Then,

$$y = \frac{e - lb_1 + lb_{1e}}{2} \tag{93}$$

Concerning the value of the lever arm between F_c and F_s, it is possible to express the horizontal equilibrium in the middle of the pile cap to determine its value.

Which consists on expressing that $F_c = F_s$. Moreover, when flexural failure occurs, it is commonly admitted that $\eta = 1$. Thereby, it can be successively written that:

$$A_s.f_y = \lambda x.\eta f_c.b \tag{94}$$

$$\Rightarrow \lambda x = \frac{A_s.f_y}{f_c.b} \tag{95}$$

The, it is possible to express the lever arm z based on the value of the effective height d and λx previously determined:

$$z = d - \frac{\lambda x}{2} \tag{96}$$

$$\Rightarrow z = d - \frac{A_s.f_y}{2f_c.b} \tag{97}$$

Which finally allows to find a new value for the vertical reaction V by reusing the values of the two lever arms y and z which have just been calculated.

$$V = \varepsilon_t E_s A_s \frac{z}{y} \tag{98}$$

It is important to note that the expression for z is strictly speaking correct only at flexural failure. This assumption could seem unrealistic knowing that the the purpose of the model is to evaluate the shear strength of the pile caps. However, as it was previously mentioned, this kind of element is usually lightly reinforced which leads to reach shear failure while the steel is close from failure and conversely. This statement could be confirmed by the crack patterns reported in the tests by *Suzuki et al. in 1998 [4]*, see Figure 54.

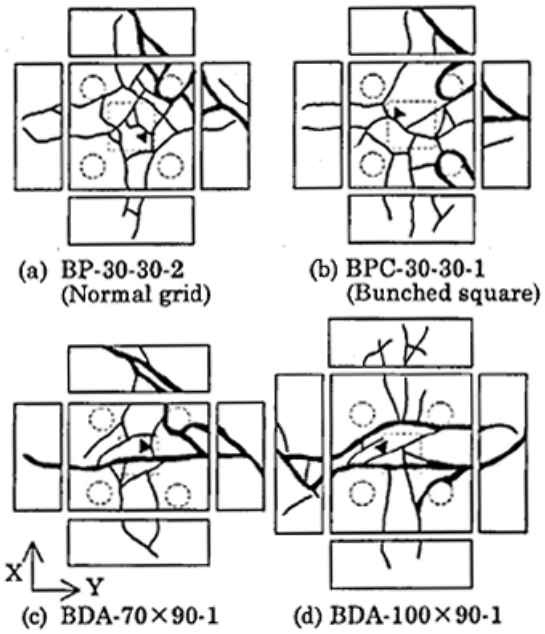

Figure 54: Crack pattern on several specimens tested by *Suzuki et al. [4]*

It can be seen that the characteristic cracks of a shear failure occurring on the periphery of the corners can be observed together with some vertical cracks on the sides of the cap, proper to the flexural failure. In conclusion, it appears that flexural and shear strength are close to each other in the case of pile caps. Thereby, evaluating z under the flexural failure does not change a lot its value and seems to be a reasonable assumption.

7.3 Critical loading zone

Once again, the modifications brought to the failure mode have a direct impact on the expression of the components of shear strength. Indeed, the kinematics of the failure is changed and affects the way the elements interact and also modifies their shape.

The previous critical loading zones assumed that the entire column surface was fully effective and can contribute to the shear strength provided by this component. However, the stress distribution is generally non-uniform, especially in the corners of the column where it is usually lower than in the rest of the surface. For that reason, the column surface used to determine the critical loading zone area was reduced by subtracting the corners. As such, the effective surface is represented by a circle inscribed if the square of the column area, see Figure 55.

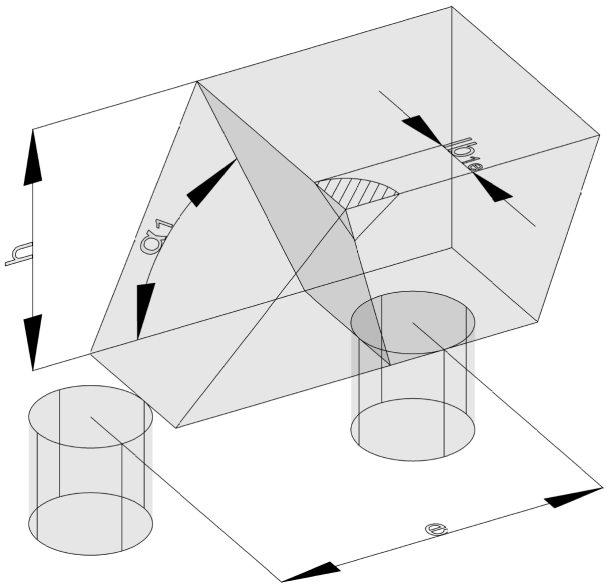

Figure 55: Illustration of the critical loading zone for the final failure mode

Figure 56 shows a close-up view of the CLZ. It can be seen that the chosen failure mode generates a double slope on the corners. Thereby, the resulting critical loading zone, located at the junction of these two tilted planes, sees its dimensions decrease in both directions which was not the case in previous models. Of course, this detail has an impact on the global strength considering the area supporting the cantilever is diminished accordingly. To take this into account, it is necessary to evaluate in which proportion the mechanical properties of the critical loading zone are affected. As such, this model assumes that the corresponding strength is reduced by a factor of 2 compared to the equivalent CLZ with a full section.

Moreover, the expression of V_{CLZ} has to be detailed a bit more. Indeed, the curved shape of the top surface of the critical loading zone implied to change the way to evaluate its projection on its thickness.

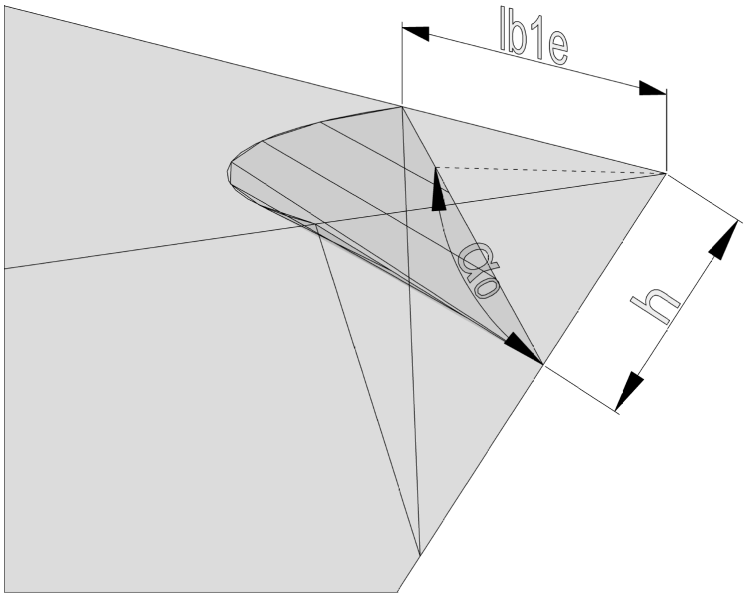

Figure 56: Focus on the shape of the critical loading zone

Where the shaded surface in Fig.56 represents the projection of the top surface on which the compressive strength of the concrete is reached. Under this configuration, it appears that the circle whose radius is equal to lb_{1e} becomes a spherical cap when it is projected. Such a surface can be expressed by the following expression

$$A_{sph} = 2\pi r.h \tag{99}$$

The angle α_0 illustrated in the Figure 56 corresponds to the slope of the intersection of the two plans composing the failure mode. As such, it represents the slope of the critical loading zone and can be expressed by:

$$\alpha_0 = atan\left(\frac{2h}{\sqrt{2}e - lb_2}\right) \tag{100}$$

It is possible to adapt the previous equation to the current configuration. As such, only a quarter of the entire spherical cap has to be considered:

$$A_{sph} = \frac{2\pi}{4} lb_{1e}^2 \sin\alpha_0 \tag{101}$$

Then, the corresponding strength of the critical loading zone is obtained by replacing the expression determined above in the initial equation of V_{CLZ}. Thereby and not forgetting the strength reduction due to the double slope of the failure mode, it can finally be written as:

$$V_{CLZ} = \frac{k.f_{avg}\frac{2\pi}{4} l_{b1e}^2 \sin^2\alpha_0}{2} \tag{102}$$

7.4 Aggregate interlock

Similarly to what was done for the critical loading zone, the modifications which will be brought in this section will result from both the changes of the failure mode and several improvements realized to increase the accuracy of the 2PKT model for pile caps. To ease the understanding of the adaptations to undertake, it is possible to reuse the failure mode described in the Figure 34 and set it to focus on the characteristics of the aggregate interlock, see Figure 57.

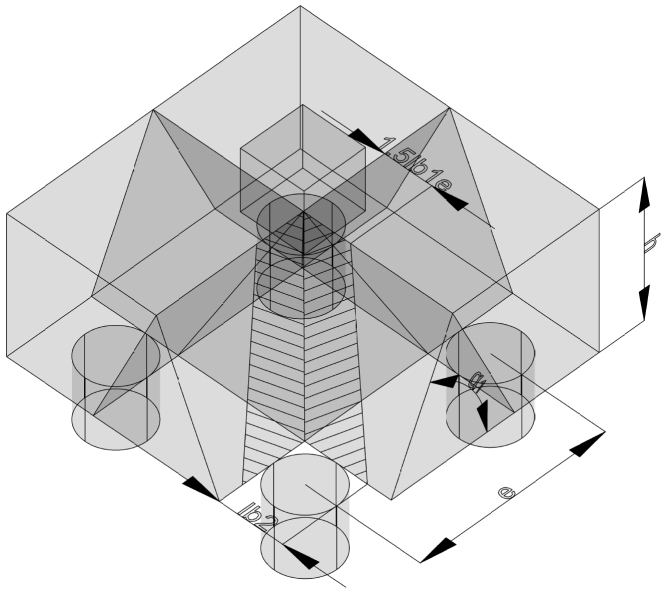

Figure 57: Illustration of the aggregate interlock for the final failure mode

For a first time, the frictions between the two faces of the critical crack extend on two different plans. Indeed, the crack pattern is such that it combines two one way shear failures oriented along two perpendicular directions. In that way, the same type of surfaces can be observed after failure but are interconnected in both directions.

First, it has to be mentioned that because of the symmetry of the pile caps, the two resulting plans will be identical. Thus it is not necessary to study the total strength provided by the aggregate interlock and it is sufficient to narrow the analysis to only one of them and then double the obtained value to retrieve the description of the whole phenomenon. Thereby, all the following developments will only concern half of the friction generated.

Secondly, some details have to be provided with regards to the relevant angles of the model. Previously, the angle α_0 was mentioned and expressed by Eq.100. Concretely it was useful during the evaluation of the strength of the critical loading zone especially because the shape of this element depends on this parameter. However, the aggregate interlock develops on the planes of the critical cracks themselves considered separately. As such, their slope is characterized by the angle α_1 shown in Fig.57 and can be expressed by the following equation:

$$\alpha_1 = atan\left(\frac{2h}{e - lb_2}\right) \tag{103}$$

Concerning the area of the crack on which the friction between the aggregates will be considered, the same basic assumptions can be made. Indeed, most of the strength are still concentrated in the struts linking the column and the piles. As such, it would be very unconservative to use the whole surface of the crack to evaluate the strength of the aggregate interlock.

For that reason,the effective surface will be determined on the same principle used for the previous models. However, some improvements can be performed. Considering the developments made by *Mihaylov et al. [1]* to detail the critical loading zone, they finally arrived to describe it following the Fig.58 which was already introduced in this work.

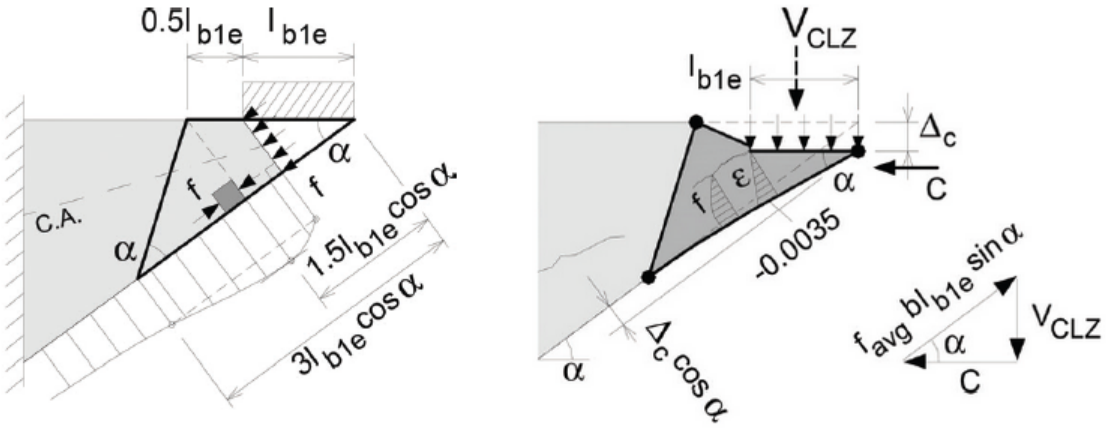

Figure 58: Zone affected by the critical loading zone [1]

It can be seen that even if the crush of concrete occurs right under the column, the critical loading zone is supposed to extend until $1.5lb_{1e}$. As such, it seems appropriate to consider that the zone influenced by the loading of the pile cap reach this value. In other words, this means that a part of the concrete around the column participate to the global strength of the element and not only the area directly in contact with the column.

The resulting surface still corresponds to a trapeze as it was previously the case. However, its dimensions have changed. Taking into account the elements discussed above, the effective are can be expressed by:

$$A = \frac{1.5lb_{1e} + lb_2}{2}d \tag{104}$$

By adding the symmetry of the system and thus multiplying the equation by 2, the expression of V_{ci} becomes:

$$V_{ci} = 2\frac{0.18\sqrt{f_c}}{0.31 + \frac{24w}{a_{ge}+16}}\frac{1.5lb_{1e} + lb_2}{2}d \tag{105}$$

One last detail has to be mentioned concerning the impact of the 3D model on the evaluation of the aggregate interlock. This remark concern the expression of the crack width and comes from the equal distribution of the transversal displacement. Indeed, it has a direct consequence on the value of w knowing that Δ_c is partially responsible of the widening of the critical crack. Thereby, taking into account the assumption of this model, it can be written:

$$w = \frac{\Delta_c}{2}\cos\alpha_1 + \frac{\varepsilon_{t,min} l_k}{2\sin\alpha_1} \tag{106}$$

Which tends to decrease the crack width and then increase the final value of the aggregate interlock.

7.5 Dowel action

Once again, the main difference between all the model depends on the way to consider the bottom reinforcement. In particular, it is related to the orientation of the critical crack considering the bar arrangements do not have the same efficiency in all directions. As such, it is better to directly convert them into the fully efficient layout in order to ease the calculation to undertake thereafter.

In the case of the 3D model, the orientation of the critical crack was already discussed and was represented in Fig.57. Compared to the disposition of the bottom reinforcement, the following observations can be made from Fig.59, where it appears that the bunched square reinforcement is perpendicular to the crack.

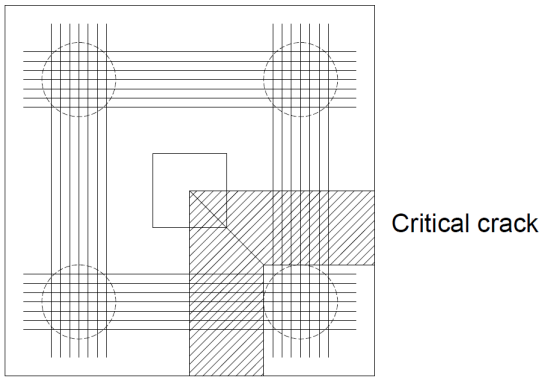

Figure 59: Orientation of the critical cracks of the 3D model

Considering that the 3D model comes from a combination of several one way shear failure, it seems logical to retrieve the same orientation and therefore solicit the different bars in the

same way. Thereby all the steel reinforcement will be converted into the bunched square arrangement in order to express them in the fully effective configuration.

Moreover, it is shown in Fig.59 that the useful steel surface is spread over the two plans of the critical crack. Once again, it is equally distributed considering the symmetry of the pile cap and especially of the bottom reinforcement. It is also illustrated that only half of the reinforcement has to be considered in each direction. Following that, each reinforcement arrangement can be expressed by:

$$A_{g\to bsq} = \frac{eff_{ratio}A_g}{2} \tag{107}$$

$$A_{bsq\to bsq} = \frac{A_{bsq}}{2} \tag{108}$$

$$A_{bd\to bsq} = \frac{A_{bd}}{\sqrt{2}} \tag{109}$$

$$\tag{110}$$

Which represents the steel area in only one direction. From this, it is possible to evaluate the strength provided by the dowel action in this particular case and then double it to take into account the same effect occurring in the other direction. This finally leads to determine the total value of V_d in this way:

$$V_d = 2n_b f_{ye}\frac{d_b^3}{3l_k} \tag{111}$$

$$\begin{aligned} f_{ye} &= f_y\left[1-\left(\frac{T_{min}}{f_y A_s}\right)^2\right] \leq 500MPa \\ &\geq 0 \end{aligned} \tag{112}$$

7.6 Solution procedure

The total strength of the pile caps is still evaluated through an iterative process during which the external force is compared to the current strength of the pile cap. The failure is reached when the value of the strain of the bottom reinforcement ε_t leads to an equilibrium between these two. Except the differences discussed above, the solution procedure remains unchanged compared to the matlab routine described for the 2D model.

7.7 Results

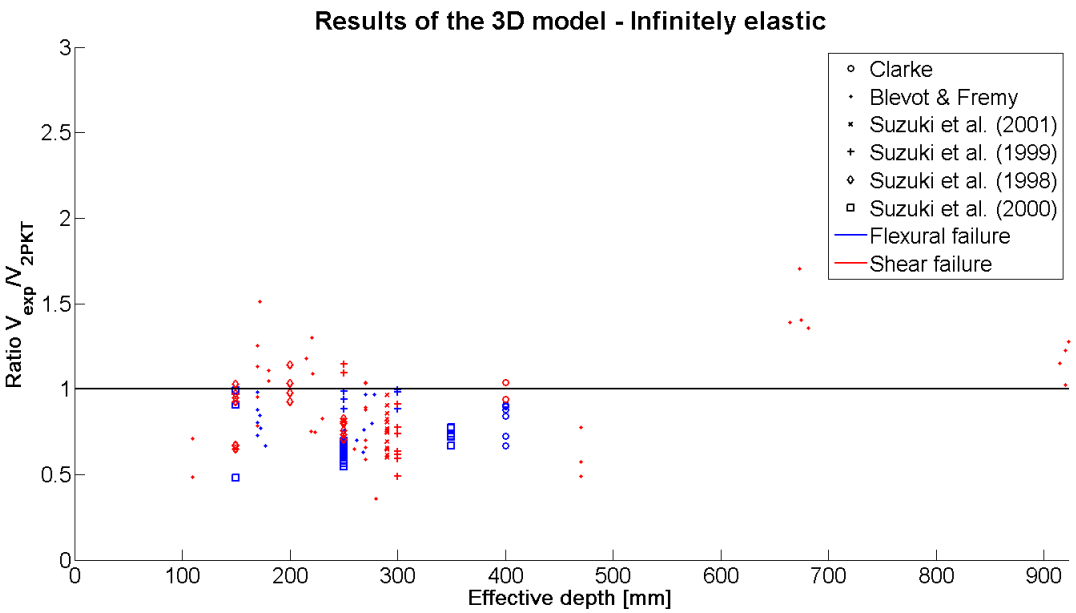

Figure 60: Results furnished by the 3D model with infinitely elastic steel

R_{min}	R_{max}	$\bar{R}$	$\sigma/\bar{R}$
0.482	1.788	0.889	29.3%

Table 5: Characteristic numbers of the 3D model with infinitely elastic steel

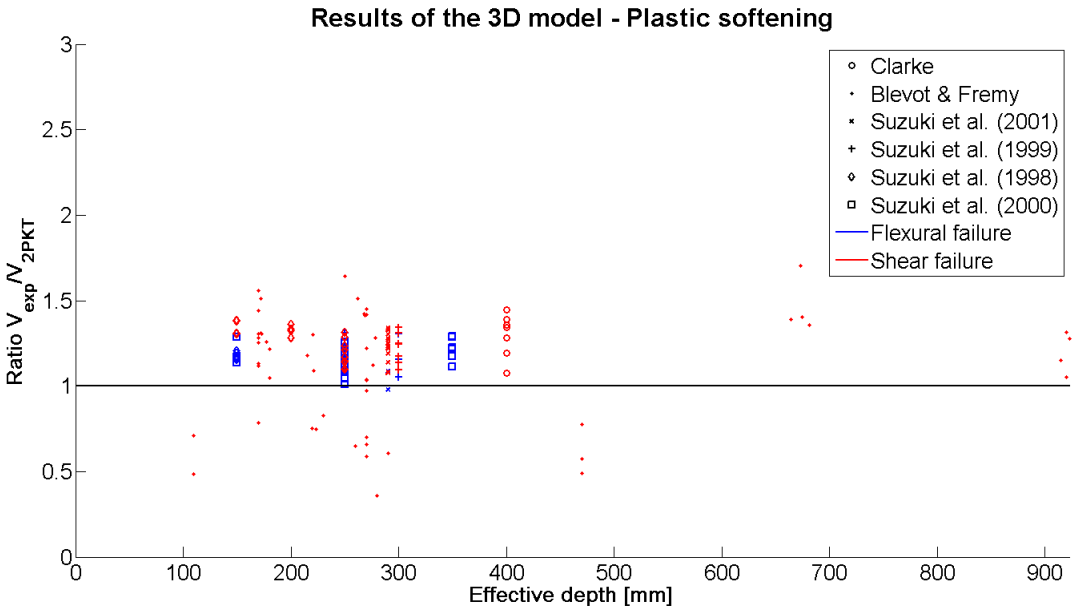

Figure 61: Results furnished by the 3D model with plastic softening steel

R_{min}	R_{max}	$\bar{R}$	$\sigma/\bar{R}$
0.657	2.23	1.242	15.7%

Table 6: Characteristic numbers of the 3D model with plastic softening steel

8 Comparison with tests

This chapter will be divided into two part. The first one will consist to introduce the results furnished by the two main models previously described. It is first necessary to evaluate the accuracy of each of them. To do so, the strength determined numerically can be compared to the experimental results. Therefore, the following ratio is defined:

$$R = \frac{V_{exp}}{V_{model}} \tag{113}$$

First of all the values given by the two models will indicate if they are accurate enough to be used into further developments. Indeed, it has to be remembered that the main purpose of this work is to determine if the 2PKT model can help to describe better the pile cap behavior. For that reason, it is necessary to check if the main objective is reached.

It is not the only characteristic this analysis could provide. Thus, reusing the ratio expressed above, it is logical to conclude that the closer from one, the better the model. However, this criteria has to be nuanced. For example, the results showing that $R < 1$ correspond to the cases for which the model is more optimistic than reality. As such, the position of the results compared to one will show whether the model tends to be conservative or not.

Moreover, the disparity of the results is a good indicator of the reliability of the model. Indeed, if it calculates some really good results but the others are scattered while the differences between the tested pile caps are small, this mitigates the confidence that can be placed in it because its accuracy is not constant and depends on the characteristics of the specimen under consideration. In this context, it is generally better to use a model whose results will be a bit less accurate on average but constant in a larger domain.

In that way, it will be possible to compare the two main models considered in this thesis. In that context, the weaknesses of each of them will be discussed in order to evaluate which one corresponds better to the objectives of this work. The comparative study will not be limited to the models themselves but will also concern the hypothesis on the steel behavior assumed in each of them. Thereby, the impacts of this choice will be represented through the results determined in each case.

However, the ratio R will not be the only value to be considered in this part. Indeed, it is not sufficient to evaluate properly the failure load of the pile caps, it is also necessary to correctly identify the failure mode. As such, the mode identified by the models will be compared to the experimental observations in order to evaluate the predicting power of the model.

8.1 2D kinematic approach

As discussed above, the results of the 2D model will be presented through the ratio defined by Eq.113. On this occasion, it is possible to take the opportunity to express them in

an useful way. To do so, it is necessary to use a parameter which represents well the size of the pile cap and have a direct impact on its strength. As such, the effective depth d fit well with these two criteria. Thereby, besides the analysis of the results themselves, some properties could be observed.

Moreover, some key values can be used to bring new informations about the characteristics of the model. In this case, this includes the extremal values of the model (namely R_{min} and R_{max}) which provide its worst predictions and which could be directly compared with the corresponding values for the other models. To these two values, it is also useful to add the mean ratio in order to determine its average accuracy and discuss about its location compared to 1. The final characteristic value represents the relative disparity of the results. In that way, it will be possible to analyze how the model behaves overall. Initially, this information is given by the standard deviation σ. However, it is better to adapt it a little in order to get a value which can be compared from a model to another. Therefore, the coefficient of variation (COV) $\frac{\sigma}{R}$ is preferred.

8.1.1 Infinitely elastic reinforcement

All the results will be sorted following the series of tests to which they belong. Indeed, each of them was performed with its own process and its own pile cap design. As such, it is important to be able to distinguish them in order to to analyze them separately. In that way, it will be possible to expose the potential inconsistencies in the experimental results and adapt the conclusions accordingly. Thereby, the analysis of the models will not only consist of a discussion of the results themselves but also making sure that the data used are relevant.

As it was mentioned, the interest is here to focus on the shear results considering it is the main purpose of this work. That said, flexural failure remains a significant part of the observed failures which means that it is also necessary to evaluate the accuracy of the model to capture this phenomenon. Thereby, flexural and shear failures are also distinguished. This is the opportunity to combine this distinction to the different representation of each series of tests which can give a quick idea if the failure mode observed experimentally are well captured or not by the model.

Following the remarks expressed above and according to the procedure described in Section 6.6, the results obtained for the 2D model when steel is modeled as infinitely elastic are shown in Fig.62.

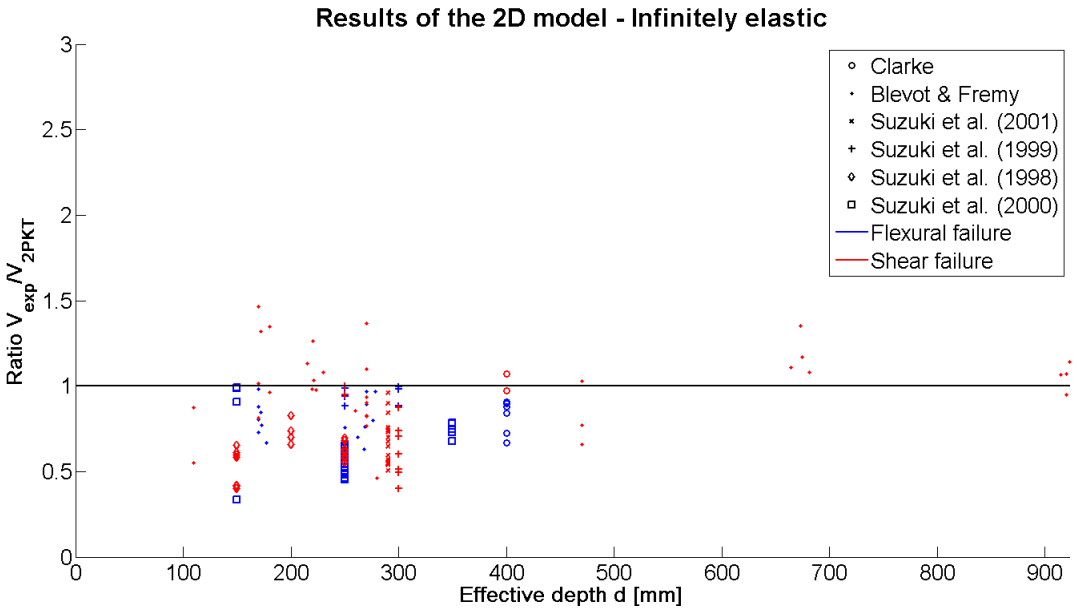

Figure 62: Results furnished by the 2D model with infinitely elastic steel

First of all, it appears that most of the values are lower than one. In other words, that means that this model is most of the time unconservative. Moreover, the graph shows that the disparity of the results tends to grow when the effective depth of the specimens decreases. As such, it seems that this observation strengthen the comment made earlier concerning the type of specimen used during the different series of tests. On this occasion, it was mentioned that the smaller the pile cap, the higher the impact of defects. Indeed, in bigger elements the defects are less important because the size is big enough to redistribute the stress elsewhere. Under this condition, the corresponding impact is more limited and will not affect much the strength of the pile cap. On the other hand, when the specimen is smaller, it does not have the ability to spread the influence of the defect and the strengths are therefore more scattered.

Considering that most of the tested specimens are relatively small compared to the usual size of such elements, this could explain why the variability observed is higher for small values of d and tends to decrease while d increase.

Concerning the failure mode, the model has apparently identified that a lot of the Japanese tests failed in flexure. This result seems to agree with the observations made experimentally knowing that in these series of tests an important number of flexural failures were reported. However, it is still necessary to determine if the results match each other.

Analyzing in more details the model, the following values can be summarized.

R_{min}	R_{max}	$\bar{R}$	$\sigma/\bar{R}$
0.335	1.687	0.827	33.2%

Table 7: Characteristic numbers of the 2D model with infinitely elastic steel

Where the minimum ratio is relatively small while the maximum one reaches reasonable values which would confirm that the model tends to overestimate the strength of the pile caps. This conclusion is also strengthened by the value of the mean which is once again lower than one. Finally, the value of the COV seems to indicate that the results are scattered.

8.1.2 Elastic-plastic reinforcement

The same king of graph was generated to illustrate the results obtained with the 2D model where the yielding was this time considered to modeled the steel behavior. The results are again plotted as a function of d, see Fig.63.

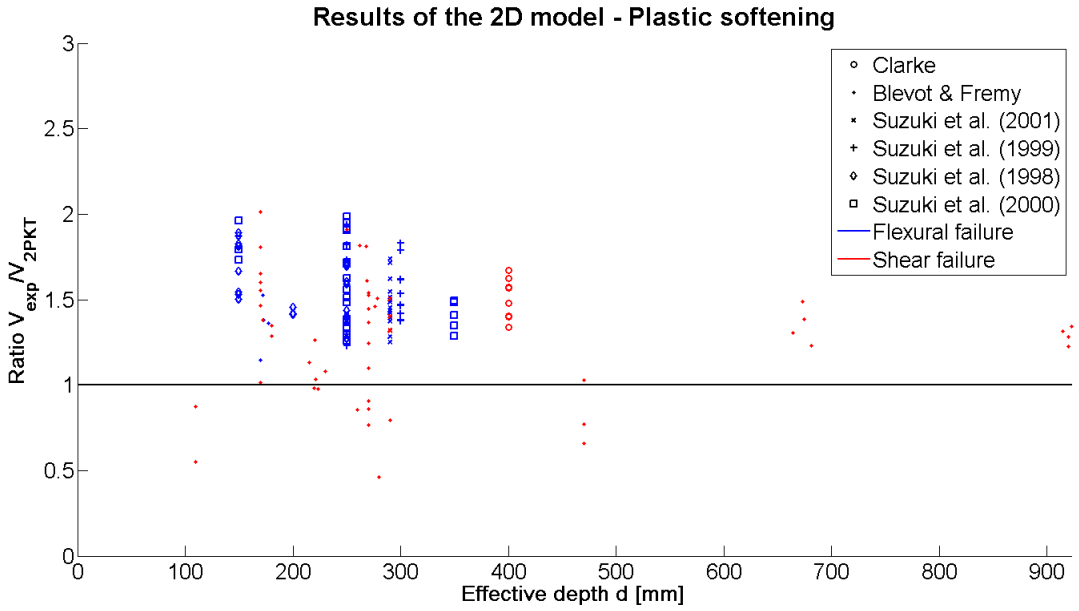

Figure 63: Results furnished by the 2D model with plastic softening steel

Once again, the graph shows that the small specimens result in a higher variability while for the biggest ones the results are closer to 1. This is assumed to come from the small size of the pile caps realized in the tests which could lead to some disparities in the experimental results.

Contrary to the infinitely elastic hypothesis, considering the yielding of the reinforcement seems to give better results. First, the values are mainly higher than one which imply that the model is conservative. Moreover, they are more accurate compared to the previous ones. This results was expected remembering the earlier discussion in this work: It was shown that in the case of pile caps, the bottom reinforcement enters most of the time into the plastic

range at failure. Thus, neglecting the plasticity causes to underestimate the value of ε_t which lead to overestimate the real strength of the element.

As it was the case for the previous model, a lot of Japanese tests are supposed to fail in flexure which still corresponds to the experimental results.

To quantify the observations made above and to compare efficiently this model with the previous one, the following table was created and contain the important numbers introduced in the beginning of this section:

R_{min}	R_{max}	$\bar{R}$	$\sigma/\bar{R}$
0.793	2.16	1.495	16.5%

Table 8: Characteristic numbers of the 2D model with plastic softening steel

These values clearly show an improvement compared to the previous model. Indeed, the minimal value is way better than before. Of course, this leads to an increase of the maximal value due to the vertical displacement of the entire graph but this is not proportional and the model tends to behave better in the entire domain which is well represented by the value of the mean ratio, now higher than one, confirming the safer approach brought by the change of the steel behavior. However, this improvement is without context best shown through the COV showing a more reliable model.

All these arguments seem to indicate that the current results are promising, especially because they come from a simplified approach performed in order to test roughly the potential of the 2PKT model for pile caps. Moreover, it is also necessary to check the base of these results by verifying if the failure mode was well captured. This could seem unnecessary considering that it was previously mentioned that the two possible failure mode (shear or flexure) were close each other due to the low ratios of reinforcement. However, the purpose of the model is also to capture well the behavior of pile caps subjected to points load. As such, it is also supposed to determine properly the failure mode even if this result has only a low impact on the final strength predictions.

At this point, some clarifications have to be made: For now, only two failure modes were considered, namely flexure and shear. Each of them respectively occurs when the reinforcement yield and when the pile cap reaches its shear strength. However, it was already mentioned that many specimens can fail in shear while the reinforcement had reached its yield strength. In that particular case, the corresponding failure mode is called flexure-shear. Unfortunately, the different series of tests did not consider the same conventions to report the experimental failure. As such, some distinguished these three cases while others only mentioned the two principle failure models. In order to stay consistent with all the different experimental results, the choice was made to only keep the flexural and shear failure and to consider the third one as shear failure. Thereby, all the results could be presented together without any risk of confusion.

Following the assumption mentioned above, the graph in Fig.64 shows which one was chosen for each specimen and compares them to the experimental results:

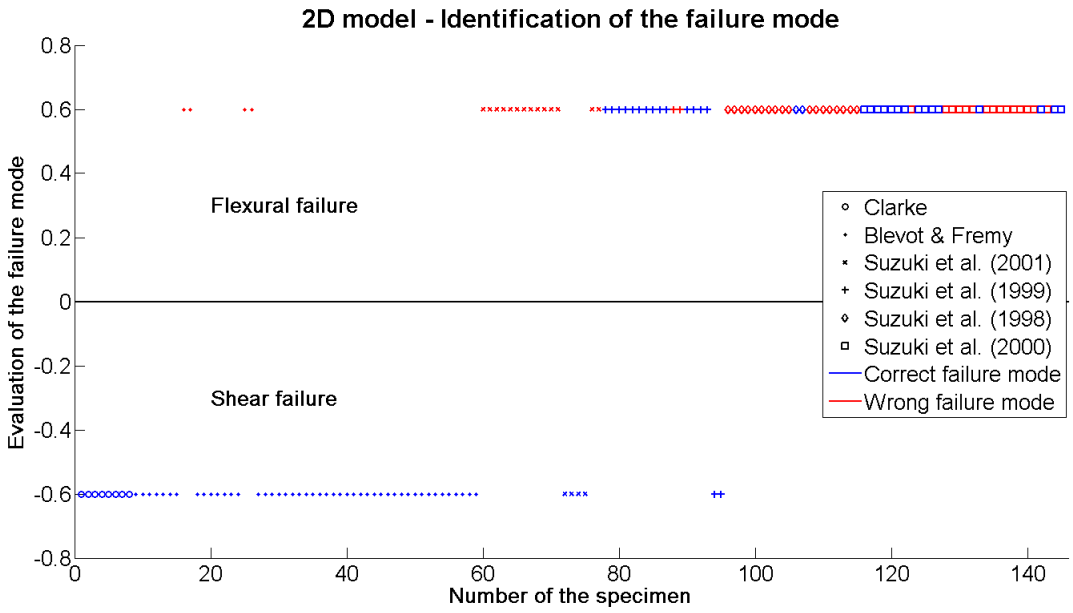

Figure 64: Accuracy of the identification of the failure mode for the 2D model

In this graph, the distinction between the Japanese tests and the other appears clearly. Moreover, it seems the failure modes were more or less correctly identified considering that the success rate reaches 63.4%. Apparently, all the errors made come from the overestimating of the shear strength which have led to the particular situation where the maximum strength of the bottom reinforcement is lower than the minimal shear strength of the pile cap. Under these conditions, the model identifies a flexural failure while the test specimens failed in shear.

Extrapolating these observations, it could mean that the 2D model tend to globally overestimate the shear strength of the pile caps. Following this idea, it should improve the expression of each of its components. As such, it is the reason why the 3D model was developed thereafter. Therefore, it remain to see if it answers to these expectations.

8.2 3D kinematic approach

Now when the results of 2D model have been presented, the interest to do the same for the 3D model is twofold. On the one hand, it will offer the possibility to evaluate its reliability through the accuracy of its results and to determine if the improvements made to realize it are effective enough to capture well the physical phenomena causing the pile cap failure. In the other hand, a comparison between the 2D and 3D model could be realized in order to determine which one gives the better results and thus if the complexity brought to the 3D model was worthed.

Thereby, the same methodology than above will be applied to the 3D model to analyze its ability to determine the shear strength of the pile caps from the database. In particular, the numerical results will be compared to the experimental values through the ratio defined by the Eq.113. Then, they will be completed by the same characteristic numbers to refine the observations that could be made.

8.2.1 Infinitely elastic reinforcement

The hypothesis of the infinitely elastic behavior has already shown its limits through the 2D model. The explanations of this were formulated on the occasion and it is likely that similar behavior will be observed in the 3D model using this hypothesis. Therefore, the purpose of the current chapter is not to repeat what was already said previously. As such, the analysis will mainly focus on the possible improvements brought by the changes made between the 2D and the 3D model.

Knowing that, the results provided by the 3D model when steel is modeled as infinitely elastic are illustrated in Fig.65:

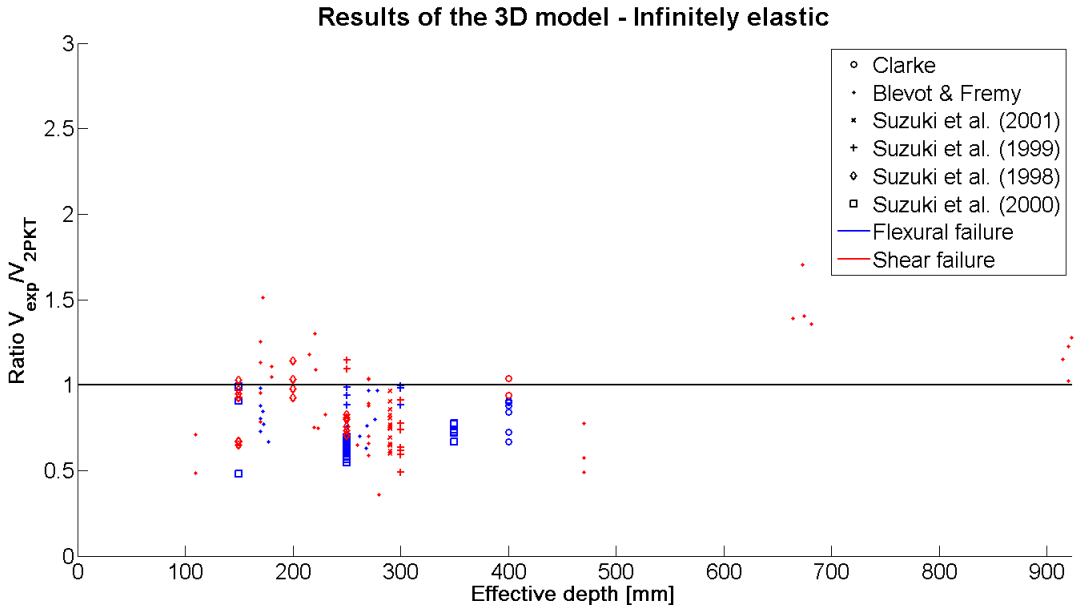

Figure 65: Results furnished by the 3D model with infinitely elastic steel

As expected, they globally show the same characteristics. Indeed, a lot of values remain lower than one, the disparity of the model increases with the decreasing of the effective depth d and most of the Japanese tests are identified as failing in flexure. However, some differences have to be mentioned. First of all, the entire graph seems to have been moved upward. In the present case, that tends to increase the unconservative results by getting closer to one. Moreover, the results distribution seems to be a bit more centered which corresponds to reach

on average better values for V_{exp}/V_{mod}. However, this translation also means that some ratios initially higher than one are getting worse. For example, it is the case for four of the biggest elements for whose their results are obviously less accurate. In order to quantify these two effects, it is necessary to analyze the characteristic statistic values related to this model:

R_{min}	R_{max}	$\bar{R}$	$\sigma/\bar{R}$
0.482	1.788	0.889	29.3%

Table 9: Characteristic numbers of the 3D model with infinitely elastic steel

Compared to the equivalent 2D model given by the Table 7, the 3D one seems to give slightly better results considering that the global graph is indeed moved upward but also improved its mean by getting closer to one. Moreover, the scatter of the results decreased a little bit which improves the reliability of the model.

8.2.2 Plastic softening

A similar approach can be followed when the steel behavior is improved to take into account the plastic range. Once again, the purpose is to compare it to the equivalent 2D model in order to draw the differences and not to observe and discuss the same trends than before. Therefore, the results obtained for the current 3D model are shown in Fig.66

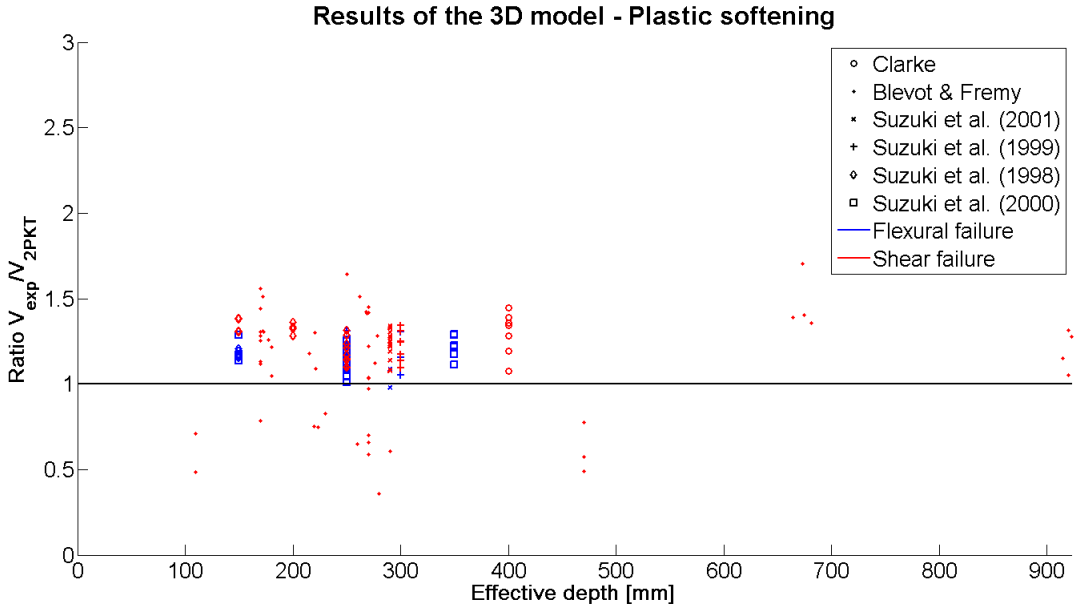

Figure 66: Results furnished by the 3D model with plastic softening steel

Passing from the infinitely elastic hypothesis to the elastic-plastic again results in diminishing shear strength predictions which correspond globally to move upward the entire graph. Thereby, most of the ratios become higher than one and offer a safer approach. In comparison

with the 2D model, it appears that the results are obviously improved by this change or at least most of them seem closer to one than previously. The only exception concern the same four large specimens discussed for the previous 3D model for which it was already observed a loss of accuracy.

This observation is difficult to interpret considering that only a few cases behaves as such while the global tendency tends to show the opposite. However, analyzing carefully their characteristics (they are respectively the specimens N° 52,53,54 and 55), it appears that the corresponding experimental results are difficult to explain. Indeed, the more reinforced specimens from them seem to fail earlier than lower one. Moreover bigger specimens with the same amount of reinforcement reached the same strength. Conversely, it is also possible that this loss of accuracy comes from a weakness of the 3D model which would not capture well a phenomenon in particular. At this stage, these explanations remain hypothetic and it is not possible to clearly identify the reason responsible of these results.

Returning to the main analysis, the characteristic values can now bring the missing informations to complete the analysis of the current model and refine the comparison with the others. In particular, the results calculated by this model gave the the following statistic data:

R_{min}	R_{max}	$\bar{R}$	$\sigma/\bar{R}$
0.657	2.23	1.242	15.7%

Table 10: Characteristic numbers of the 3D model with plastic softening steel

It can be seen that the extreme values are worse than for the corresponding 2D model (detailed in the Table 4). Moreover, the mean of the results shows a slight improvement. These take apart could lead to the conclusion that the 3D model behaves better on average but suffers from a reduced stability which means that the numerical strength calculated through this model considered separately are less accurate but are distributed in such a way that the average is improved. However, the value of the COV shows that this conclusion is not correct. Indeed, the lower the value of $\sigma/\bar{R}$, the lower the scatter of the results and thus the more uniform the accuracy. In that way, the worse external values correspond to some isolated cases which do not represent well the global behavior of the model. In particular, this phenomenon is well represented in the Fig.61.

Concerning the evaluation of the failure mode, the results should be similar to those obtained for the 2D model even if some differences can be observed. This seems logical considering the calculation process remain unchanged and only some parameters of the components differ. Thereby, the failure modes identified by the 3D model are gathered in Fig.67.

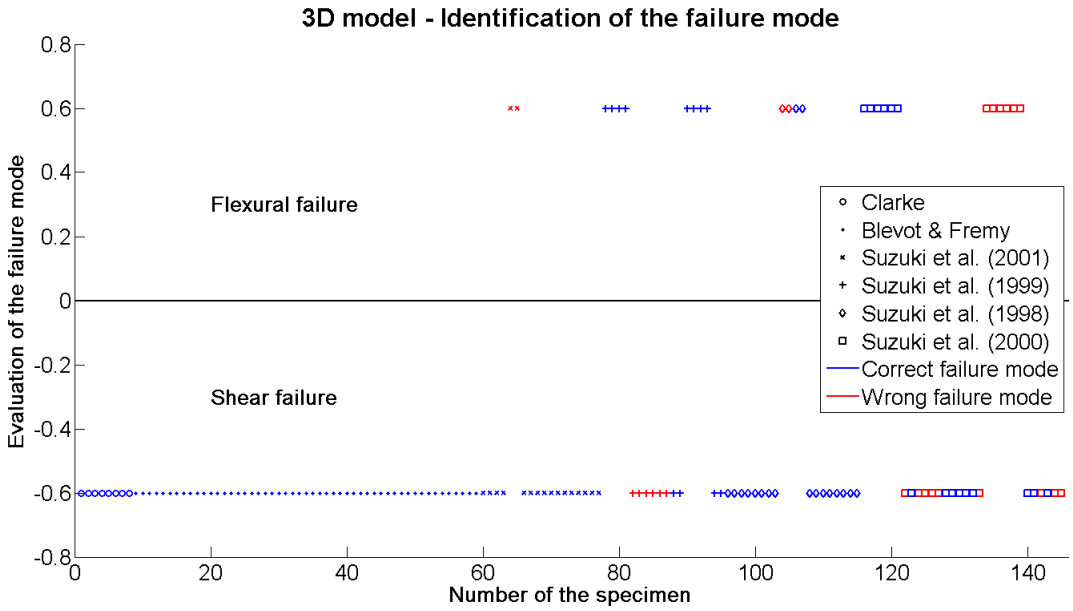

Figure 67: Accuracy of the identification of the failure mode for the 3D model

Regarding the first series of tests, it is obvious that the results remain relatively unchanged. The main differences compared to the 2D model come from the evaluations of the Japanese tests. Indeed, even if many of them are still associated to flexural failure, some inversions can be noticed. As such, it seems that the changes performed between the 2D and 3D model have not changed much the results on the predicted strength but were sufficient to introduce the modification of the failure mode. Once again, that illustrates well the proximity between flexural and shear failure when both occur while the reinforcement has reached its yield strength.

Secondly, this graph shows that errors were made on both sides unlike the 2D model which only overestimated the shear strength. This observation seems to correspond with the global improvement of the results. Indeed, the Figure 61 showed that the predictions were improved on average. Considering that the two failure modes reach close values in several cases, that means that better results are closer from these two. In particular, this graph tends to show that the predictions of 3D model are on average between the real values of flexural and shear failure. In that way, the variability of the model can lead either to overestimate the shear strength and then identify a flexural failure while it should be shear or underestimate the shear strength and thus predict a shear failure while experimentations reported a flexural one.

Finally, the picture clearly illustrate that this model identifies better the failure mode compared to the previous one considering the proportion of correct evaluations. This observation is also confirmed by the success ratio which reaches this time 82.8%.

8.3 Choice of the model

All along this chapter, the differences between the 2D and 3D model were discussed. As such, it appeared that even if it is a bit more complex regarding the failure it describes, the improvements brought by the 3D model allow to reach better results and accuracy. Another way to illustrate this it to express the previous graphs differently. Thus, by opposing the predicted strengths to the experimental ones for both models, the result is shown in Fig.68.

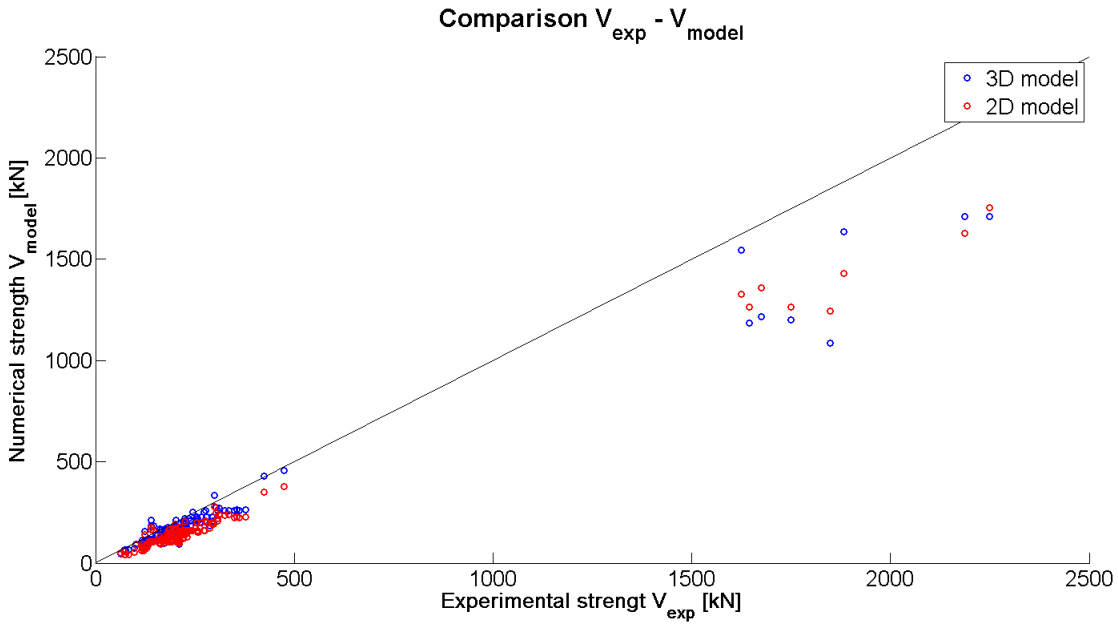

Figure 68: Final values calculated by the two models

Where once again, the predictions of the 3D model are obviously more accurate than the 2D one. The main exception concerns some isolated cases as the four large specimens previously mentioned and for whom no satisfying explanation permit to justify these results at the moment. In particular, these four are located on the upper part of the picture and tend to show that the 3D model is slightly worse than the 2D model.

In summary, the properties targeted for the 2PKT model for pile caps are:

- Being able to describe both corner shear and punching shear failure
- Correspond well with the experimental observations
- Be conservative
- Provide results as accurate as possible
- Remain simple enough to be used with basic analytic tools

Knowing that, the 3D model was initially performed because it captures better the possible crack patterns and failure modes of pile caps because the 2D one was limited and did not fit well with the experimental observations. Moreover, it was shown that the results it provides

are more accurate and more reliable while remaining conservative. Of course, it was necessary to increase the complexity of the model to reach this efficiency. However, the process remained unchanged and only some details through some parameters of each components were modified. This means that finally the complexity did not rise as much.

As such the 3D model fits better with the researched properties and will be preferred to the 2D one. Thus, it represents the final version of the 2PKT model extended for pile caps. Therefore, the global efficiency of this approach will be determine according to the global accuracy of its results. As such, it was already shown that regarding its predictions, the 2PKT for pile caps permits to reach some good results whose disparity remains reasonable. That means that the first purpose of this thesis, which was to develop a numerical model able to predict the shear strength of pile caps is reached. However, it is now necessary to verify if it offers the opportunity to improve significantly the current design methods. In that way, the model will have proved both its efficiency and its utility.

8.4 Comparison with the strut-and-tie model

Before comparing the results given by the 2PKT model and the strut-and-tie model, it is first useful to analyze separately the different results given by the strut-and-tie model in order to identify its properties which will be used during the comparison. Thereby, Figure 69 gathers the results furnished by the strut-and-tie model when the confinement reaches its minimum value:

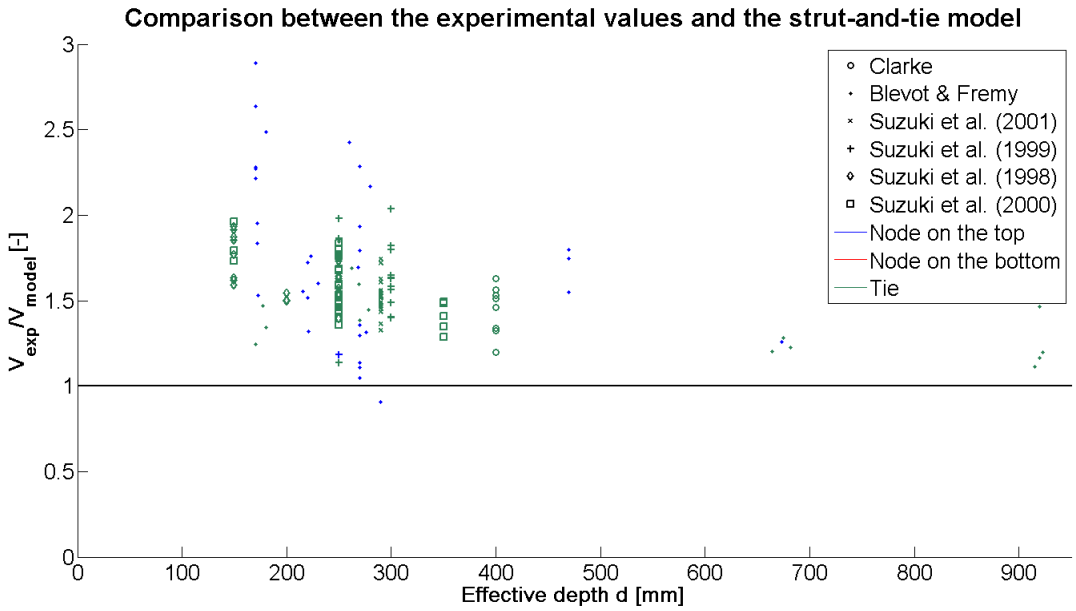

Figure 69: Results of the strut-and-tie model with the minimum confinement

First of all, it appears that this model only identifies two failure modes from the three possible. Indeed, no specimen was predicted to fail by excess of compression in the bottom node.

Thereby, the represented failure mode are respectively the shear failure by excess of compression in the top node and flexural failure by excess in tension in the tie. As such, many pile caps are predicted to fail in flexure, especially the specimens relative to the Japanese tests. Once again, this observation fit well with the experimental results.

Then, most of the specimens reach a ratio > 1 which means that the strut-and-tie model offers the possibility to evaluate the strength of the pile caps in a safe approach. Moreover, the global accuracy of this model seems pretty good considering its value should turn around 1.5 which corresponds to a good result compared to some results obtained by the models previously analyzed.

Concerning the disparity of this model, many specimens are regrouped which tends to indicate a good behavior of the model on the entire domain. However, several others are spread and can reach much higher values. Thereby, the disparity of the results seem better than the models with infinitely elastic steel but it would not reach the same stability than the final model.

The same analyzed can be performed for the strut-and-tie model considering this time the maximum confinement. Thereby, Figure 70 describes the corresponding results:

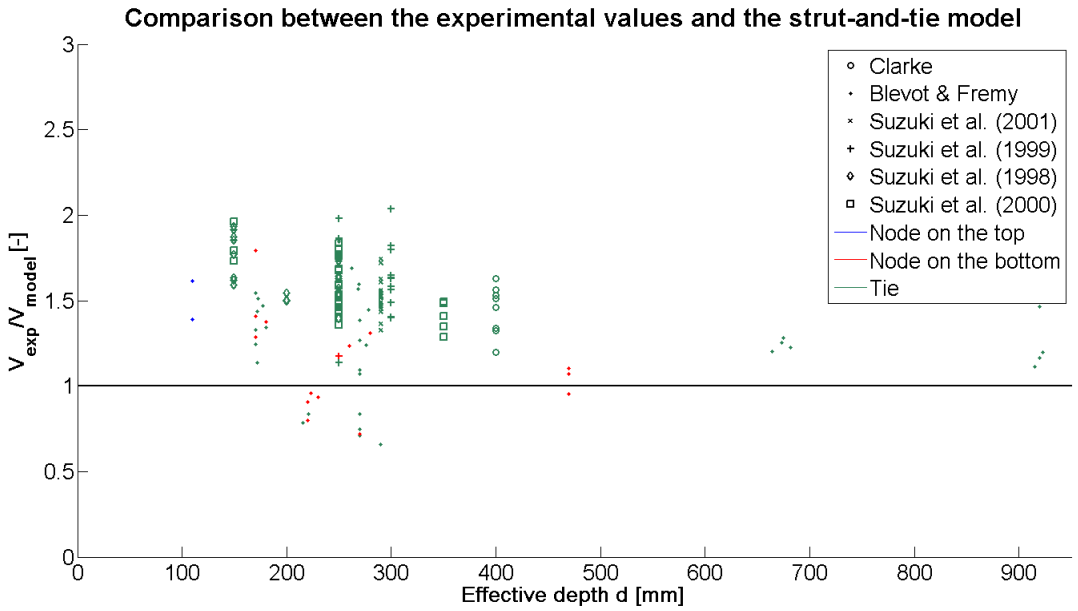

Figure 70: Results of the strut-and-tie model with the maximum confinement

This time, the trend reversed regarding the weakest element identified by the model. Indeed, while the bottom node was not represented in the previous mode, the top one almost disappeared in this one. Thereby, the three failure modes are now described in this model where flexural failure still occurs by excess of tension in the tie but where shear failure can either occur by excess of compression in the top node or in the bottom one.

The change on the confinement only affects the specimens which were identified to fail in shear considering only the strength of the top node is increased. As such, these results are similar to the previous one knowing that a lot of specimens are supposed to fail in flexure and only some particular predictions has changed.

In particular, that led to lower significantly the strength of some pile caps whose ratio could decrease even under one. Thereby it appears that the approach of this model is less safe than the previous one. However, this also led to improve a little the global accuracy of the strut-and-tie model which seems to be a bit lower than previously. It finally improved the stability of the model considering the isolated points are now closer to the general trend which corresponds to a lower the disparity of the results.

The general observations are now made for both models. It is now possible to start the comparison strictly speaking. It will consist on opposing the 3D model with strain hardening steel to the two strut-and-tie model analyzed above. In order to bring more precise informations, the statistic values of each of them will be used. As such, they are summarized in Table 11:

Strut-and-tie			
Confinement min			
R_{min}	R_{max}	$\bar{R}$	$\sigma/\bar{R}$
0.908	3.87	1.655	25.8%
Confinement max			
R_{min}	R_{max}	$\bar{R}$	$\sigma/\bar{R}$
0.659	2.03	1.461	19.7%
3D model			
Strain hardening			
R_{min}	R_{max}	$\bar{R}$	$\sigma/\bar{R}$
0.657	2.23	1.242	15.7%

Table 11: Comparison between the statistic values of each model

Globally, it can be observed that the extreme values of the 3D model seems worse than those of the strut-and-tie models. However, it was already mentioned that these only concerned isolated specimens and thus do not represent the global behavior of the model. Therefore, it is more usefull to concentrate on the two last values.

Concerning the average get by each model, it appears that the best one correspond to the 3D model. More precisely, it shows an improvement of around 40% compared to the lower bound of the confinement and this improvement falls to 20% when compared to the upper bound. The same observation can be made for the coefficient of variation, where the 3D model can bring some improvements but which remain limited considering the increase of complexity to implement this model. Indeed, the results of the strut-and-tie models were

already accurate. In that way, it is difficult to improve further the predictions and the it will remain low compared to the initial model.

However, it is necessary to necessary to mitigate the results of the strut-and-tie models and especially those when the upper bound of the confinement. Indeed, the assumptions to consider the maximum value of the confinement seems a bit unrealistic in the case of a current design method. In practical, it is more common to use the lowest value or if the configuration requires, something in between. In that way, the results brought by the 3D model are even a bit more accurate which could justify to consider this approach in some particular cases, for example when an extra precision is necessary. Otherwise, it seems that the 3D model would require too much effort.

9 Parametric studies

Now the 2PKT model for pile caps has proven its reliability, it can be used to evaluate some properties of the pile caps and especially try to understand the impact of some key parameters on the strength of the element. It is also the opportunity to check if the behaviors announced by the model correspond well with reality by comparing the numerical curves with some experimental results. Finally, it is the occasion to divide the total strength into each of its components and to study them separately in order to represent how changes their relative importance.

Ideally, such an approach require to consider several specimens whose characteristics are identical except for the considered parameter. Thus, it is simply necessary to generate elements based on these specimens and vary the component to study. In that way, experimental results correspond better with the evaluated situation which permits to easily compare them to the predictions and determine if the model capture well or not the corresponding behavior.

Unfortunately, non of the series of tests performed such an analysis which means that the specimens have systematically at least two or more different components. As such, it is difficult to evaluate the accuracy of the described phenomena considering that the others characteristics of the points of comparison do not match perfectly with the predictions. Moreover, it was previously mentioned that most of the specimens were relatively small compared to real pile caps which increases the risk to obtain disturbed experimental results. Therefore, these specimens can potentially bring some more disturbances in the results which could pervert the observations and thus bring to false conclusions.

However, it is possible to try to diminish these parasitic effects by trying to use the biggest tests available and to select those whose characteristics are as close as possible. In that way, the disturbances are limited and it is easier to evaluate the results. Under these conditions, it is also necessary to adapt accordingly the values of the numerical elements. Indeed, the model has to remain consistent with all the experimental tests used to control the predictions. Thereby, only use the characteristics of one of them would lead to center the results on this one in particular and would not represent them all. For that reason, the values used through the model will correspond to the average of all the tests used as comparatives.

By analyzing the different specimens which constitute the database, it appears that eight of them meet these criteria. In particular, they correspond to the specimens N°52-N°59 which represent the biggest pile caps realized by *Blévot and Frémy [2]*. Thereby, their characteristics are given in Figure 71.

N°	b, m	h, m	d, m	e, m	a,m	lb1, m	lb2, m	ag	dg	Ag	ng	dbsq	Absq	nbsq	dbd
52	1.85	0.75	0.67461538	1.2	0.6	0.5	0.35	9.5	16	1407.43351	7	32	6433.98175	8	0
53	1.85	0.75	0.68164447	1.2	0.6	0.5	0.35	9.5	12	791.681349	7	25	3926.99082	8	0
54	1.85	0.75	0.66409301	1.2	0.6	0.5	0.35	9.5	0	0	0	32	4825.48632	6	25
55	1.85	0.75	0.67303738	1.2	0.6	0.5	0.35	9.5	0	0	0	25	2945.24311	6	20
56	1.85	1	0.92	1.2	0.6	0.5	0.35	9.5	12	904.778684	8	28.714108	5180.48629	8	0
57	1.85	1	0.92	1.2	0.6	0.5	0.35	9.5	10	628.318531	8	22.6384628	3220.13247	8	0
58	1.85	1	0.915	1.2	0.6	0.5	0.35	9.5	0	0	0	25	3926.99082	8	25
59	1.85	1	0.9225	1.2	0.6	0.5	0.35	9.5	0	0	0	20	2513.27412	8	20

Abd	nbd	eu	fc, MPa	fyg, MPa	fug, Mpa	fybsq, MPa	fubsq, Mpa	fybd, MPa	fubd, Mpa	|Nf,e|, kN	EFL	Name	Serie N°
0	0	0	37.25	279.3	401	276.2	401.5	277.75	401.5	7000	c	Blevot - 4N1	2
0	0	0	40.8	516.7	822.7	443	764	479.55	764	6700	c	Blevot - 4N1 bis	2
1963.49541	4	0	37.1	278.5	407.5	278.5	407.5	300.3	431.7	6580	c	Blevot - 4N2	2
1256.63706	4	0	34.15	498	819	498	819	474.5	776.5	7390	c	Blevot - 4N2 bis	2
0	0	0	34.15	293.1	397.4	262.1979381	382.6810188	274.96	382.681019	6500	c	Blevot - 4N3	2
0	0	0	49.3	429.5	683.5	469.4756098	805.0853659	453.33	805.085366	9000	c	Blevot - 4N3 bis	2
1963.49541	4	0	35.35	291.4	412.9	291.4	412.9	291.4	412.9	7530	c	Blevot - 4N4	2
1256.63706	4	0	42.3	486.4	811.3	486.4	811.3	486.4	811.3	8750	c	Blevot - 4N4 bis	2

Figure 71: Characteristics of the control specimens

These data show that the only difference comes from the two possible values of the effective depth, considering that the amount of reinforcement and the steel strength can differ but the number $As.f_y$ is keep constant for each specimen. Concerning this ratio, there is an alternation between two values of A_s and two values of f_y. Thereby, four specimens have less reinforcement but the bars used have a higher yielding strength while it is the opposite for the others. Moreover, each of these four are distributed two by two between the possible values of d.

Using the average of all of these values, it is now possible to decide which parameter could be interesting to study, depending in their impact on the shear stress of the pile cap. Thereby, the following terms were identified:

- Effective depth d

It is obviously one of the most important parameter influencing the ultimate strength considering it has an impact on every terms which composed it. Generally, it can be considered that the higher, the more strengthened the pile cap. The purpose is now to determine how each component is influenced and quantify the effect on the total strength.

- Reinforcement ratio ρ_l

It represents the relative importance of the bottom reinforcement and give an idea if the pile cap is heavily or slightly reinforced. In particular, the strain on the steel has a direct impact on the crack width (see Equation 37). Thereby, it has an indirect impact on the terms depending on w but also influence directly the dowel effect generated by the bottom reinforcement itself.

9.1 Influence of the effective depth d

In this study, a distinction was made between the eight tests used to control the predictions of the model. Indeed, four of them correspond to some litigious specimens for whom it is difficult to explain their results. Knowing that they are now used as comparatives, some precautions have to be taken. Indeed, considering the fact that no justification has been validated yet, it is impossible to properly interpret the differences between the model and these results. Moreover, it could lead to disturb the results and bring to some wrong conclusions. As such distinguish these four from the others offers the possibility to analyze them separately which permits to mitigate the results and decide if they are relevant or not.

Following these, Figure 72 resumes the predictions of the model for the impact of the effective depth.

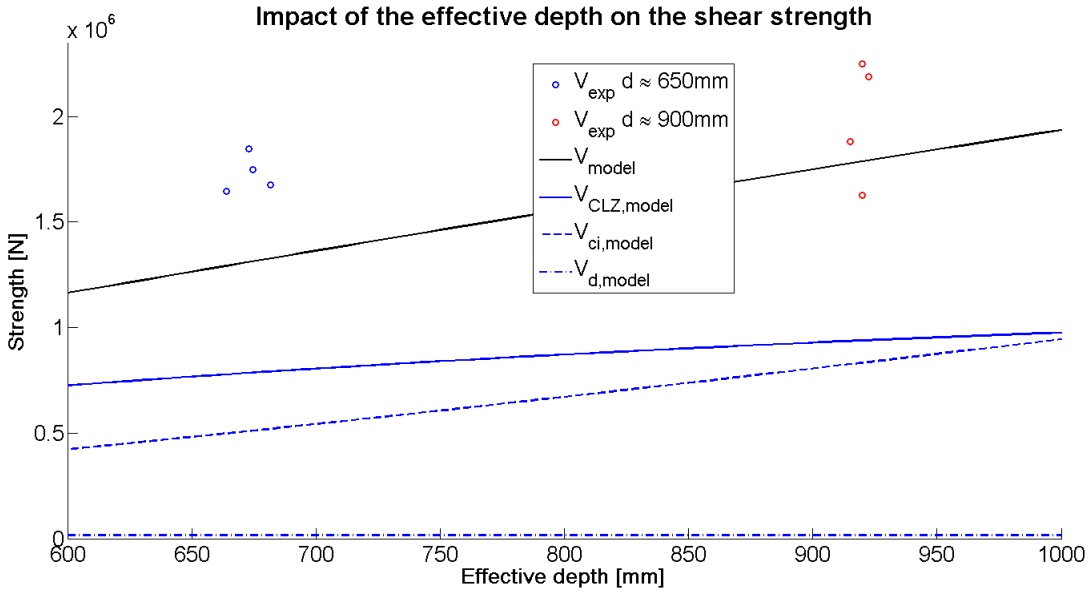

Figure 72: Study of the influence of the effective depth d

This graph clearly shows that the effective depth d represents well the main difference between all the specimens, considering they are split into two distinct groups. Thereby, the experimentations determined that these two groups reached more or less the same strength while the only parameter differentiating them is a decrease of d.

This results can be a bit confusing compared to the expectations that assume that d has a positive impact on the strength of the pile cap. In particular, this is confirmed by the predictions of the 2PKT model which clearly depict an improvement on the ultimate load when d is increased. The mismatch between predictions and experimentations can could comes from two different sources.

The first one consists to say the comparatives values are correct. In that way, even if the

common sense tends to show the opposite, the experimental results are consistent and can be explained by a physical phenomenon. In particular, this means that the 3D model is not able to capture this phenomenon and that some improvements have to be performed to correct this defect.

The second one is the exact opposite. It appears that something went wrong during the experimentations (either during the cast of concrete or the during the test itself) which altered the final results. Thereby, the reported strengths of the pile caps do not correspond any more to reality and the behavior they describe is disturbed.

In this case, determine to which situation correspond these tests would require to perform some more analysis on the database and push the developments of the model further to try to identify some leads. However, this approach exceed the purpose of this thesis. For that reason and because the results cannot be trusted under the current conditions, the only remaining solution is to purely exclude them from the comparative study in order to suppress the problem instead of solving it.

Regarding now the predictions of the model, Figure 72 illustrates that the global strength of the pile cap tends to increase steadily with the effective depth d. To demonstrate that, it is necessary to study each component of the strength separately. As a reminder, here are the equations expressed for the 3D model of the three terms which contribute to the shear strength of piles caps:

$$V_{CLZ} = \frac{k.f_{avg}\frac{2\pi}{4}l_{b1e}^2 \sin^2\alpha_0}{2} \tag{114}$$

$$V_{ci} = 2\frac{0.18\sqrt{f_c}}{0.31+\frac{24w}{a_{ge}+16}}\frac{1.5lb_{1e}+lb_2}{2}d \tag{115}$$

$$V_d = 2n_b f_{ye}\frac{d_b^3}{3l_k} \tag{116}$$

First, it was previously shown that the dowel effect contributes relatively little to the total strength of the pile caps. Thereby, any change impacting V_d will not be impact much the global strength. As such, only the two other components will be analyzed.

Concerning the aggregate interlock, the relation is immediate because V_ci is linearly dependent of d. Indeed, it only develops between the two sides of the critical crack. Thereby, the higher d, the longer the crack and the larger the surface on which will develop friction.

The link between d and the critical loading zone is a bit more difficult to evaluate. Indeed, it does not impact directly V_{CLZ} but influences the angle of the critical crack α_0. This describes the fact that when the effective depth increases, the critical crack tends to straighten. Thereby, the area on which is reached the concrete strength increases which influences accordingly the corresponding strength.

Finally, it can be concluded that the physical phenomena described above are consistent with the predictions of the 3D model represented in Figure 72 considering that both of them describe the positive effect of d on the shear strength of the pile cap. However, because of the exclusion of some of the comparative specimens, it was not possible to determine if it was also the case with the experimental results.

9.2 Influence of the reinforcement ratio ρ_l

The next parameter to be studied is the reinforcement ratio. It represents the relative importance of the bottom steel reinforcement compared to the concrete section. As such, it takes an important place in the determination of the shear strength of pile caps especially because it has a direct impact on the crack widening at failure through its strain value ε_t.

Thereby, to try to describe the influence of this parameter, a set of data will be created based on some particular pile caps of the database, in the same way that was done for the effective depth d. However, the number of comparative specimens is now reduced by two according the the discussion conducted above. In that way, Figure 73 describes the results determined by the model by varying the value of the reinforcement ratio while the other parameters are fixed.

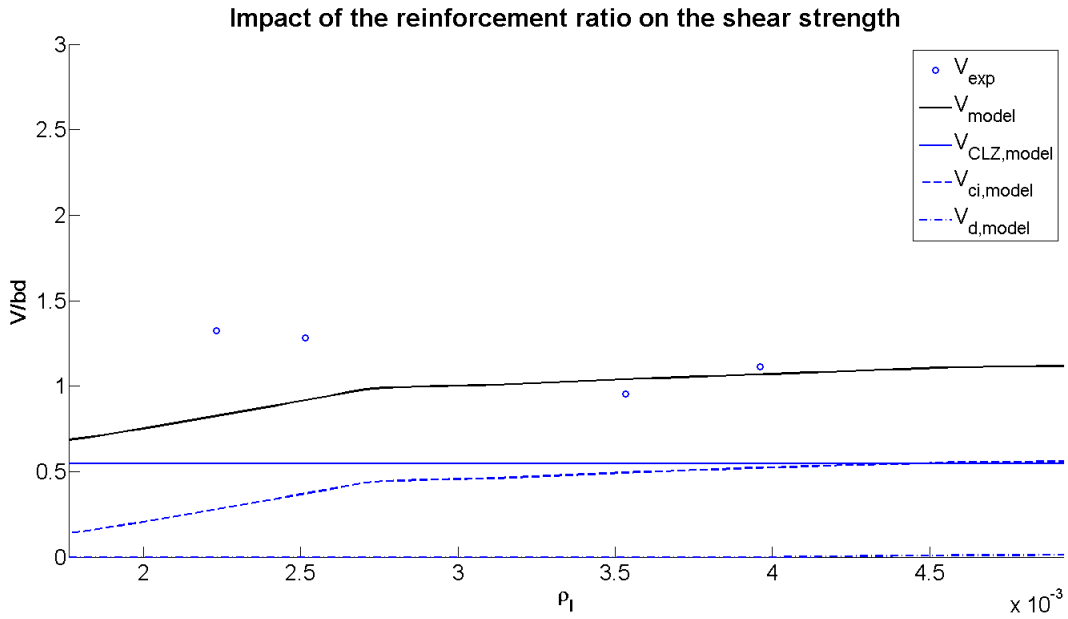

Figure 73: Study of the influence of the reinforcement ratio ρ_l

In particular, the 3D model tends to show that ρ_l also has a beneficial effect on the shear strength of the pile cap. However, this property does not evolve constantly and a change of the slope can be noticed. Concerning the impact on each of the components of the shear strength, the observations differ from one to another.

Thereby, the strength of the critical loading zone remains unchanged considering it is not influenced by the bottom reinforcement.

Concerning the aggregate interlock, it shows the same properties than the total shear strength which means that it is this term which lead to observe this phenomenon. In particular, the reinforcement ratio for which the change of slope occurs corresponds to the value which marks the transition between the plastic and the elastic range of the steel. For lower one, the reinforcement is more solicited at failure and the corresponding stress is higher than the yielding strength. Thereby, by progressively increasing ρ_l, the stress at failure will gradually decrease and finally reach f_y to stay in the elastic range for higher values of the reinforcement ratio.

Moreover, this observation is directly linked to the change of slope. Indeed, the strain in the plastic range is way higher than in elastic one. Therefore, a small increase of ρ_l under this condition will lead to decrease significantly the strain on the reinforcement at failure. The corresponding impact on the elastic range is thus less important considering the smaller variations of the strain. Following this, it appears that it has a direct impact on the final crack width knowing that it depends especially on the strain ε_t in the reinforcement. Thereby, Figure 74 describes predicted final crack width for the considered values of ρ_l.

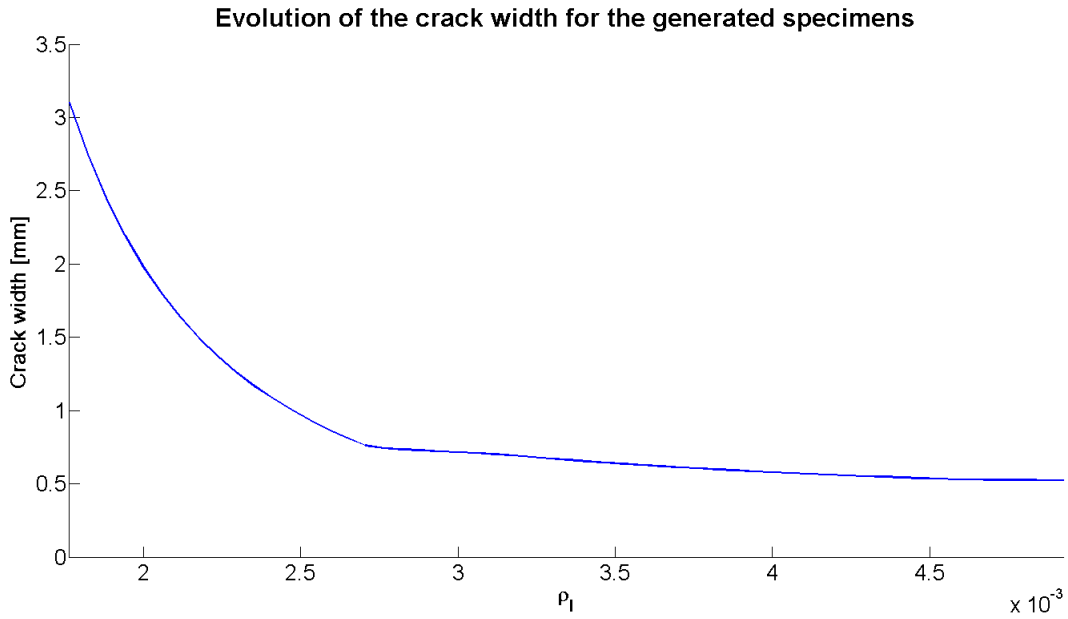

Figure 74: Evolution of the crack width for several reinforcement ratio ρ_l

This graph clearly shows that the decrease observed for the crack width is clearly more significant for lower values of ρ_l for which the plastic range have been reached. Then, developing the reasoning a bit further, it was previously mentioned that the strength provided by the aggregate interlock decreased when the crack width increased. As such, the more significant the decrease of the crack width, the more significant the strengthening of the aggregate in-

terlock. This explains why the slope of V_{ci} is bigger in the plastic range than in the elastic one.

A similar explanation can justify the behavior of the dowel effect which is equal to zero until the reinforcement ratio reaches a sufficiently high value. This particular point corresponds once again to the transition between the plastic and the elastic range of the steel. Indeed, the bottom reinforcement is not able to develop a dowel effect if it has reached plasticity which means that V_d falls 0.

Even if it is not clear in Figure 73, the entrance into the plastic range occurs at the same time for both the aggregate interlock and the dowel effect. However, the fact that V_d remains small compared to the other components tends to make difficult the moment from when it differs from 0

Now the predictions of the 3D model are explained, it is possible to compare them to the experimental results. However they seem to represent that ρ_l has no impact on the ultimate load considering that the comparative specimens reaches more or less the same ultimate load for different values of the reinforcement ratio. The reason for this is simple: These four pile caps were designed in such a way that the number $A_s.f_y$ is more or less constant which means that the less the reinforcement, the higher the yielding strength. Therefore, these specimens get some extra strength due to this increase which is not represented through the generated specimen considering that $A_s.f_y$ progressively decreases with lower values of A_s.

In conclusion, the differences between the comparative specimens does not offers the possibility to represent experimentally the impact of only the amount of reinforcement. Thereby, this study will be once again limited to discuss the model predictions only without verifying if it corresponds well to reality.

10 Conclusion

Through this thesis, a new model was developed to predict the shear strength of deep pile caps. In particular, it is based on the same principles than the 2PKT model for deep beams and thus is governed by the same physical phenomena. As such, several crack patterns were compared to determine which one fit better with reality, based on the observations made during some experimental tests found on the literature. At this occasion, two main failure modes were chosen and the initial 2PKT was adapted accordingly to take into account the changes of configuration.

The first one models a one-way shear failure, similar to what happens for deep beams and correspond to the "2D model". The second one, called "3D model", is in fact a combination between the one way shear failure used in the first model and the punching shear failure. In that way, this model is able to capture both corner shear failure and punching shear failure which represents the two main failure modes observed experimentally. Both of them are respectively represented in Figure 75 and 76 .

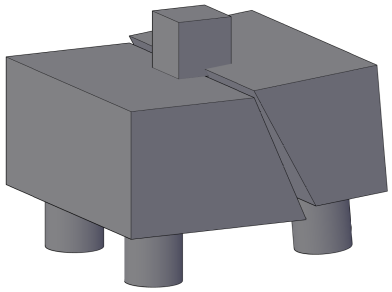

Figure 75: 2D model

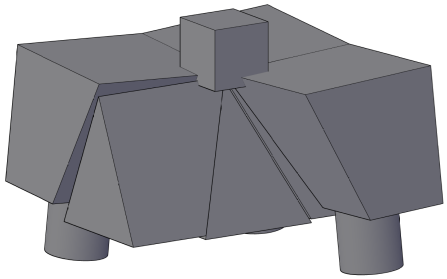

Figure 76: 3D model

Then, the characteristics of the pile caps described during the experimental tests were used through the these two models to evaluate the strength of these elements. Therefore, it was possible to compare their predictions to the ultimate load reported by the tests. At this occasion, a comparative study was performed to try to determine which model fit better with reality by evaluating their respective accuracy regarding the ratio R between the experimental and the predicted strength. Thereby, it was demonstrated that the 3D model offered a better efficiency and corresponded better to reality. In particular, the Table 12 illustrates the characteristics of the results predicted by this model:

R_{min}	R_{max}	$\bar{R}$	$\sigma/\bar{R}$
0.657	2.23	1.242	15.7%

Table 12: Results of the 3D model

Which shows that the predictions globally reaches a good accuracy.

In parallel, a strut-and-tie model was developed to represent a classical design method used for pile caps. For that reason, the model had to stay simple and followed reasonable assumptions in order to correspond as well as possible with what is done in practice. In that way, it was also possible to evaluate the efficiency of common way to design such elements and thus determine if the 2PKT model for piles caps brings notable improvements.

Thereby, the strut-and-tie model showed that current design method can also predict accurate results, see Table 13.

Strut-and-tie			
Confinement min			
R_{min}	R_{max}	$\bar{R}$	$\sigma/\bar{R}$
0.908	3.87	1.655	25.8%
Confinement max			
R_{min}	R_{max}	$\bar{R}$	$\sigma/\bar{R}$
0.659	2.03	1.461	19.7%

Table 13: Results of the strut-and-tie model

As such, the 2PKT model only provides slight improvements compared to what is being done nowadays, which means that its utility seem limited to specific cases where accuracy prevails over simplicity.

Finally, a parametric study was performed on two important parameters of the shear strength of the pile cap. Thereby, the model clearly described how they impact the global strength of the element through the different elements which compose it.

Concerning the possible improvements which can be brought to the 2PKT model for pile cap, this mainly concerns some particular specimens for which the model seemed to deviate from reality by predicting really conservative strength while the other one were globally way better predicted. Therefore, it should investigate the reasons why these particular ones are so badly predicted and especially by determining which are the main differences between these and the rest of the specimens evaluated.

For now, one lead looks promising. It assumes that these results comes from the fact that actually, the 3D model does not take into account the confinement right under the column. Globally, that corresponds to underestimate the strength provided by this area. As such, as long as this one is not too significant compared to the other components, the final strength is not affected much. However, as soon as this changes, the prediction of the ultimate strength of the pile cap could be significantly underestimated which could lead to this kind of phenomena.

Moreover, it is also possible to refine the model in order to take into account the potential asymmetry of pile caps. Indeed, it would have an impact on most of the parameters of the model and on some properties used because of the symmetry of the system. Therefore, it would be necessary to express each component in both directions and would increase the complexity of the model.

References

[1] B. Mihaylov, E. Bentz, and M. Collins, "Two-parameter kinematic theory for shear behavior of deep beams," *ACI Structural Journal*, vol. 110, no. 3, pp. 447–455, 2013. cited By 1.

[2] J. Blévot and R. Frémy, "Semelles sur pieux," *Annales de l'Institut Technique du bâtiment et des Travaux Publics*, vol. 20, pp. 223–279, February 1967.

[3] J. Clarke, "Behaviour and design of pile caps with four piles," *Technical report of the Cement and Concrete Association*, vol. 42, pp. 1–19, November 1973.

[4] K. Suzuki, K. Otsuki, and T. Tsubata, "Influence of bar arrangement on ultimate strength of four-pile caps," *Transactions of the Japan Concrete Institute*, vol. 20, pp. 195–202, 1998.

[5] K. Suzuki, K. Otsuki, and T. Tsubata, "Experimental study on four-pile caps with taper," *Transactions of the Japan Concrete Institute*, vol. 21, pp. 327–334, 1999.

[6] K. Suzuki, K. Otsuki, and T. Tsuchiya, "Influence of edge distance on failure mechanism of pile caps," *Transactions of the Japan Concrete Institute*, vol. 22, pp. 361–368, 2000.

[7] K. Suzuki and K. Otsuki, "Experimental study on corner shear failure of pile caps," *Transactions of the Japan Concrete Institute*, vol. 23, pp. 303–310, 2001.

[8] U. b. Jensen and L. Hoang, "Collapse mechanisms and strength prediction of reinforced concrete pile caps," *Engineering Structures*, vol. 35, pp. 203–214, 2012. cited By 1.

Appendix

Geometrical properties					Experimental failure		2D model				3D model				Strut-and-tie model			
							Infinitely elastic		Strain hardening		Infinitely elastic		Strain hardening		Lower bound		Upper bound	
N°	Name	b, m	d, m	a/d	EFL	Fexp, kN	Fmod, kN	Ratio	Fmod, kN	Ratio	Fmod, kN	Ratio	Fmod, kN	Ratio	Fmod, kN	Ratio	Fmod, kN	Ratio
1	Clarke - A1	0.95	0.4	0.75	c	1110	1180.72502	0.94010035	969.038961	1.14546478	1182.13543	0.93897871	1031.8065	1.0757831	927.398151	1.19689693	927.398151	1.19689693
2	Clarke - A2	0.95	0.4	0.75	c	1420	1395.49422	0.89577571	278.03095	5.10734507	1336.7694	0.89577571	1045.50821	1.35819115	927.398151	1.53116544	927.398151	1.53116544
3	Clarke - A3	0.95	0.4	0.75	c	1340	1505.14311	0.66761178	275.236598	4.86853859	1411.09892	0.66761178	1044.12276	1.28337399	918.07733	1.45957204	918.07733	1.45957204
4	Clarke - A4	0.95	0.4	0.75	c	1230	1183.72654	1.03909134	971.618918	1.26592842	1184.35328	1.03854147	1031.98609	1.19187653	927.398151	1.32629119	927.398151	1.32629119
5	Clarke - A5	0.95	0.4	0.75	c	1400	1372.92205	0.90829624	278.03095	5.03541063	1320.88201	0.90829624	1043.96877	1.34103628	927.398151	1.50959973	927.398151	1.50959973
6	Clarke - A6	0.95	0.4	0.75	c	1230	1346.22713	0.72630724	275.236598	4.46888244	1300.44481	0.72630724	1032.71406	1.19103636	918.07733	1.33975642	918.07733	1.33975642
7	Clarke - A8	0.95	0.4	0.75	c	1510	1395.49422	0.84238511	278.03095	5.43105004	1336.7694	0.84238511	1045.50821	1.44427369	927.398151	1.62821114	927.398151	1.62821114
8	Clarke - A9	0.95	0.4	0.75	c	1450	1372.92205	0.87697568	278.03095	5.21524672	1320.88201	0.87697568	1043.96877	1.38893043	927.398151	1.56351401	927.398151	1.56351401
9	Blevot - 1,1	0.6	0.25	0.84	c	850	638.933363	0.75482678	526.849067	1.61336529	647.846196	0.75482678	517.960158	1.64105286	461.253551	1.84280424	461.253551	1.84280424
10	Blevot - 1,2	0.6	0.268	0.78358209	c	880.4	638.479511	0.62981789	522.206691	1.68592248	667.786374	0.62981789	619.161537	1.42192295	519.919018	1.69334063	561.220028	1.5687252
11	Blevot - 1,3	0.6	0.262	0.80152672	c	871	679.94142	0.69866284	559.081968	1.55791109	695.317463	0.69866284	575.979735	1.51220598	516.024561	1.68790416	516.024561	1.68790416
12	Blevot - 2,1	0.6	0.2781	0.75512406	c	747.5	768.987185	0.96571574	592.63737	1.26131094	777.425494	0.96571574	583.753741	1.28050571	516.912847	1.44608517	516.912847	1.44608517
13	Blevot - 2,2	0.6	0.276	0.76086957	c	810	760.921524	0.79871657	599.857177	1.35032143	778.149354	0.79871657	720.957953	1.12350519	616.494474	1.31388039	654.106106	1.2383312
14	Blevot - 2,3	0.6	0.269	0.78066914	c	740	717.217102	0.76271257	125.673977	5.88825161	734.437026	0.76271257	524.001725	1.41220909	464.1256	1.594396	464.1256	1.594396
15	Blevot - 3,1	0.6	0.18	1.16666667	c	475	394.017599	1.20552991	334.971007	1.41803317	428.239225	1.10919312	391.194643	1.21422931	354.232656	1.34092662	354.232656	1.34092662
16	Blevot - 3,2	0.6	0.177	1.18644068	c	540	725.555687	0.67024119	99.2031338	5.44337643	629.308337	0.67024119	429.49953	1.25727728	367.045954	1.47120543	367.045954	1.47120543
17	Blevot - 3,3	0.6	0.173	1.21387283	c	510	631.609127	0.77297055	92.5027993	5.51334666	557.656399	0.77297055	391.298944	1.30335133	333.131969	1.53092482	337.669683	1.51035176
18	Blevot - 1A,1	0.6	0.27	0.77777778	c	1150	859.316018	1.33827367	859.316018	1.33827367	1106.74442	1.03908362	1106.74442	1.03908362	503.132752	2.28567907	907.875098	1.26669407
19	Blevot - 1A,2	0.6	0.27	0.77777778	c	900	824.821708	1.0911449	824.821708	1.0911449	870.632014	1.0337318	870.632014	1.0337318	664.282486	1.35484529	1074.20806	0.83782652
20	Blevot - 1A,2 bi	0.6	0.27	0.77777778	c	1177.5	773.461528	0.8928975	773.461528	1.52237695	830.437702	0.8928975	830.437702	1.41792695	609.417814	1.93217194	1074.20806	1.09615637
21	Blevot - 1A,3	0.6	0.27	0.77777778	c	1185	810.63872	0.96629492	771.412104	1.5361439	815.874279	0.96629492	815.874279	1.45242966	661.292023	1.79194661	935.613007	1.2665493
22	Blevot - 3A,1	0.6	0.17	1.23529412	c	815	556.325569	1.46496952	556.325569	1.46496952	718.470126	1.13435475	718.470126	1.13435475	308.958819	2.63789201	633.996325	1.28549641
23	Blevot - 3A,2	0.6	0.17	1.23529412	c	900	769.809316	0.72935288	159.825751	5.63113262	688.342195	0.72935288	688.342195	1.30748922	396.571324	2.26945305	676.681082	1.33002093
24	Blevot - 3A,3	0.6	0.172	1.22093023	c	665	393.951839	1.68802359	393.951839	1.68802359	440.382872	1.51004965	440.382872	1.51004965	340.43803	1.95336579	585.507161	1.13576749
25	Blevot - 3A,3 bi	0.6	0.172	1.22093023	c	842.5	860.881632	0.84385462	137.91256	6.10894324	732.086699	0.84385462	643.507378	1.3092313	458.722189	1.8366236	585.507161	1.43892348
26	Blevot - Q,1	0.6	0.17	1.23529412	c	408	396.294871	1.02953641	336.527454	1.21238251	428.700041	0.95171439	364.45009	1.11949485	327.776403	1.24475098	327.776403	1.24475098
27	Blevot - Q,2	0.6	0.27	0.77777778	c	650	720.252197	0.90246167	571.103613	1.13814724	741.105349	0.87706829	669.241442	0.97124888	570.824369	1.13870401	605.94602	1.07270281
28	Blevot - Q,2 bis	0.6	0.27	0.77777778	c	510	532.489491	0.95776538	411.433971	1.23956706	572.241553	0.89123203	417.066015	1.222828	368.545468	1.3838184	368.545468	1.3838184
29	Blevot - 6,1	0.6	0.11	1.90909091	c	250	285.837116	0.874624	285.837116	0.874624	352.493392	0.70923315	352.493392	0.70923315	74.8687571	3.33917658	179.685017	1.39132357
30	Blevot - 6,2	0.6	0.11	1.90909091	c	290	529.410732	0.54777885	529.410732	0.54777885	598.17416	0.48480864	598.17416	0.48480864	74.8687571	3.87344483	179.685017	1.61393535
31	Blevot - 6,3	0.6	0.18	1.16666667	c	650	487.776142	1.3325785	487.776142	1.3325785	621.502648	1.04585234	621.502648	1.04585234	261.493015	2.48572605	471.849619	1.37755754
32	Blevot - 6,4	0.6	0.17	1.23529412	c	850	846.202341	1.00448789	846.202341	1.00448789	1080.50505	0.78666916	1080.50505	0.78666916	322.197883	2.6381303	661.163435	1.28561254
33	Blevot - 6,5	0.6	0.26	0.80769231	c	842.5	1009.23566	0.83479016	1009.23566	0.83479016	1293.07383	0.65154826	1293.07383	0.65154826	347.144659	2.42694214	682.602638	1.23424662
34	Blevot - 6,6	0.6	0.28	0.75	c	810	1792.67316	0.4518392	1792.67316	0.4518392	2255.55849	0.35911283	2255.55849	0.35911283	373.975382	2.16591797	618.599279	1.30940987
35	Blevot - 9,A1	0.6	0.47	0.44680851	c	1200	1640.77804	0.73136035	1640.77804	0.73136035	2091.05243	0.5738737	2091.05243	0.5738737	774.839346	1.54870814	1259.37092	0.95285668
36	Blevot - 9,A2	0.6	0.47	0.44680851	c	1900	2990.65414	0.63531251	2990.65414	0.63531251	3878.37683	0.48989567	3878.37683	0.48989567	1089.06882	1.74460967	1770.09804	1.07338687
37	Blevot - 9,A3	0.6	0.47	0.44680851	c	1700	1692.10165	1.00466778	1692.10165	1.00466778	2188.55585	0.77676793	2188.55585	0.77676793	946.139143	1.79677589	1537.78991	1.10548261
38	Blevot - 10,1a	0.6	0.23	0.91304348	c	850	790.619043	1.07510691	790.619043	1.07510691	1028.67297	0.82630732	1028.67297	0.82630732	530.364893	1.60267018	908.483864	0.93562476
39	Blevot - 10,1b	0.6	0.2211	0.94979647	c	800	707.571166	1.13062832	707.571166	1.13062832	733.236731	1.09105282	733.236731	1.09105282	605.778108	1.32061557	958.111479	0.83497591
40	Blevot - 10,2a	0.6	0.22	0.95454545	c	750	766.326564	0.97869503	766.326564	0.97869503	995.961028	0.75304151	995.961028	0.75304151	494.957472	1.5152817	940.472133	0.7974718
41	Blevot - 10,2b	0.6	0.2202	0.95367847	c	800	565.313551	1.41514386	565.313551	1.41514386	614.376582	1.30213297	614.376582	1.30213297	464.301551	1.72301815	880.407227	0.90867041
42	Blevot - 10,3a	0.6	0.2231	0.94128194	c	760	789.456579	0.96268753	789.456579	0.96268753	1018.81114	0.7459675	1018.81114	0.7459675	431.814441	1.76001525	794.664266	0.95637873
43	Blevot - 10,3b	0.6	0.2154	0.97493036	c	740	582.772486	1.26979227	582.772486	1.26979227	627.076786	1.18007877	627.076786	1.18007877	475.791781	1.55530219	941.037288	0.78636629
44	Blevot - 11,1a	0.6	0.27	0.77777778	c	562.5	674.498171	0.83395334	654.608756	0.8592919	853.982504	0.6586786	853.982504	0.6586786	507.791643	1.10773781	792.774951	0.70953301
45	Blevot - 11,1b	0.6	0.27	0.77777778	c	492.5	645.71998	0.76271451	645.71998	0.76271451	839.514134	0.58664885	839.514134	0.58664885	380.202831	1.29536121	686.054887	0.71787259
46	Blevot - 11,2a	0.6	0.29	0.72413793	c	557.5	772.918295	0.72129228	710.268546	0.78491439	919.726139	0.6061587	919.726139	0.6061587	613.596447	0.90857762	845.528793	0.6593507
47	Blevot - 11,2b	0.6	0.27	0.77777778	c	585	708.20306	0.82603427	649.061132	0.90130185	836.69695	0.69917788	836.69695	0.69917788	558.806847	1.04687336	780.135586	0.74986965
48	Blevot - 12,1a	0.6	0.17	1.23529412	c	840	416.167669	0.80574199	416.167669	2.01841724	539.097454	0.80574199	539.097454	1.55815984	228.592872	3.67465526	469.082066	1.79073143
49	Blevot - 12,1b	0.6	0.17	1.23529412	c	692.5	416.512777	0.9809484	416.512777	1.66261406	540.523059	0.9809484	540.523059	1.28116643	239.538494	2.89097585	491.542935	1.40882912
50	Blevot - 12,2a	0.6	0.17	1.23529412	c	750	398.7123	0.88124731	398.7123	1.88105559	520.622335	0.88124731	520.622335	1.4405836	338.618432	2.21488239	485.623568	1.5444061
51	Blevot - 12,2b	0.6	0.17	1.23529412	c	640	391.658334	1.63407732	391.658334	1.63407732	509.535776	1.25604527	509.535776	1.25604527	280.452447	2.2820268	481.165238	1.3301044
52	Blevot - 4N1	1.85	#REF!	#REF!	c	7000	5748.2046	1.21777154	5338.40015	1.31125427	4987.04498	1.40363683	4987.04498	1.40363683	5466.40235	1.28054972	5466.40235	1.28054972
53	Blevot - 4N1 bi	1.85	#REF!	#REF!	c	6700	6086.40141	1.10081468	5735.76547	1.16810913	4939.0936	1.3565242	4939.0936	1.3565242	5464.62568	1.22606751	5464.62568	1.22606751
54	Blevot - 4N2	1.85	#REF!	#REF!	c	6580	5705.84632	1.15320316	5313.58867	1.23833447	4742.20621	1.38753983	4742.20621	1.38753983	5480.49924	1.20062055	5480.49924	1.20062055
55	Blevot - 4N2 bi	1.85	#REF!	#REF!	c	7390	5298.88072	1.39463415	5065.67385	1.45883849	4336.63282	1.70408709	4336.63282	1.70408709	5876.83721	1.25747911	5891.53185	1.25434271

56	Blevot - 4N3	1.85	0.92	0.65217391	c	6500	7875.8725	0.82530539	1595.88677	4.07297066	6341.16786	1.02504777	6171.36617	1.05325139	5585.08317	1.16381436	5585.08317	1.16381436
57	Blevot - 4N3 bi	1.85	0.92	0.65217391	c	9000	10122.2209	0.88913294	2061.11039	4.36657834	7334.13221	1.22713905	6844.25733	1.31497101	6135.06407	1.46697735	6135.06407	1.46697735
58	Blevot - 4N4	1.85	#REF!	#REF!	c	7530	8149.14413	0.92402342	7333.23901	1.02683139	6540.15048	1.15134966	6540.15048	1.15134966	6773.45282	1.11169299	6773.45282	1.11169299
59	Blevot - 4N4 bi	1.85	#REF!	#REF!	c	8750	9153.21465	0.9559483	8469.37776	1.03313375	6845.73646	1.27816781	6845.73646	1.27816781	7295.23664	1.19941277	7295.23664	1.19941277
60	uki - BPL 35/3	0.8	0.29	0.86206897	c	960	1419.86003	0.67612298	158.586128	6.05349288	1388.94592	0.69117162	843.325907	1.13834995	633.44728	1.51551681	633.44728	1.51551681
61	uki - BPL 35/3	0.8	0.29	0.86206897	c	941	1486.15502	0.63317755	158.586128	5.93368417	1440.5559	0.65322005	874.903	1.0755478	633.44728	1.48552221	633.44728	1.48552221
62	uki - BPB 35/3	0.8	0.29	0.86206897	f+c	1029	1402.0272	0.73393726	158.586128	6.48858769	1374.9867	0.74837088	835.21868	1.23201268	633.44728	1.62444458	633.44728	1.62444458
63	uki - BPB 35/3	0.8	0.29	0.86206897	f+c	1103	1393.08545	0.79176765	158.586128	6.95521109	1367.9746	0.80630152	831.223847	1.32695904	633.44728	1.74126567	633.44728	1.74126567
64	uki - BPH 35/3	0.8	0.29	0.86206897	c	980	1739.11764	0.56350415	158.586128	6.17960732	1633.75576	0.59984486	999.581225	0.98041057	633.44728	1.54709008	633.44728	1.54709008
65	uki - BPH 35/3	0.8	0.29	0.86206897	f+c	1088	1789.23433	0.60808134	158.586128	6.86062527	1671.40132	0.65095079	999.849659	1.0881636	633.44728	1.71758572	633.44728	1.71758572
66	uki - BPL 35/2	0.8	0.29	0.86206897	f+c	902	1218.37641	0.7403295	158.586128	5.68776102	1210.94968	0.74486993	710.710308	1.26915283	591.217461	1.52566536	591.217461	1.52566536
67	uki - BPL 35/2	0.8	0.29	0.86206897	c	872	1168.35975	0.74634547	158.586128	5.49858937	1171.9428	0.74406362	699.700533	1.24624744	591.217461	1.47492261	591.217461	1.47492261
68	uki - BPB 35/2	0.8	0.29	0.86206897	f+c	911	1086.84899	0.83820292	158.586128	5.74451252	1107.57567	0.82251717	685.379215	1.32919117	591.217461	1.54088818	591.217461	1.54088818
69	uki - BPB 35/2	0.8	0.29	0.86206897	f+c	921	1103.99045	0.83424635	158.586128	5.80756974	1121.19786	0.82144288	688.05857	1.33854884	591.217461	1.55780243	591.217461	1.55780243
70	uki - BPH 35/2	0.8	0.29	0.86206897	c	882	1521.7125	0.57961014	158.586128	5.56164659	1440.65004	0.61222363	816.582803	1.08011092	591.217461	1.49183686	591.217461	1.49183686
71	uki - BPH 35/2	0.8	0.29	0.86206897	c	951	1561.70568	0.60894957	158.586128	5.99674139	1470.16263	0.64686721	834.40386	1.13973586	591.217461	1.60854518	591.217461	1.60854518
72	uki - BPL 35/2	0.8	0.29	0.86206897	c	755	859.865955	0.87804383	158.586128	4.76081992	881.714818	0.85628594	619.917119	1.21790474	554.26637	1.36216094	554.26637	1.36216094
73	uki - BPL 35/2	0.8	0.29	0.86206897	c	735	832.742624	0.88262565	158.586128	4.63470549	860.37585	0.85427781	618.480367	1.18839666	554.26637	1.32607721	554.26637	1.32607721
74	uki - BPB 35/2	0.8	0.29	0.86206897	f+p	755	802.518056	0.9407888	158.586128	4.76081992	836.383896	0.90269552	616.935474	1.22379087	554.26637	1.36216094	554.26637	1.36216094
75	uki - BPB 35/2	0.8	0.29	0.86206897	f+c	804	796.976624	1.00881253	158.586128	5.06980029	831.960102	0.9663925	616.657002	1.30380422	554.26637	1.45056609	554.26637	1.45056609
76	uki - BPH 35/2	0.8	0.29	0.86206897	c	813	1089.19358	0.74642379	158.586128	5.12655179	1055.7939	0.77003665	635.531656	1.27924391	554.26637	1.46680377	554.26637	1.46680377
77	uki - BPH 35/2	0.8	0.29	0.86206897	c	794	1074.31242	0.73907737	158.586128	5.00674307	1044.80699	0.75994897	634.245161	1.25188184	554.26637	1.43252422	554.26637	1.43252422
78	Suzuki - TDL1 1	0.9	0.3	1	f	392	1055.32537	0.8826245	53.58195	7.31589649	936.197951	0.8826245	300.04829	1.30645637	192.374905	2.03768781	192.374905	2.03768781
79	Suzuki - TDL1 2	0.9	0.3	1	f	392	985.379271	0.88210715	53.58195	7.31589649	889.701057	0.88210715	299.975269	1.30677439	192.374905	2.03768781	192.374905	2.03768781
80	Suzuki - TDL2 1	0.9	0.3	1	f	519	1013.28069	0.99616824	80.372925	6.45739843	959.344847	0.99616824	449.362443	1.15496969	288.562358	1.79857139	288.562358	1.79857139
81	Suzuki - TDL2 2	0.9	0.3	1	f	472	1018.53282	0.46341168	80.372925	5.87262439	963.06984	0.49009945	449.375318	1.05034696	288.562358	1.63569498	288.562358	1.63569498
82	Suzuki - TDL3 1	0.9	0.3	1	f	608	1052.80457	0.57750509	107.1639	5.67355238	1021.83078	0.59501046	555.391998	1.09472229	384.749811	1.58024769	384.749811	1.58024769
83	Suzuki - TDL3 2	0.9	0.3	1	f	627	1044.91265	0.60005016	107.1639	5.85085089	1016.02202	0.61711261	551.699763	1.13648771	384.749811	1.62963043	384.749811	1.62963043
84	Suzuki - TDS1 1	0.9	0.3	0.75	f	921	1277.70788	0.98123108	128.59668	7.16192673	1268.97726	0.98123108	686.650813	1.3412931	506.093982	1.8198201	506.093982	1.8198201
85	Suzuki - TDS1 2	0.9	0.3	0.75	f	833	1328.75862	0.62690092	128.59668	6.47761668	1308.069	0.63681656	708.28484	1.17608052	506.093982	1.64593935	506.093982	1.64593935
86	Suzuki - TDS2 1	0.9	0.3	0.75	f	1005	1352.90176	0.74284773	171.46224	5.86134883	1358.71203	0.73967109	803.743108	1.25039953	674.791975	1.48934788	674.791975	1.48934788
87	Suzuki - TDS2 2	0.9	0.3	0.75	f	1054	1356.55454	0.7769684	171.46224	6.14712604	1361.58892	0.77409561	804.516281	1.310104	674.791975	1.56196285	674.791975	1.56196285
88	Suzuki - TDS3 1	0.9	0.3	0.75	f+c	1299	1400.19222	0.92772977	235.76058	5.50982696	1426.88551	0.91037437	1042.25603	1.24633484	927.838966	1.40002743	927.838966	1.40002743
89	Suzuki - TDS3 2	0.9	0.3	0.75	f+c	1303	1403.86389	0.92815266	235.76058	5.52679333	1429.85914	0.91127858	1042.53614	1.24983677	927.838966	1.40433852	927.838966	1.40433852
90	uzuki - TDM1	0.9	0.25	1	f	490	970.267772	0.8838158	63.27162	7.7443884	927.523714	0.8838158	373.380093	1.31233563	247.591627	1.97906531	247.591627	1.97906531
91	uzuki - TDM1	0.9	0.25	1	f	461	938.38686	0.93903204	63.27162	7.28604705	903.984442	0.93903204	373.308784	1.23490263	247.591627	1.86193696	247.591627	1.86193696
92	uzuki - TDM2	0.9	0.25	1	f	657	1041.37316	0.98527815	94.90743	6.92253494	1022.23259	0.98527815	559.147482	1.17500305	371.38744	1.76904205	371.38744	1.76904205
93	uzuki - TDM2	0.9	0.25	1	f	657	988.450296	0.98438897	94.90743	6.92253494	981.448599	0.98438897	558.910749	1.17550074	371.38744	1.76904205	371.38744	1.76904205
94	uzuki - TDM3	0.9	0.25	1	c	1245	1010.25041	1.23236772	902.393738	1.37966383	1084.45988	1.14803694	1084.45988	1.14803694	1050.17442	1.18551736	1058.57581	1.17610849
95	uzuki - TDM3	0.9	0.25	1	c	1210	1037.91318	1.16580078	926.801055	1.30556606	1106.10054	1.09393311	1106.10054	1.09393311	1065.10667	1.13603645	1065.10667	1.13603645
96	Suzuki - BP 20 1	0.9	0.15	1.8	f+c	519	500.123644	1.03774338	77.77404	6.67317784	533.390047	0.97302153	376.394931	1.37887085	293.562942	1.76793432	293.562942	1.76793432
97	Suzuki - BP 20 2	0.9	0.15	1.8	f+c	480	483.810464	0.99212406	77.77404	6.17172517	518.613159	0.92554535	367.914692	1.30465026	293.562942	1.63508377	293.562942	1.63508377
98	uzuki - BPC 20	0.9	0.15	1.8	f+p	519	511.904735	1.01386052	86.4156	6.00586005	546.760271	0.94922771	396.403704	1.30927132	326.181046	1.59114089	326.181046	1.59114089
99	uzuki - BPC 20	0.9	0.15	1.8	f+p	529	475.598513	1.1122827	86.4156	6.1215799	513.646271	1.02989164	382.065302	1.38458006	326.181046	1.62179871	326.181046	1.62179871
100	Suzuki - BP 25 1	0.9	0.2	1.35	c	735	762.691953	0.96369183	129.6234	5.6702725	795.664826	0.9237558	573.141898	1.28240494	489.271569	1.50223321	489.271569	1.50223321
101	Suzuki - BP 25 2	0.9	0.2	1.35	c	755	734.178134	1.02836078	129.6234	5.82456563	770.922627	0.97934601	565.419682	1.33529133	489.271569	1.5431103	489.271569	1.5431103
102	uzuki - BPC 25	0.9	0.2	1.35	f+c	818	666.948997	1.22648059	144.026	5.67953008	715.858337	1.14268418	601.171951	1.36067559	543.635077	1.50468584	543.635077	1.50468584
103	uzuki - BPC 25	0.9	0.2	1.35	f+p	813	748.874868	1.08562863	144.026	5.64481413	788.17606	1.03149543	613.432278	1.32532967	543.635077	1.49548849	543.635077	1.49548849
104	zuki - BP 20/3(	0.8	0.15	1.66666667	f+c	485	720.172937	0.67344936	64.10583	7.56561455	727.079464	0.66705226	402.287998	1.20560395	250.606768	1.93530288	250.606768	1.93530288
105	zuki - BP 20/3(	0.8	0.15	1.66666667	f+c	480	733.537451	0.65436332	64.10583	7.48761852	738.544747	0.64992677	402.399179	1.19284538	250.606768	1.91535131	250.606768	1.91535131
106	uki - BPC 20/3	0.8	0.15	1.66666667	f	500	734.392389	0.68083494	68.379552	7.31212746	742.045072	0.67381352	428.897118	1.16578074	267.313886	1.87046026	267.313886	1.87046026
107	uki - BPC 20/3	0.8	0.15	1.66666667	f	495	734.392389	0.67402659	68.379552	7.23900619	742.045072	0.66707538	428.897118	1.15412293	267.313886	1.85175566	267.313886	1.85175566
108	zuki - BP 30/3(	0.8	0.25	1	c	916	1273.67371	0.71917949	142.4574	6.4299924	1248.29503	0.73380089	801.812409	1.14241185	556.903929	1.64480793	556.903929	1.64480793
109	zuki - BP 30/3(	0.8	0.25	1	f+c	907	1316.1261	0.68914369	142.4574	6.36681562	1281.95089	0.7075154	825.494788	1.09873498	556.903929	1.62864716	556.903929	1.62864716
110	uki - BPC 30/3	0.8	0.25	1	f+c	1039	1332.41137	0.7797892	151.95456	6.83757039	1301.10127	0.79855429	841.176595	1.23517464	594.030857	1.74906739	594.030857	1.74906739
111	uki - BPC 30/3	0.8	0.25	1	f+c	1029	1402.19063	0.73385172	151.95456	6.77176124	1356.2841	0.7586906	879.900611	1.16945026	594.030857	1.73223325	594.030857	1.73223325
112	zuki - BP 30/2(	0.8	0.25	1	f+c	794	1086.7908	0.73059139	142.4574	5.57359604	1083.72453	0.73265851	656.44027	1.20955407	519.777	1.52757817	519.777	1.52757817
113	zuki - BP 30/2(	0.8	0.25	1	c	725	964.045248	0.75203939	142.4574	5.08924071	985.9236	0.7353511	619.309958	1.17065775	519.777	1.39482894	519.777	1.39482894
114	uki - BPC 30/2	0.8	0.25	1	f+c	853	1041.81216	0.81876564	151.95456	5.61352025	1053.59973	0.80960537	663.602311	1.28540842	554.4288	1.53852037	554.4288	1.53852037

115	:uki - BPC 30/2	0.8	0.25	1	f+c	872	1044.47324	0.8348706	151.95456	5.73855763	1055.72852	0.82596992	664.284124	1.31269131	554.4288	1.57278987	554.4288	1.57278987
116	ki - BDA 20/25	0.7	0.15	1.5	f	294	590.575775	0.49781927	42.43776	6.92779261	609.147731	0.48264154	258.723008	1.13635043	169.645735	1.73302323	169.645735	1.73302323
117	ki - BDA 20/25	0.7	0.15	1.5	f	304	590.575775	0.98881207	42.43776	7.16343181	609.147731	0.98881207	258.723008	1.1750018	169.645735	1.7919696	169.645735	1.7919696
118	ki - BDA 20/25	0.8	0.15	1.5	f	304	578.501226	0.99070565	42.43776	7.16343181	598.973222	0.99070565	258.968406	1.17388837	169.645735	1.7919696	169.645735	1.7919696
119	ki - BDA 20/25	0.8	0.15	1.5	f	304	578.501226	0.99070565	42.43776	7.16343181	598.973222	0.99070565	258.968406	1.17388837	169.645735	1.7919696	169.645735	1.7919696
120	ki - BDA 20/25	0.9	0.15	1.5	f	333	585.409782	0.9063521	42.43776	7.8467855	604.891909	0.9063521	259.241551	1.28451631	169.645735	1.96291406	169.645735	1.96291406
121	ki - BDA 20/25	0.9	0.15	1.5	f	333	585.409782	0.9063521	42.43776	7.8467855	604.891909	0.9063521	259.241551	1.28451631	169.645735	1.96291406	169.645735	1.96291406
122	ki - BDA 30/20	0.7	0.25	0.9	f	534	829.199028	0.64399497	106.0944	5.0332534	839.66176	0.63597037	462.618244	1.15429948	393.820457	1.35594784	393.820457	1.35594784
123	ki - BDA 30/20	0.7	0.25	0.9	f+c	549	815.005768	0.67361486	106.0944	5.17463693	828.610816	0.66255471	460.553032	1.19204513	393.820457	1.39403627	393.820457	1.39403627
124	ki - BDA 30/20	0.8	0.25	0.9	f	568	829.199028	0.68499839	106.0944	5.35372272	839.777426	0.67636969	462.996091	1.22679222	393.820457	1.4422816	393.820457	1.4422816
125	ki - BDA 30/20	0.8	0.25	0.9	f	564	861.992736	0.65429786	106.0944	5.31602045	865.132017	0.65192362	468.25895	1.20446176	393.820457	1.43212469	393.820457	1.43212469
126	ki - BDA 30/20	0.9	0.25	0.9	f	583	847.9924	0.68750616	106.0944	5.49510625	854.426542	0.68232899	466.194065	1.25055217	393.820457	1.48037003	393.820457	1.48037003
127	ki - BDA 30/20	0.9	0.25	0.9	f	588	850.331376	0.69149512	106.0944	5.54223409	856.232939	0.68672901	466.573123	1.26025262	393.820457	1.49306617	393.820457	1.49306617
128	ki - BDA 30/25	0.7	0.25	0.9	f+c	662	1151.45546	0.57492454	111.6558	5.92893517	1141.9624	0.57970385	656.052939	1.00906491	453.731262	1.45901342	453.731262	1.45901342
129	ki - BDA 30/25	0.7	0.25	0.9	f+c	676	1082.29094	0.624601	111.6558	6.05432051	1087.44219	0.62164224	622.544049	1.08586694	453.731262	1.48986869	453.731262	1.48986869
130	ki - BDA 30/25	0.8	0.25	0.9	f+c	696	1169.28756	0.59523425	111.6558	6.23344242	1156.04284	0.60205381	665.150245	1.04638013	453.731262	1.53394764	453.731262	1.53394764
131	ki - BDA 30/25	0.8	0.25	0.9	f+c	725	1121.54551	0.64642941	111.6558	6.49316919	1118.60491	0.64812875	641.398955	1.13034172	453.731262	1.59786213	453.731262	1.59786213
132	ki - BDA 30/25	0.9	0.25	0.9	f+c	764	1157.40886	0.66009517	111.6558	6.84245691	1146.86102	0.66616616	659.236475	1.15891646	453.731262	1.68381609	453.731262	1.68381609
133	ki - BDA 30/25	0.9	0.25	0.9	f	764	1091.38814	0.70002593	111.6558	6.84245691	1094.89585	0.69778327	627.079233	1.21834684	453.731262	1.68381609	453.731262	1.68381609
134	ki - BDA 30/30	0.7	0.25	0.9	f+c	769	1405.31131	0.54720971	106.0944	7.24826193	1364.93194	0.56339806	701.521795	1.09618832	459.4572	1.67371411	459.4572	1.67371411
135	ki - BDA 30/30	0.7	0.25	0.9	f+c	730	1369.1918	0.53316124	106.0944	6.88066477	1336.41986	0.54623552	701.321147	1.04089261	459.4572	1.58883134	459.4572	1.58883134
136	ki - BDA 30/30	0.8	0.25	0.9	f+c	828	1429.24445	0.57932707	106.0944	7.80437045	1383.89493	0.59831132	702.354208	1.17889235	459.4572	1.80212651	459.4572	1.80212651
137	ki - BDA 30/30	0.8	0.25	0.9	f+c	809	1429.24445	0.56603333	106.0944	7.62528465	1383.89493	0.58458195	702.354208	1.15184047	459.4572	1.76077336	459.4572	1.76077336
138	ki - BDA 30/30	0.9	0.25	0.9	f+c	843	1421.27949	0.59312754	106.0944	7.94575397	1377.74529	0.61186927	702.870997	1.1993666	459.4572	1.83477373	459.4572	1.83477373
139	ki - BDA 30/30	0.9	0.25	0.9	f+c	813	1312.45579	0.61944944	106.0944	7.66298692	1291.62603	0.62943916	702.383343	1.15748759	459.4572	1.76947929	459.4572	1.76947929
140	ki - BDA 40/25	0.7	0.35	0.64285714	c	1019	1525.69252	0.66789342	198.04288	5.14535034	1524.26865	0.66851733	913.566448	1.11540874	791.680098	1.28713606	791.680098	1.28713606
141	ki - BDA 40/25	0.7	0.35	0.64285714	f+c	1068	1478.4062	0.72239957	198.04288	5.3927715	1487.57439	0.71794729	908.091819	1.17609252	791.680098	1.34902974	791.680098	1.34902974
142	ki - BDA 40/25	0.8	0.35	0.64285714	f	1117	1551.27845	0.72005126	198.04288	5.64019267	1544.193	0.72335518	917.527852	1.21740174	791.680098	1.41092343	791.680098	1.41092343
143	ki - BDA 40/25	0.8	0.35	0.64285714	f+c	1117	1508.55522	0.74044356	198.04288	5.64019267	1511.1855	0.73915479	912.272392	1.224415	791.680098	1.41092343	791.680098	1.41092343
144	ki - BDA 40/25	0.9	0.35	0.64285714	f	1176	1517.13203	0.77514678	198.04288	5.93810795	1517.97195	0.77471788	913.868789	1.28683681	791.680098	1.48544848	791.680098	1.48544848
145	ki - BDA 40/25	0.9	0.35	0.64285714	f	1181	1529.9668	0.77191218	198.04288	5.96335501	1527.89728	0.77295772	915.409925	1.2901324	791.680098	1.49176416	791.680098	1.49176416